APPLICATIONS OF QCD FACTORIZATION IN MULTISCALE HADRONIC SCATTERING

Approved by:

Dr. Pavel Nadolsky

Dr. Fredrick Olness

Dr. Kent Hornbostel

Dr. Stephen Sekula

APPLICATIONS OF QCD FACTORIZATION IN MULTISCALE HADRONIC SCATTERING

A Dissertation Presented to the Graduate Faculty of the

Dedman College of Humanities and Sciences

Southern Methodist University

in

Partial Fulfillment of the Requirements

for the degree of

Doctor of Philosophy

with a

Major in Physics

by

Bowen Wang

(B.A., University of Science and Technology of China, 2009)

August 4, 2015

ACKNOWLEDGMENTS

I want to express my deep gratitude to my advisor Pavel Nadolsky, who has shaped my view in doing research in theoretical physics, and has always been a role model for me as a diligent researcher as well as an honest person. Without his patient explanations in our numerous discussions, it would not have been possible for me to overcome the barriers of my research in the intricate theories of hadronic physics. During my years in Dallas, Pavel is like family to me. I'll always cherish the enjoyable times I've spent at his house hanging our with him and his family.

I must also thank the rest of my thesis committee Kent Hornbostel, Fredrick Olness, and Stephen Sekula. They've provided lots of good advice for my research on the thesis projects. Their hard questions have driven me to improve my understanding about the subjects.

I'm indebted to Marco Guzzi, from whom I learned a lot about programming and data analysis through our collaboration on several projects. I'm truely grateful to Ted Rogers, who not only improved my knowledge on TMD factorization through discussions and lectures, but also opened the door for my future career. I enjoyed collaborating with David Clark, and thank him for always being supportive and encouraging. Keping Xie has made an important cross check of the calculations in this thesis, and has carefully read it. I'm grateful of his help.

My appreciation also goes to Jingbo Ye, who was supportive during my application for the Ph.D. program at SMU, and helped me get used to the life in the US when I first came here. I worked shortly in 2011 with Robert Kehoe, who taught me important knowledge about experimental collider physics, and provided me the great opportunity to visit Fermilab, of which I am sincerely grateful.

During the first few years at SMU I had enjoyed the lectures from Kent Hornbostel, Roberto Vega, Fredrick Olness, Robert Kehoe, Simon Dalley, Randall J. Scalise, and Pavel Nadolsky. I thank them for their courses that had built up my knowledge in particle physics needed by my future research. I thank Shirley Melton, Carol Carroll, Michele Hill, and Lacey Porter, for their administrative work that has made my life at SMU a lot easier.

I thank Zhihua Liang, Jun Gao, Huanzhao Liu, Lin Zhu, Hang Qiu, Tingting Cao, and many other friends and colleagues with whom I've had a lot of fun during my years at SMU. Our friendship is of great value to me.

I own my inexpressible gratitude to my parents, and grandparents. Their love and encouragement have always been a strong power to get me through the difficult times of my oversea life.

Wang , Bowen B.A., University of Science and Technology of China, 2009

Applications of QCD Factorization in Multiscale Hadronic Scattering

Advisor: Professor Pavel Nadolsky

Doctor of Philosophy degree conferred August 4, 2015
Dissertation completed August 4, 2015

In this thesis I apply QCD factorization theorems to two important hadronic processes. In the first study, I treat the inclusive cross section of the production of massive quarks through neutral current deep inelastic scattering (DIS). I work out a method to consistently organize the QCD radiative contributions up to $O(\alpha_s^3)$ (N3LO), with a proper inclusion of the heavy quark mass dependence at different momentum scales. The generic implementation of the mass dependence developed in this thesis can be used by calculations in both an intermediate-mass factorization scheme and a general-mass factorization scheme. The mass effect is relevant to the predictions for Higgs, and W and Z cross sections measured at the LHC. The second study examines the transverse-momentum distribution of the lepton-pair production in Drell-yan process. Theory predictions based on the Collins-Soper-Sterman (CSS) resummation formalism at NNLL accuracy are compared with the new data on the angular distribution ϕ_η^* of Drell-Yan pairs measured at the Tevatron and the LHC. The main finding is that the nonperturbative component of the CSS resummed cross section plays a crucial part in explaining the data in the small transverse momentum region.

TABLE OF CONTENTS

LIST OF FIGURES

LIST OF TABLES

To my parents

Zhengxue Wang and Wenping Zhang.

Chapter 1

Introduction

The concept of factorization [1] is crucial in today's applications of quantum chromodynamics (QCD) to particle scattering involving hadrons. There are several fundamental properties of strong interactions between quarks and gluons (the assumed constituents of hadrons, often called partons) that necessitate the use of factorization methods in calculations.

First, QCD is a renormalizable non-Abelian gauge theory with $SU(3)$ color symmetry [1–3]. The most prominent difference between QCD and an Abelian gauge theory (quantum electrodynamics or QED) is revealed in their renormalization of charges. The behavior of the renormalized strong coupling differs from that of electromagnetic coupling in that the gauge-field self-interaction, which is absent in QED, introduces an anti-screening effect that weakens the interaction at short distances [1–3]. This interaction turns out to dominate the evolution of the coupling and results in the famous property of asymptotic freedom [4,5]. In today's experiments, the strong coupling at the electroweak scale (e.g. Z boson mass $m_Z \approx 90$ GeV) is determined to be $\alpha_s(m_Z) \approx 0.118$ [6], a value small enough for carrying out a perturbative calculation to account for high order contributions from strong interactions. Thus, such a hard momentum scale is necessary in all perturbative QCD calculations.

On the other hand, as the momentum scale decreases, the strong coupling becomes larger and eventually renders any perturbative calculation meaningless. This behavior is consistent with the fact that free quarks or gluons have not been so far observed, which is known as the "confinement". The only strong interaction participants registered by detectors are color neutral states (hadrons). The mechanism that transforms hadrons into quarks and gluons, or that does the inverse, is nonperturbative and is largely unknown.

Moreover, even at large momentum scale, one has to define carefully the quantities to which perturbative calculation can reliably apply. In a typical QCD process, contribution from individual Feynman diagrams generally contains singularities as a result of long distance interactions. It is already shown (Kinoshita-Lee-Nauenberg theorem [7, 8]) that part of the singularities cancel for sufficiently inclusive cross sections. The other part of singularities does not cancel, however, for many important processes, these divergences can be absorbed into one or more universal scalar functions that describe the probability of transformation between hadrons and their constituent particles. The uncancelled divergence is associated with the collinear radiation of massless particles from a parton inside a hadron. The scalar functions are referred to as a parton distribution functions (or PDFs, for an initial hadron), or a fragmentation functions (or FFs, for a final hadron). Factorization theorems are proved for these processes (see reviews in [1, 9–11]) to ensure that the scalar functions carrying long distance information are process independent and are factorized out from the short distance interaction. The hard-scattering cross sections can be computed in perturbation theory order by order, while the nonperturbative hadronic functions can only be obtained from experiments. Factorization is more difficult to carry out for processes with more than one momentum scales, especially when the various scales are well separated. A generic perturbative calculation in this case contains logarithms of the ratio of the separated scales in the form $\ln^n(s_1/s_2)$ at each order, where s_1 and s_2 are two scales satisfying $s_1/s_2 \gg 1$ or $s_1/s_2 \ll 1$, and n is some power constrained by the order of the calculation. The appearance of these log terms can be problematic if they are large enough to ruin the convergence of perturbation series. A consistent factorization procedure needs to sum these logarithms to all orders using the renormalization group invariance of the cross sections, and recover the convergence of the hard scattering processes. Furthermore, various approximations are to be made as part of the prescription of the factorization to pick up important contributions and to simplify calculations. It can be a challenging task to accommodate the prescriptions at different scales.

In this thesis I present two studies that apply QCD factorization theorems in multiscale processes, where I deal with the complications related with the factorization in each case. In one application I treat the inclusive cross section of the production of massive quarks through neutral current deep inelastic scattering (DIS): $e^- + p \rightarrow e^- + X(q_h)$. In this study I work out a method to consistently organize the QCD radiative contributions up to $O(\alpha_s^3)$ (N3LO), with a proper inclusion of the heavy quark mass dependence at different momentum scales. The study is of interest to the phenomenology of hadronic physics for three reasons. First, it is the first study of massive quark production in DIS at an accuracy of N3LO. Second, it results in a generic framework of classifying contributions with various mass dependences at N3LO, which applies not only for the current numerical calculation, but also for future implementations when the calculation of the hard scattering process reaches a new accuracy. Third, the mass dependence from heavy quark flavors not only manifests itself in DIS, but has shown its importance in global QCD analysis at an accuracy relevant for the measurements at the Large Hadron Collider (LHC). Fig. 1.1 shows the sensitivity of the experiments in CTEQ14 fits to the Higgs cross section, where S_n is a quantity defined in [12], which provides a measure of the goodness-of-fit to each individual experiment. From this figure we see that a prediction for the Higgs boson production cross section σ_H, the key electroweak observable at the LHC, is sensitive to the goodness-of-fit to the charm production (experiment number 147) and total inclusive (experiment number 159) DIS measurements at HERA. The mutual sensitivity is introduced through the shared degrees of freedom in parton distribution functions, which in turn are affected by the N3LO contributions to heavy-quark hard scattering in DIS that I am computing. Fig. 1.2 gives the W and Z correlation in lepton production processes. It shows that allowing intrinsic charm contribution leads to cross sections that deviate significantly from the tolerance ellipse of the CTEQ6.6 fit. These figures show affirmatively the relevance of charm quark effects in DIS to predictions for the LHC measurements.

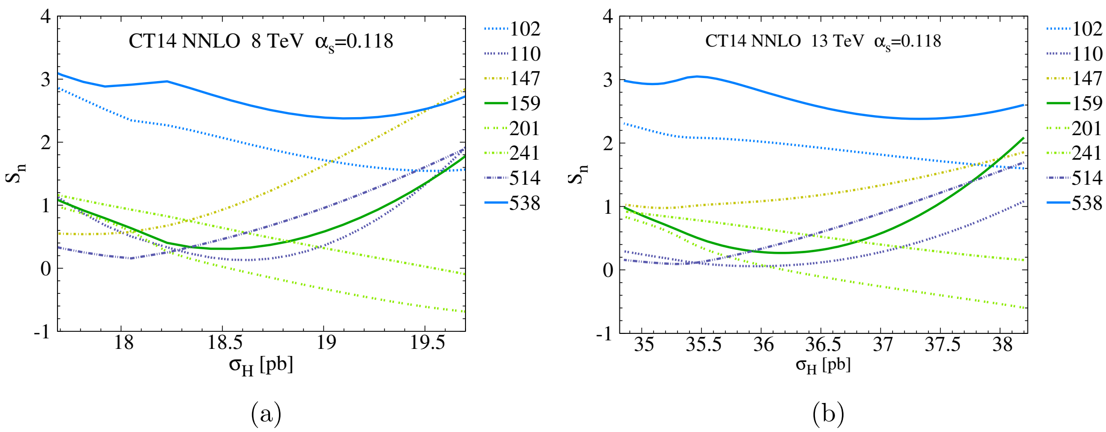

Figure 1.1. From [13]: The equivalent Gaussian variable S_n versus σ_H (in pb) at the LHC for two center-of-mass energies.

In the other study I and my collaborators examine factorization for Drell-Yan production of lepton pairs at hadron colliders: $h_1 + h_2 \rightarrow (Z/\gamma^* \rightarrow l_1 + l_2) + X$. This process shows its two-scale character conspicuously when the distribution of the transverse momentum Q_T of the lepton pair is computed at a value $Q_T \ll Q$, where Q denotes the invariant mass of the lepton pair. At this region perturbation series receives large corrections from soft emission of gluons. In each order n they are of the

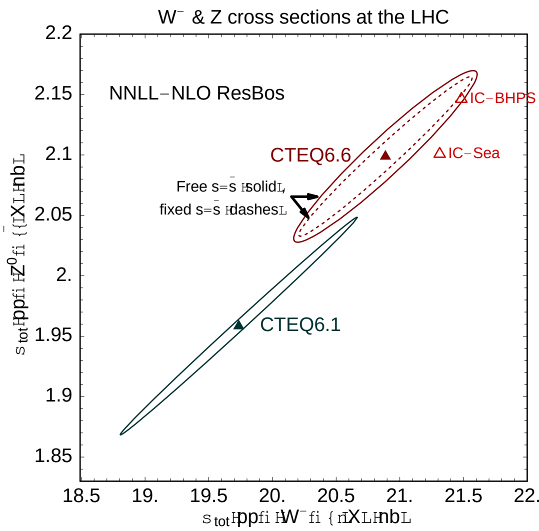

(a)

Figure 1.2. From [14]: W and Z correlation ellipses at the LHC

form $\alpha_s^n ln^m(Q^2/Q_T^2)$, with $m = 0, 1, ...2n - 1$. In addition to factorizing the collinear singular contributions into parton distribution functions, these large logs must be summed properly to all orders into a soft factor. Factorization in such a manner is variously called transverse momentum dependent (TMD) factorization, Q_T factorization, or Q_T resummation. It was first established by Collins, Soper, and Sterman (CSS) [1, 15–18]. One subtlety of TMD factorization is that if Q_T is of a small value comparable to the intrinsic transverse motion of the partons, long distance interaction becomes important and one has to introduce an additional factor to describe the nonperturbative transverse dynamics. As with PDFs and FFs, this nonperturbative contribution can only be parameterized and fitted with data. In this study, we give a detailed analysis regarding the parameterization of the nonperturbative factor as well as the effects of several perturbative parameters. Motivated by the new measurements from the LHC [19, 20] and the TEVATRON [21], we are able to perform the analysis at an unprecedented level of accuracy and have obtained a conclusive evidence regarding the significance of the nonperturbative small Q_T contribution.

The rest of this thesis is organized as follows. In Ch. 2 I summarize the basics of perturbative QCD as a background for discussions in other chapters. In Ch. 3 I discuss the kinematics of DIS, give an explicit calculation of a DIS structure function to the lowest non-trivial order, and thereby introduce the idea of factorization. In Ch. 4 I treat heavy quark production in inclusive DIS in a particular factorization scheme at N3LO, and discuss its numerical implications. In Ch. 5 I present an analysis of the nonperturbative contribution to a Q_T related distribution for Drell-Yan production of a lepton pair using TMD factorization, in which theoretical predictions are compared with new measurements from hadron colliders. Appendix A contains the factorization scale dependent DIS hard coefficients at N3LO that are used in Ch. 4 to compute the scale uncertainty of DIS structure functions.

Chapter 2

Basics of Perturbative QCD

Quark model was first proposed in early 1960's to explain the hadron spectra discovered at that time. In this model hadrons are composed of fermions called quarks. It was not long before people realized that this model needed to be extended to allow additional degree of freedom for the quarks, otherwise, the newly discovered baryon states $\triangle^{++}$ and Ω^- would not exist, since they are made of three quarks of the same flavor with parallel spins, which are prohibited by Pauli's exclusion principle. Since 1973, a field theory with the name quantum chromodynamics (QCD) has been developed to explain interactions of quarks on the basis of the gauge invariance principle. The hypothesized gauge group was $SU(3)$, which introduces a new quantum number color to quarks as well as the gauge bosons called gluons. Unlike the photons in quantum electrodynamics (QED), the gluons in QCD are able to interact with themselves because of the non-abelian nature of the $SU(3)$ color group. This property finally has lead to the discovery of asymptotic freedom of strong interactions [4, 5]. To give an introductory account of the basic results in QCD, we start by writing down the QCD Lagrangian.

2.1. QCD Lagrangian

The QCD Lagrangian is given by

$$\mathcal{L} = \mathcal{L}_{gauge-invariant} + \mathcal{L}_{gauge-fixing} + \mathcal{L}_{ghost}, \tag{2.1}$$

where the gauge-invariant part has the Yang-Mills [22] form

$$\mathcal{L}_{gauge-invariant} = \bar{\psi}_i(i\gamma^\mu\partial_\mu\delta_{ij} - g_s\gamma^\mu t^a_{ij}A^a_\mu - m\delta_{ij})\psi_j - \frac{1}{4}F^b_{\mu\nu}F^{b\,\mu\nu}. \tag{2.2}$$

In Eq. (2.2) the sum over quark flavors is implicit, and repeated indices are summed over. ψ_i and A^a_μ are quark (with mass m) and gluon fields, respectively. γ^μ are the Dirac γ-matrices. g_s is the strong coupling constant. t^a_{ij} are the generators of the SU(3) group in its fundamental representation, with i, j running from 1 to $N = 3$. This value of N, the number of independent quark colors, is supported by experiment. The field strength tensor is $F^a_{\mu\nu} = \partial_\mu A^a_\nu - \partial_\nu A^a_\mu - g_s f_{abc}A^b_\mu A^c_\nu$, where f_{abc} are the structure constants of the SU(3) group defined by the commutator

$$\left[t^a, t^b\right] = if_{abc}t^c. \tag{2.3}$$

The indices a, b, c are subjected to the transformation in the adjoint representation, and run from 1 to $N^2 - 1 = 8$. In fact, the matrix $(t^a)_{bc} \equiv f_{abc}$ serves as the a^{th} generator of the adjoint representation.

$\mathcal{L}_{gauge-invariant}$ of the form in Eq. (2.2) is invariant under the local gauge transformations of the SU(3) group:

$$\psi'_i = U(\theta(x))\psi_i, \tag{2.4}$$

$$t^a A'^a_\mu = (i/g)(\partial_\mu U(\theta(x)))U^{-1}(\theta(x)) + U(\theta(x))t^a A^a_\mu U^{-1}(\theta(x)), \tag{2.5}$$

where

$$U(\theta(x)) = e^{-it^a\theta^a(x)}. \tag{2.6}$$

The gauge-fixing term is introduced in order to define a suitable form for the gluon propagator, which is necessary for the calculation of scattering amplitudes. One common choice is the R_ζ gauge

$$\mathcal{L}_{gauge-fixing} = \frac{1}{2\zeta}(\partial^\mu A^a_\mu)(\partial^\mu A^a_\mu). \tag{2.7}$$

There is a freedom of choosing the parameter ζ. For instance, most calculations of matrix elements are easily performed with Feynman gauge where ζ is set to 1. However, calculations with R_ζ gauge contain contribution from unphysical gluon polarization states. The way to overcome this difficulty is to introduce the unobservable ghost fields η^a residing in

$$\mathcal{L}_{ghost} = -\bar{\eta}^a(\partial^2\delta^{ab} + g_s\partial^\mu f_{abc}A^c_\mu)\eta^b. \tag{2.8}$$

The ghost contribution to an S-matrix element serves to cancel the effect of unphysical gluon states. Another useful choice for the gauge-fixing Lagrangian is the axial gauge

$$\mathcal{L}_{gauge-fixing} = \frac{1}{2\zeta}(n^\mu A^a_\mu)(n^\mu A^a_\mu), \tag{2.9}$$

with a constant ζ and a 4-vector n.

2.2. Renormalization of QCD

Just as in many other quantum field theories, a perturbative calculation in QCD may suffer from ultra-violet divergences produced by loop momentum integrals. Renormalization is the procedure to cancel the divergences systematically and obtain finite physical results. The fields and coupling constant in the Lagrangian Eq. (2.1) are the bare quantities: $\psi_0, g_{0\,s}, A^b_{0\,\mu}$, though the subscript 0 is suppressed there. Using the standard notations, the renormalized quantities, which are related to physical observables, can be expressed in terms of the bare ones using the renormalization constants Z_i:

$$\psi = Z_\psi^{-1/2}\psi_0,\ A^a_\mu = Z_A^{-1/2}A^a_{0\,\mu},\ \eta^a = Z_\eta^{-1/2}\eta^a_0. \tag{2.10}$$

We can write similar relations for the coupling constant and fermion mass

$$g_{s\,0} = Z_g\mu^\epsilon g_s, \tag{2.11}$$

$$m_0 = Z_m m, \tag{2.12}$$

where we use dimensional regularization to evaluate the divergent integrals at the dimension $n = 4 - 2\epsilon$.

2.3. The β function and Asymptotic freedom

Dimensional regularization introduces the parameter μ with the unit of momentum to make up for the dimension of loop integrals in a perturbative calculation of the renormalization constants. While S-matrix elements and bare quantities such as ψ_0 make no reference to μ, renormalized quantities depend on it. One important case is the renormalized strong coupling constant g_s, of which the μ dependence can be derived from Eq. (2.11). If we plug in the one-loop value of Z_g (see for example [2]), we can rewrite it as

$$g_{s\,0} = \left[1 - \frac{b\alpha_s}{2\pi\epsilon}\right] \mu^{\epsilon} g_s, \tag{2.13}$$

where $\alpha_s \equiv g_s^2/4\pi$, and

$$b \equiv \frac{11}{12} C_A - \frac{1}{3} T_F N_f, \tag{2.14}$$

where $C_A = 3$, $T_F = 1/2$ and N_f stands for the number of active quark flavors. $g_{s\,0}$ is independent of μ, therefore taking the logarithm of Eq. (2.13) and differentiating with respect to lnμ gives

$$\mu \frac{\mathrm{d}g_s}{\mathrm{d}\mu} = -\epsilon g_s \frac{1 - \frac{bg_s^2}{8\pi^2\epsilon}}{1 - \frac{3bg_s^2}{8\pi^2\epsilon}}. \tag{2.15}$$

If we retain terms up to $O(g_s^3)$ on the right hand side and take the limit $\epsilon \to 0$ at the end, we obtain a simpler form

$$\beta \equiv \mu \frac{\mathrm{d}g_s}{\mathrm{d}\mu} = -\frac{b}{4\pi^2} g_s^3 + O(g_s^5), \tag{2.16}$$

where we have defined the β function and obtained its value to one loop. It can be shown in general that the β function takes the form

$$\beta = -g_s \sum_{n=0}^{\infty} \beta_n \left(\frac{\alpha_s}{4\pi}\right)^{n+1}, \tag{2.17}$$

where β_n are perturbatively calculable constants with $\beta_0 = 4b = \frac{11}{3}C_A - \frac{4}{3}T_F N_f$. It is straightforward to integrate Eq. (2.16) to obtain

$$\frac{1}{g_s^2(\mu)} - \frac{1}{g_s^2(\mu_0)} = \frac{\beta_0}{8\pi^2} \tag{2.18}$$

or equivalently,

$$\alpha_s(\mu) = \frac{\alpha_s(\mu_0)}{1 + \frac{\beta_0 \alpha_s(\mu_0)}{2\pi} \ln\left(\frac{\mu}{\mu_0}\right)}. \tag{2.19}$$

For $N_f < 33/2$, $\alpha_s(\mu)$ becomes smaller for larger value of μ. This property is named asymptotic freedom and is one of the key features of QCD that is different from QED, for which the coupling strength increases as the momentum scale becomes large. The behavior is consistent with the fact that all particles with non-zero color charge are not directly observed. The interaction between colored particles tends to become stronger at long distances. Eventually, the large value of α_s deteriorates the perturbative prediction and some non-perturbative effect not fully known causes the confinement. It is convenient to introduce a scale Λ at which perturbation theory breaks down. It is defined by

$$\ln\frac{\mu^2}{\Lambda^2} = -\int_{\alpha_s(\mu)}^{\infty} \frac{4 \mathrm{d}\alpha_s}{g_s \beta(\alpha_s)}. \tag{2.20}$$

Therefore α_s would diverge at this scale. Integrating Eq. (2.20) using the one loop beta function Eq. (2.16) gives

$$\alpha_s(\mu) = \frac{4}{\beta_0 \ln(\mu^2/\Lambda^2)}. \tag{2.21}$$

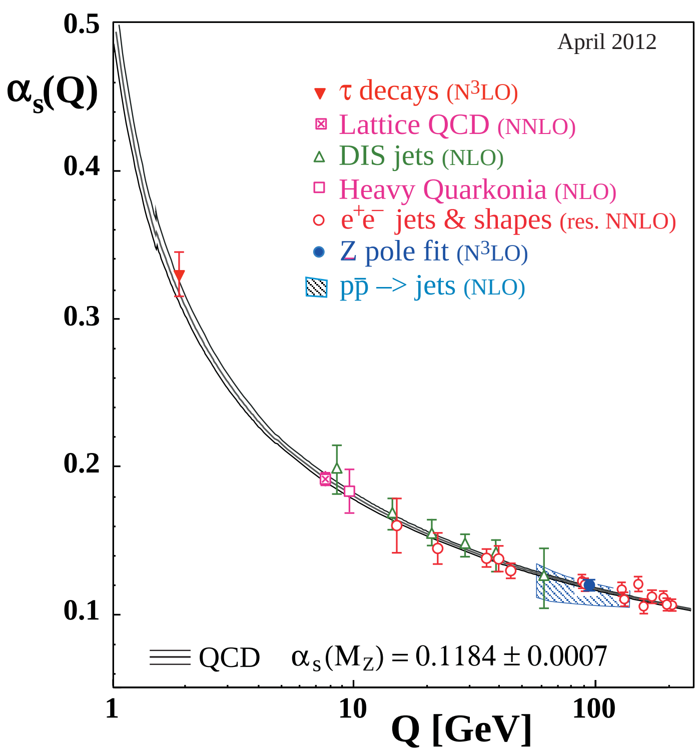

Figure 2.1. From [6]: measurements of α_s as a function of the energy scale Q.

Λ depends on the renormalization scheme and the number of active flavors N_f. It can be determined by the experimental measurement of α_s. However, a small uncertainty in α_s can lead to a much larger uncertainty in Λ due to the form of Eq. (2.21). The approximate value given by the experiment measurements is

$$\Lambda \approx 200\,\mathrm{MeV}. \tag{2.22}$$

2.4. Quark masses

The quark mass is another quantity that needs to be renormalized. The definition of the renormalized quark mass is not unique and depends on the renormalization scheme used. A commonly used definition is the $\overline{MS}$ mass. As with the case of the coupling, the masses in this scheme also depend on the scale μ. Starting from Eq. (2.12) a calculation similar to what is done for the running coupling can be performed to give the scale dependence of m. In this case we define the γ_m function by

$$\gamma_m \equiv -\frac{\mu}{m}\frac{\mathrm{d}m}{\mathrm{d}\mu}, \tag{2.23}$$

where γ_m has the expansion

$$\gamma_m = \sum_{n=0}^{\infty} \gamma_n \left(\frac{\alpha_s}{\pi}\right)^{n+1}. \tag{2.24}$$

The scale dependence is fully determined by Z_m:

$$\gamma_m = \frac{\partial \ln Z_m}{\partial \ln \mu}. \tag{2.25}$$

The one-loop expression of Z_m [1] then gives the first coefficient $\gamma_0 = 2$. Therefore the running of the quark mass obeys

$$\mu\frac{\mathrm{d}m(\mu)}{\mathrm{d}\mu} = \left(-\frac{2\alpha_s(\mu)}{\pi} + O(\alpha_s^2)\right) m(\mu). \tag{2.26}$$

Neglecting the $O(\alpha_s^2)$ terms in the brackets, one can integrate the equation using Eq. (2.21) and get

$$m(\mu) = \left[\frac{\ln(\mu_0/\Lambda)}{\ln(\mu/\Lambda)}\right]^{4/\pi\beta_0} m(\mu_0). \tag{2.27}$$

2.5. The decoupling of heavy flavors and matching of the coupling

Note that the running of both the coupling and the mass depend on the number of active quark flavors N_f, through β_0. There remains the problem of choosing the appropriate value for N_f. For a quantity such as the running coupling, which is free of any singularity in the zero quark mass limit, it is safe to set $m = 0$ in a perturbative calculation where the mass of a quark flavor satisfies $m \ll \mu$. However, in practice, the quark masses extend from less than 1 GeV for the light flavors to nearly 200 GeV for the top quark. A large part of the perturbative region is covered in this range. The mass effect of a heavy flavor needs to be taken seriously. Fortunately, it is proved that the inclusion of a heavy flavor with the mass m only contributes finite terms to the renormalized quantities of the form $(\mu/m)^\lambda$, with $\lambda \geq 1$. It means that the heavy flavor can be dropped as long as $\mu \ll m$. Note that automatic decoupling can be realized in momentum subtraction factorization schemes, but for $\overline{MS}$ one has to use an alternative approach [23]. For instance, to obtain the evolution of $\alpha_s(\mu)$, we include one more active flavor in N_f as μ crosses a heavy flavor mass threshold, and specify the matching conditions of the evolutions with N_f and $N_f + 1$ flavors. A detailed description of the method can be found in [24–26].

Chapter 3

Deep Inelastic Scattering

High-energy collisions between hadrons and leptons can serve as probes of the hadron structure. At sufficiently high energy, such collisions, through exchange of vector bosons, can break the hadrons and produce complex hadronic states. Therefore, this kind of processes is called deep inelastic scattering (DIS). In this chapter, we first summarize the basic aspects of a perturbative calculation in Quantum Chromodynamics, then turn to the factorization of inclusive DIS. The purpose of this chapter is to introduce key concepts describing DIS on the example of a one-loop QCD calculation for this process.

3.1. Kinematics of Deep Inelastic Scattering

A diagram of electron-proton scattering is shown in Fig. 3.1, in which the collision occurs through one-photon exchange. In fact, the one-photon exchange has been experimentally confirmed to be a good approximation in calculation of cross sections, although multiple-photon processes can contribute. The hadronic part of the final state is not shown explicitly which indicates that the measured cross section is inclusive: only the final state of the electron is observed and hadronic final states are summed over in calculation of the cross section. In this section we will derive a general form of cross section for this process. The discussion here is based on [2, 3, 27, 28].

The S-matrix element of this process can be written as

$$S_{fi} = S\left(\mathrm{e}^-(k)\,\mathrm{p}(p) \to \mathrm{e}^-(k')\,\mathrm{X}(p')\right)$$

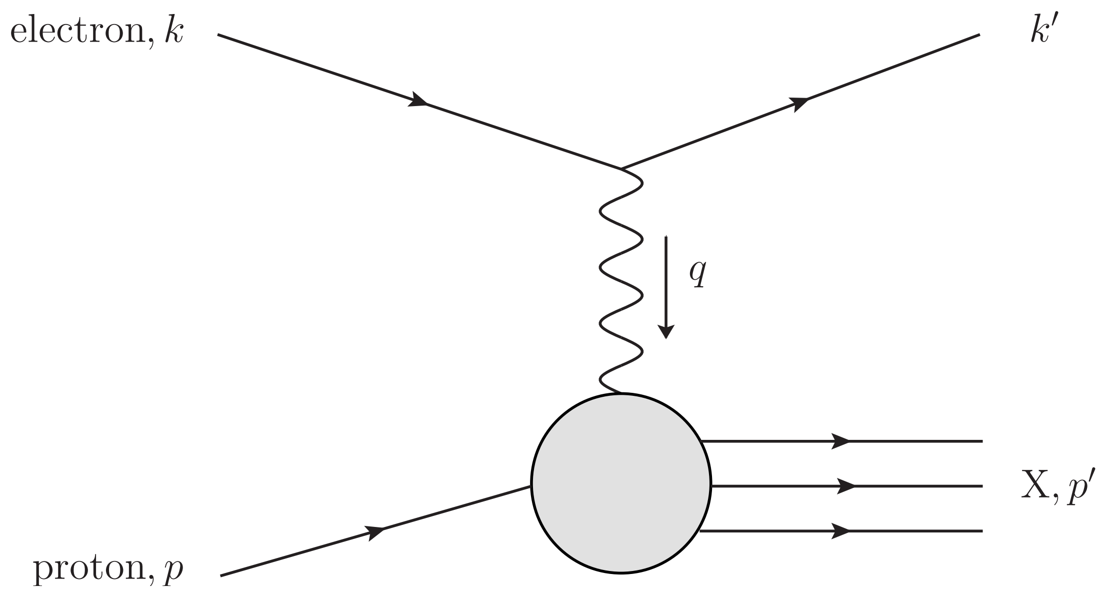

Figure 3.1. Deep inelastic scattering of an electron and a proton.

$$= \bar{u}(k', s')(ie\gamma^{\mu})u(k, s)\left(\frac{-i}{q^2}\right)\int d^4x e^{iq\cdot x}\langle \mathrm{X}|\, j^{(em)}_{\mu}(x)\,|\mathrm{p}(p, r)\rangle\,, \qquad (3.1)$$

where the spin indices of initial and final state electrons, and of the initial state proton are shown explicitly as s, s', and r. $e = -|e|$ is the electron charge. The initial and final hadronic states are represented by $|\mathrm{p}(p, r)\rangle$ and $|\mathrm{X}\rangle$, where $j^{\mu}_{(em)} = i\sum_q Q_q\bar{\psi}_q\gamma^{\mu}\psi_q$ is the electromagnetic current for the proton. Q_q are the charge fractions of the quarks. $q^{\mu} = k^{\mu\prime} - k^{\mu}$ is the 4-momentum transfer from the lepton to the proton; x^{μ} is the position 4-vector that is Fourier-conjugate to q^{μ}. The integral over x can be further simplified:

$$\int d^4x e^{-iq\cdot x}\langle \mathrm{X}|\, j^{(em)}_{\mu}(x)\,|\mathrm{p}(p, r)\rangle = \int d^4x e^{-i(q+p-p')\cdot x}\langle \mathrm{X}|\, j^{(em)}_{\mu}(0)\,|\mathrm{p}(p, r)\rangle$$
$$= (2\pi)^4\langle \mathrm{X}|\, j^{(em)}_{\mu}(0)\,|\mathrm{p}(p, r)\rangle\,\delta^4(q + p - p'). \qquad (3.2)$$

To obtain a transition rate we square the S-matrix element, sum and average over the electron and proton spins, sum over all possible quantum numbers associated with the unknown state $|\mathrm{X}\rangle$, and divide the result by the space-time volume VT. We then obtain the transition probability per unit time and per unit volume

$$P_{fi} = \frac{\frac{1}{4}\sum_{s,s',r,X}|S_{fi}|^2}{VT} = \frac{1}{q^4}L^{\mu\nu}W_{\mu\nu}, \tag{3.3}$$

where we express the transition rate as contraction of the leptonic tensor,

$$\begin{aligned} L^{\mu\nu} &= \frac{e^2}{2}\,\mathrm{Tr}\,[\not{k}\gamma^\mu\not{k}'\gamma^\nu] \\ &= 2e^2[k'^\mu k^\nu + k'^\nu k^\mu + (q^2/2)g^{\mu\nu}], \end{aligned} \tag{3.4}$$

in which the electron mass is neglected for high energy collisions. The hadronic tensor is

$$\begin{aligned} W_{\mu\nu} = &\frac{e^2}{2}\sum_{\mathrm{X},r}\langle \mathrm{p}(p,r)|\, j_\mu^{(em)}(0)\,|\mathrm{X}\rangle\,\langle \mathrm{X}|\, j_\nu^{(em)}(0)\,|\mathrm{p}(p,r)\rangle \\ &\times (2\pi)^4\delta^4(q+p-p'). \end{aligned} \tag{3.5}$$

We need to simplify the hadronic tensor $W_{\mu\nu}$. Before making any assumptions regarding the details of the hadronic current $j_\mu^{(em)}$, and of the initial proton state $|\mathrm{p}(p,r)\rangle$, all we can do is to construct the tensor $W_{\mu\nu}$ by using $g_{\mu\nu}$ and the hadron and photon momentum vectors, of which p and q are two independent ones. For the parity conserving current $j_\mu^{(em)}$, the general form of $W_{\mu\nu}$ is

$$W_{\mu\nu} = p_\mu p_\nu g_1 + p_\mu q_\nu g_2 + q_\mu p_\nu g_3 + q_\mu q_\nu g_4 + g_{\mu\nu}q^2 g_5, \tag{3.6}$$

where g_i are functions of Lorentz scalars p^2, q^2, and $p\cdot q$. In the last term q^2 is factored out so that all g_i have the same unit. The number of the scalar functions g_i can be reduced by the requirement of current conservation in the following form:

$$q^\mu W_{\mu\nu} = 0, \tag{3.7a}$$

$$q^\mu W_{\nu\mu} = 0. \tag{3.7b}$$

Plugging Eq. (3.6) into Eq. (3.7a) and Eq. (3.7b) and subtracting the resulting equations yield $g_2 = g_3$. Contracting Eq. (3.7a) with q^ν and p^ν will give another two independent relations, from which we can express g_3 and g_4 in terms of g_1 and g_5. Consequently, Eq. (3.6) simplifies to

$$W_{\mu\nu} = q^2(g_{\mu\nu} - \frac{q_\mu q_\nu}{q^2})g_5 + [p_\mu - q_\mu(p \cdot q/q^2)][p_\nu - q_\nu(p \cdot q/q^2)]g_1. \tag{3.8}$$

It is conventional to extract some constant factors out of g_1 and g_5 and define another two scalar functions, W_1 and W_2:

$$\begin{aligned} W_{\mu\nu} &= -4\pi e^2(g_{\mu\nu} - \frac{q_\mu q_\nu}{q^2})W_1(x, Q^2, p^2) \\ &+ 4\pi e^2[p_\mu - q_\mu(p \cdot q/q^2)][p_\nu - q_\nu(p \cdot q/q^2)]W_2(x, Q^2, p^2), \end{aligned} \tag{3.9}$$

where we define $Q^2 \equiv -q^2 > 0$, and

$$x \equiv \frac{Q^2}{2p \cdot q}. \tag{3.10}$$

The next step is to give an expression of the differential cross section. This is done by inserting the flux factor and the phase space of the outgoing electron

$$d\sigma = \frac{P_{fi}}{4|p \cdot k|}\frac{d^3\mathbf{k}'}{(2\pi)^3 2|\mathbf{k}'|} = \frac{1}{2s}\frac{L^{\mu\nu}W_{\mu\nu}}{Q^4}\frac{d^3\mathbf{k}'}{(2\pi)^3 2E'}, \tag{3.11}$$

where the Mandelstam variable $s = (k+p)^2$, and $E' \equiv |\mathbf{k}'|$. The proton mass is also ignored in the flux in high energy case. Eq. (3.11) works equally well in all frames associated by boosts along the initial beam direction. In terms of spherical variables, this becomes

$$d\sigma = \frac{1}{4s}\frac{L^{\mu\nu}W_{\mu\nu}}{Q^4}\frac{E'dE'd(-\cos\theta)}{(2\pi)^2}, \tag{3.12}$$

where the azimuthal angle is integrated over because of azimuthal symmetry. It is often convenient to write the differential cross section as a function of Lorentz invariant variables. For this purpose we introduce another commonly used quantity

$$y \equiv \frac{p \cdot q}{p \cdot k} = \frac{2p \cdot q}{s}. \tag{3.13}$$

Now we can change variables from E' and $-\cos\theta$ to Q^2 and y:

$$Q^2 = 2EE'(1 - \cos\theta), \tag{3.14}$$

$$y = 1 - \frac{2|\mathbf{p}|E'(1 + \cos\theta)}{s}, \tag{3.15}$$

where E denotes the initial proton energy. The Jacobian of this transformation gives

$$dE' d(-\cos\theta) = (1/2E')dydQ^2. \tag{3.16}$$

It is not difficult to evaluate the tensor contraction in Eq. (3.12). The result is

$$L^{\mu\nu}W_{\mu\nu} = 8\pi e^4[xysW_1 + \frac{1}{2}s^2(1-y)W_2]. \tag{3.17}$$

These DIS cross sections are usually expressed in terms of structure functions defined as

$$F_1(x, Q^2) \equiv W_1(x, Q^2), \tag{3.18a}$$

$$F_2(x, Q^2) \equiv \nu W_2(x, Q^2), \tag{3.18b}$$

where $\nu \equiv p \cdot q$. Collecting all the pieces we find the cross section

$$\frac{d\sigma}{dydQ^2} = \frac{4\pi\alpha^2}{Q^4}\left(xyF_1 + \frac{1-y}{y}F_2\right), \tag{3.19}$$

where $\alpha = e^2/4\pi$ is the fine-structure constant. One can also change variables to x and Q^2 using $Q^2 = sxy$ and obtain

$$\frac{d\sigma}{dxdQ^2} = \frac{4\pi\alpha^2}{Q^4}\left(y^2F_1 + \frac{1-y}{x}F_2\right). \tag{3.20}$$

Eq. (3.19) and Eq. (3.20) are invariant under beam direction boosts.

We can compute the cross sections of the process $\gamma \mathrm{p} \to \mathrm{X}$ for transversely and longitudinally polarized photons absorbed by the proton. It can be shown [27] that the former is proportional to F_1 and the latter is proportional to $F_L \equiv F_2 - 2xF_1$, which is called the longitudinal structure function. Thus, the cross section Eq. (3.20) can also be written as

$$\frac{d\sigma}{dxdQ^2} = \frac{4\pi\alpha^2}{Q^4}\left[[1+(1-y)^2]F_1 + \frac{1-y}{x}F_L\right]. \tag{3.21}$$

3.2. The Parton Model

It was observed in early experiments that, to a good approximation, the structure functions scale with x. That is, instead of depending on x and Q^2 separately, they depend only on one variable x (Fig. 3.2). This is known as Bjorken scaling [29, 30].

Feynman proposed the parton model [30,31] to describe the scaling behavior of the structure functions. Essentially, a hadron is seen as consisting of pointlike particles called partons. In the standard model of particle physics, these are further assumed to be charged fermions, called "quarks", and a vector boson called "gluon". Each parton carries a fraction ξ of the proton momentum in the beam direction, with $0 < \xi < 1$, and a negligible[1] momentum transverse to the beam. The momentum distribution of a parton can be described by a function $f_i(\xi)$ which gives the probability of finding a parton of the type i with a fraction ξ of the proton momentum. With these assumptions, inelastic scattering of an electron and a proton can be expressed as a superposition of elastic scatterings of an electron and charged partons. The squared

[1] Neglecting the transverse momenta of initial partons is not valid if they are comparable to the net transverse momentum of the particles produced by the parton scattering. We will see such an example in Ch. 5.

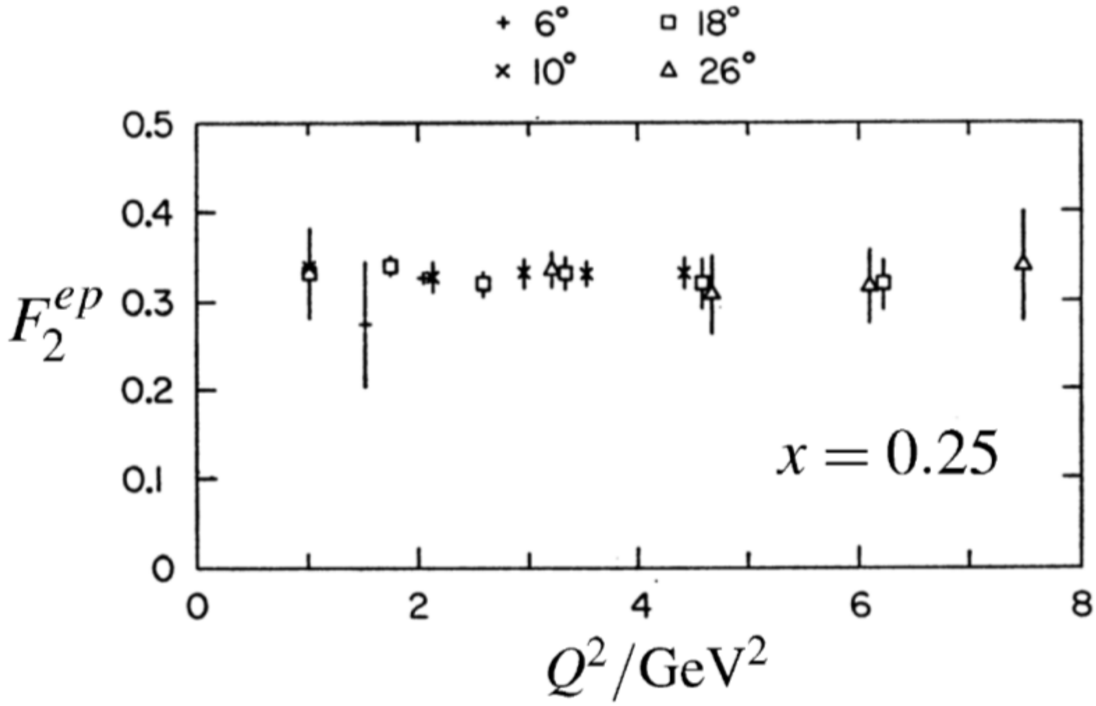

Figure 3.2. Bjorken scaling observed by the SLAC experiments (Friedman and Kendall 1972). F_2 is shown to have no significant Q^2 dependence.

matrix element of this process is known from QED:

$$\begin{aligned}
&\overline{\sum} \left|\mathcal{M}\left(\mathrm{e}^-(k)\,\mathrm{q}(\xi p) \to \mathrm{e}^-(k')\,\mathrm{q}\left(p'_q\right)\right)\right|^2 \\
&= 2e^4 Q_q^2 \frac{\hat{s}^2 + \hat{u}^2}{\hat{t}^2} (2\pi)^4 \delta^4(q + \xi p - p'_q),
\end{aligned} \tag{3.22}$$

where by our assumption, the initial quark momentum is written as $\hat{p} = \xi p$. Here and in what follows "ˆ" is used to signify a parton-level quantity. $\overline{\sum}$ denotes the average over initial colors and spins and the sum over final colors and spins. Q_q is the quark charge in the unit of $|e|$. The parton-level Mandelstam variables $\hat{s} = (k + \hat{p})^2$, $\hat{t} = (k - k')^2 = -Q^2$, and $\hat{u} = (\hat{p} - k')^2$ are used. After including the flux factor and the electron phase space, as well as performing the integral over the final-state quark phase space, we get the parton-level cross section

$$\frac{d^2\hat{\sigma}}{dxdQ^2} = \frac{2\pi Q_q^2\alpha^2}{Q^4}[1+(1-y)^2]\delta(x-\xi). \tag{3.23}$$

The parton-level structure functions are easily read off from Eq. (3.21):

$$\hat{F}_2^{(0)} = 2\hat{F}_1^{(0)} = \sum_q Q_q^2\delta(1-\frac{x}{\xi}), \tag{3.24}$$

$$\hat{F}_L^{(0)} = 0. \tag{3.25}$$

To obtain a hadron-level cross section we need to multiply Eq. (3.26) by $f_q(\xi)$, integrate over all possible momentum fraction ξ, and sum over all quark flavors

$$\begin{aligned}\frac{d^2\sigma}{dxdQ^2} &= \sum_q \int_0^1 f_q(\xi)\frac{2\pi Q_q^2\alpha^2}{Q^4}[1+(1-y)^2]\delta(x-\xi) \\ &= \sum_q f_q(x)\frac{2\pi Q_q^2\alpha^2}{Q^4}[1+(1-y)^2]. \end{aligned} \tag{3.26}$$

Comparing this expression with Eq. (3.21) we find the leading-order prediction given by the parton model:

$$F_1 = \frac{1}{2}\sum_q Q_q^2 f_q(x), \tag{3.27a}$$

$$F_2 = 2xF_1 = \sum_q Q_q^2 x f_q(x). \tag{3.27b}$$

The parton-model calculation gives structure functions scaling to x. The relation $F_2 = 2xF_1$, or $F_L = 0$, is called the Callan-Gross relation [32]. It follows from our assumption that the electron scatters off spin-$\frac{1}{2}$ quarks. In contrast, scattering on a spin-0 particle will yield $F_1 = 0$. Experiments have confirmed the Callan-Gross relation and therefore the spin-$\frac{1}{2}$ of quarks.

3.3. One-loop correction and the breaking of Bjorken scaling

The parton model calculation we have done is of the leading order in QCD ($O(\alpha_s^0)$), as shown in Fig. 3.3(a). In this section we consider the next-to-leading order corrections. These include processes with one gluon emitted by a quark, as in Figs. 3.3 (b-d)(along with a mirror diagram of (c)) and the vertex correction from one virtual gluon. These diagrams represent the tensor $\hat{W}_{\mu\nu}$ for an incoming quark, which will

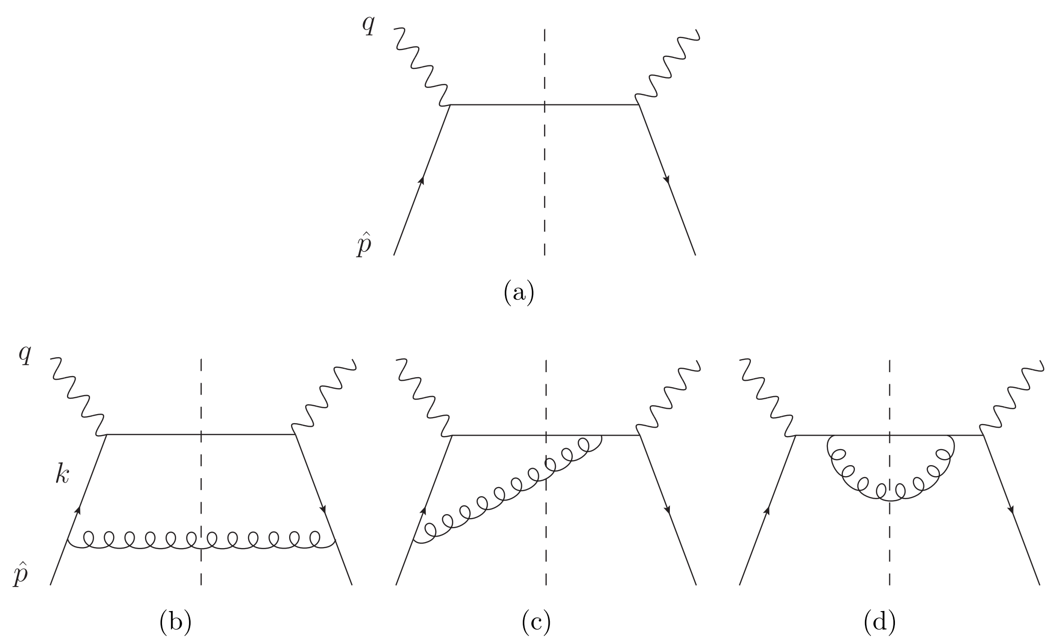

Figure 3.3. Parton level DIS diagrams at (a)the leading order, and (b)(c)(d)the next-to-leading order with one gluon emitted.

be used to obtain the structure functions. The parton level $\hat{W}_{\mu\nu}$ depends on Q and $z \equiv Q^2/(2\hat{p} \cdot q) = x/\xi$. The leading order result $z = 1$ becomes $z < 1$ with gluon emissions, which can be seen from that the invariant mass squared $(\hat{p} + q)^2$ is larger than 0.

We will perform the calculation using dimensional regularization [33], which preserves the gauge invariance, and does not complicate phase space integration. We use Feynman gauge, defined in Eq. (2.7) with $\zeta = 1$, which is normally simpler in calculations. To obtain the structure functions, simply compute the contractions in dimension $n = 4 - 2\epsilon$.

$$\frac{1}{4\pi e^2} g^{\mu\nu} \hat{W}_{\mu\nu} = -(3-2\epsilon)\hat{F}_1 + \hat{F}_2/2z = (3-2\epsilon)\hat{F}_L/2z - (1-\epsilon)\hat{F}_2/z, \tag{3.28}$$

$$\frac{1}{4\pi e^2} \hat{p}^\mu \hat{p}^\nu \hat{W}_{\mu\nu} = (\hat{\nu}/4z^2)(\hat{F}_2 - 2z\hat{F}_1) = (Q^2/8z^3)\hat{F}_L. \tag{3.29}$$

We first compute the contribution of the real gluon diagrams Fig. 3.3 (b),(c), and (d) to $g^{\mu\nu}\hat{W}_{\mu\nu}$. It is given by

$$g^{\mu\nu}\hat{W}^r_{\mu\nu} = \frac{e^2}{2}\int \frac{d^n l}{(2\pi)^{n-1}} \frac{d^n r}{(2\pi)^{n-1}} \overline{\sum} \left|\mathcal{M}(\gamma^*(q)q(\hat{p}) \to g(r)q(l))\right|^2_{\mu\nu} g^{\mu\nu}$$
$$\times\, \delta^+(l^2)\delta^+(r^2)(2\pi)^n \delta^n(\hat{p} + q - l - r), \tag{3.30}$$

where an average/sum over color is imposed. Using the Feynman rules for QCD, the squared and contracted matrix element can be expressed as the sum of four traces

$$\overline{\sum} |\mathcal{M}|^2_{\mu\nu} g^{\mu\nu} = -Q_q^2 \mu^{2\epsilon} g_s^2 C_F (\mathrm{Tr}\,[\hat{\not p}\gamma^\mu(\hat{\not p} + \not q)\gamma^\nu \not l \gamma_\nu(\hat{\not p} + \not q)\gamma_\mu]/(\hat{p}+q)^4$$
$$+ \mathrm{Tr}\,[\hat{\not p}\gamma^\mu(\hat{\not p} + \not q)\gamma^\nu \not l \gamma_\mu(\hat{\not p} - \not r)\gamma_\nu]/(\hat{p}+q)^2(\hat{p}-r)^2$$
$$+ \mathrm{Tr}\,[\hat{\not p}\gamma^\nu(\hat{\not p} - \not r)\gamma^\mu \not l \gamma_\nu(\hat{\not p} + \not q)\gamma_\mu]/(\hat{p}-r)^2(\hat{p}+q)^2$$
$$+ \mathrm{Tr}\,[\hat{\not p}\gamma^\nu(\hat{\not p} - \not r)\gamma^\mu \not l \gamma_\mu(\hat{\not p} - \not r)\gamma_\nu]/(\hat{p}-r)^4), \tag{3.31}$$

where the overall minus sign is from using $-g^{\mu\nu}$ for the gluon polarization sum in Feynman gauge. The color factor is $\frac{1}{3}\sum_a \mathrm{Tr}\,[t^a t^a] = C_F$. The traces can be evaluated with, for instance, *FeynCalc* [34], to give

$$\overline{\sum} |\mathcal{M}|^2_{\mu\nu} g^{\mu\nu} = -8Q_q^2 \mu^{2\epsilon} g_s^2 C_F (1-\epsilon)\left[(\epsilon - 1)\left(\frac{\hat{t}}{\hat{s}} + \frac{\hat{s}}{\hat{t}}\right) + \frac{2Q^2\hat{u}}{\hat{t}\hat{s}} + 2\epsilon\right], \tag{3.32}$$

where the sum over all quark flavors q is implicit. The Mandelstam variables are defined as usual: $\hat{s} = (\hat{p}+q)^2$, $\hat{t} = (\hat{p}-r)^2$, and $\hat{u} = (\hat{p}-l)^2$. The phase space of Eq. (3.30) can be simplified by integrating over l and r^0

$$g^{\mu\nu}\hat{W}^r_{\mu\nu} = \frac{e^2}{2}\frac{1}{(2\pi)^{n-2}}\int \frac{d^{n-1}r}{2r}\overline{\sum}\left|\mathcal{M}(\gamma^*(q)q(\hat{p}) \to g(r)q(\hat{p}+q-r))\right|^2_{\mu\nu} g^{\mu\nu} \\ \times \delta^+((\hat{p}+q-r)^2). \tag{3.33}$$

where for simplicity r denotes both the n-vector and the magnitude of the corresponding spatial $(n-1)$-vector, which can be distinguished by context. Integration over space components of r can be done using spherical coordinates in n dimensional space:

$$\int \mathrm{d}^{n-1}r = \int_0^\infty \mathrm{d}r r^{n-2}\int \mathrm{d}\Omega_{n-2} = \int_0^\infty \mathrm{d}r r^{n-2} \times \frac{2(\pi)^{(n-2)/2}}{\Gamma((n-2)/2)}\int_0^\pi d\theta \sin^{n-3}\theta. \tag{3.34}$$

The integral in Eq. (3.30) is Lorentz invariant, hence can be done in any frame. A convenient choice is the center-of-mass frame of the initial quark and photon. If we choose the last spatial axis along the direction of the incoming quark, then θ becomes the polar angle between the initial quark and gluon. Let $y = \cos\theta$, then in this frame it is straightforward to show that

$$\hat{p}^0 = \frac{Q}{2}\sqrt{\frac{1}{z(1-z)}}, \tag{3.35}$$

$$r^0 = \frac{Q}{2}\sqrt{\frac{1-z}{z}}, \tag{3.36}$$

$$\hat{s} = Q^2\frac{1-z}{z}, \tag{3.37}$$

$$\hat{t} = -Q^2\frac{1-y}{2z}, \tag{3.38}$$

$$\hat{u} = -Q^2\frac{1+y}{2z}. \tag{3.39}$$

Integrating over r will eliminate the remaining delta function

$$\begin{aligned}
&\int_0^\infty dr r^{1-2\epsilon}\delta((\hat{p}+q)^2 - 2(\hat{p}+q)\cdot r) \\
&= \int_0^\infty dr r^{1-2\epsilon}\delta(s - 2\sqrt{s}\, r) \\
&= 2^{-(2-2\epsilon)} s^{-\epsilon}.
\end{aligned} \tag{3.40}$$

After changing the integration variable from θ to y, Eq. (3.33) becomes

$$g^{\mu\nu}\hat{W}^r_{\mu\nu} = -\frac{1}{4} C_F g_s^2 e^2 Q_q^2 \mu^{2\epsilon} 2^{4\epsilon} \pi^{-(1-\epsilon)} \frac{1}{\Gamma(1-\epsilon)} \left(\frac{Q^2(1-z)}{z}\right)^{-\epsilon}$$
$$\times \int_{-1}^1 dy (1-y^2)^{-\epsilon} \times (1-\epsilon) \left[(1-\epsilon)\left(\frac{1-y}{2(1-z)} + \frac{2(1-z)}{1-y}\right) + \frac{2z(1+y)}{(1-z)(1-y)} + 2\epsilon\right]. \tag{3.41}$$

Using the relation

$$\int_{-1}^1 dy (1+y)^A (1-y)^B = 2^{A+B+1} \frac{\Gamma(A+1)\Gamma(B+1)}{\Gamma(A+B+2)} \tag{3.42}$$

to evaluate the y integral, we obtain

$$g^{\mu\nu}\hat{W}^r_{\mu\nu} = -\frac{1}{4} C_F g_s^2 e^2 Q_q^2 2^{2\epsilon} \pi^{-(1-\epsilon)} \left(\frac{Q^2}{\mu^2}\right)^{-\epsilon} \frac{\Gamma(1-\epsilon)}{\Gamma(1-2\epsilon)} (1-\epsilon)$$
$$\times \frac{z^\epsilon}{(1-z)^{1+\epsilon}} \left[\frac{1-\epsilon}{1-2\epsilon} - \frac{2(1-\epsilon)(1-z)^2}{\epsilon} - \frac{4z(1-\epsilon)}{\epsilon(1-2\epsilon)} + \frac{4\epsilon(1-z)}{1-2\epsilon}\right], \tag{3.43}$$

where the $1/\epsilon$ pole is produced by the y integral in Eq. (3.41) near $y = 1$. It corresponds to the collinear configuration of the gluon and initial quark. The Born level contribution in Fig. 3.3 (a) is also corrected by virtual gluon processes at $O(\alpha_s)$. To obtain an inclusive cross section where all hadronic final states are summed over, virtual gluon contribution must be included as well.

Diagrams with virtual gluons are shown in Fig. 3.4. Contribution from these diagrams (including their mirror diagrams), as well as the corresponding counter terms, constitutes the virtual gluon correction at 1 loop level. The requirement of gauge invariance ensures that renormalization constants for the QED vertex satisfy the relation

$$Z_1 = Z_\psi. \tag{3.44}$$

Therefore the counter terms will cancel each other. It turns out that the quark self

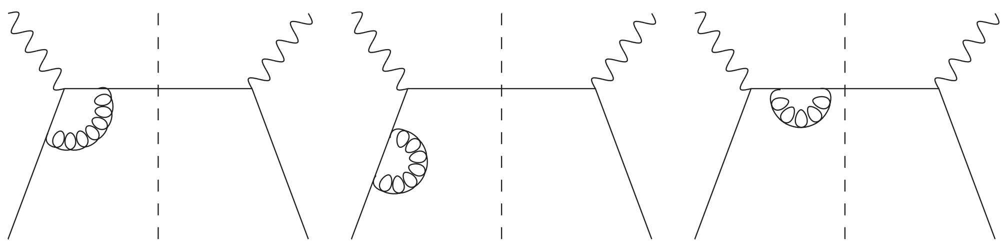

(a) (b) (c)

Figure 3.4. Virtual gluon diagrams:(a)the vertex correction, and (b)(c):quark self energy.

energy diagram also vanishes in zero quark mass limit for on-shell momenta $\hat{p} = 0$ or $l^2 = 0$, which is discussed in detail in [2] and will be skipped here. We are left with the vertex correction Fig. 3.4 (a) to calculate. In this case the contraction is

$$\begin{aligned}
g^{\mu\nu}\hat{W}^{v}_{\mu\nu} &= \frac{e^2}{2}Q_q^2\mu^{2\epsilon}g_s^2 C_F \times 2Re[\int d^n r \,\mathrm{Tr}\,[\not{\hat{p}}\gamma^\sigma(\not{\hat{p}} - \not{r})\gamma^\mu(\not{l} - \not{r})\gamma_\sigma \not{l}\gamma_\mu] \\
&\times \frac{i}{r^2(\hat{p}-r)^2)(l-r)^2}(2\pi)^{-n+1}\delta((\hat{p}+q)^2)] \\
&= \frac{e^2}{2}Q_q^2\mu^{2\epsilon}g_s^2 C_F \times (2\pi)^{-n+1}\delta((\hat{p}+q)^2) \times 8(\epsilon - 1) \times 2Re\left(\int d^n r \frac{(-i)N(\hat{p},q,r,l)}{r^2(\hat{p}-r)^2(l-r)^2}\right),
\end{aligned} \tag{3.45}$$

where an imaginary part $i\epsilon$ is omitted in each factor of the denominator. The factor $N(\hat{p}, q, r, l)$ is

$$N(\hat{p}, q, r, l) = \epsilon q^2 r^2 + 4\hat{p}\cdot r l \cdot r + 2q^2(\hat{p}\cdot r + l \cdot r) + q^4. \tag{3.46}$$

Using Feynman parameters to combine the denominators, the integral inside brackets is rewritten as

$$I = \int_0^1 dx_1 \int_0^{1-x_1} dx_2 \int d^n r \frac{(-2i)N(\hat{p}, q, r, l)}{(r^2 - 2x_1\hat{p}\cdot r - 2x_2 l\cdot r)^3}. \tag{3.47}$$

Make the substitution

$$r_\mu r_\nu \to \frac{1}{n} r^2 g_{\mu\nu}, \tag{3.48}$$

and we can express the integral using Gamma functions

$$\begin{aligned} I &= -Q^{2-2\epsilon}\pi^{2-\epsilon}\frac{\Gamma^2(1-\epsilon)\Gamma(1+\epsilon)}{\Gamma(1-2\epsilon)}\left(\frac{1}{\epsilon^2} + \frac{3+\epsilon}{2(1-2\epsilon)}\frac{1}{\epsilon} + \frac{1}{2(1-2\epsilon)}\right) \\ &= -Q^{2-2\epsilon}\pi^{2-\epsilon}\frac{\Gamma^2(1-\epsilon)\Gamma(1+\epsilon)}{\Gamma(1-2\epsilon)}\left(\frac{1}{\epsilon^2} + \frac{3}{2}\frac{1}{\epsilon} + 4\right), \end{aligned} \tag{3.49}$$

where in the second line the $O(\epsilon)$ term is omitted. The ultra-violet pole $1/\epsilon$ is analytically continued from $\epsilon > 0$ to $\epsilon < 0$ to give an infrared pole. Thus the virtual gluon contribution in Eq. (3.45) is found to be

$$\begin{aligned} g^{\mu\nu}\hat{W}^v_{\mu\nu} &= e^2 Q_q^2 \mu^{2\epsilon} g_s^2 C_F \pi^{\epsilon-1} Q^{-2\epsilon} 2^{2\epsilon}(1-\epsilon) \\ &\times \frac{\Gamma^2(1-\epsilon)\Gamma(1+\epsilon)}{\Gamma(1-2\epsilon)}\left(\frac{1}{\epsilon^2} + \frac{3}{2}\frac{1}{\epsilon} + 4\right)\delta(1-z) \end{aligned} \tag{3.50}$$

At this point if we add the contractions in Eq. (3.43) and Eq. (3.50) together, the infrared poles will not cancel manifestly. The way to proceed is to interpret the RHS of Eq. (3.43) as a distribution in the limit $\epsilon \to 0$. This is achieved by making the substitution [1]

$$\frac{z^\epsilon}{(1-z)^{1+\epsilon}} = -\frac{\delta(1-z)}{\epsilon} + \frac{1}{(1-z)_+} + \epsilon\left[\frac{\ln z}{1-z} - \left(\frac{\ln(1-z)}{1-z}\right)_+\right] + O(\epsilon^2), \tag{3.51}$$

where the "plus" functions are defined to remove the divergence produced by the integral of $1/(1-z)$ near $z = 1$:

$$\int_x^1 dz\, f(z)_+ g(z) \equiv \int_x^1 dz\, f(z)g(z) - \int_0^1 dz\, f(z)g(1). \tag{3.52}$$

Since the leading term of the RHS of Eq. (3.51) is proportional to $1/\epsilon$, we expand the terms in the square brackets of Eq. (3.43) to $O(\epsilon)$ and obtain

$$\begin{aligned}
g^{\mu\nu}\hat{W}^r_{\mu\nu} &= -\frac{1}{4}C_F g_s^2 e^2 Q_q^2 2^{2\epsilon}\pi^{-(1-\epsilon)}\left(\frac{Q^2}{\mu^2}\right)^{-\epsilon}\frac{\Gamma(1-\epsilon)}{\Gamma(1-2\epsilon)}(1-\epsilon) \\
&\times \frac{z^\epsilon}{(1-z)^{1+\epsilon}}\left[\frac{-2(z^2+1)}{\epsilon}+2z^2-8z+3+\epsilon(5-12z)\right] \\
&= C_F g_s^2 e^2 Q_q^2 2^{2\epsilon}\pi^{-(1-\epsilon)}\left(\frac{Q^2}{\mu^2}\right)^{-\epsilon}\frac{\Gamma(1-\epsilon)}{\Gamma(1-2\epsilon)}(1-\epsilon) \\
&\times \left[-\delta(1-z)\left(\frac{1}{\epsilon^2}+\frac{3}{4\epsilon}+\frac{7}{4}\right)+\frac{z^2+1}{2(1-z)_+}\frac{1}{\epsilon}-\frac{3}{2}+\frac{z}{2}\right. \\
&\left. +\frac{3}{4(1-z)_+}+\frac{(z^2+1)\ln z}{2(1-z)}-\frac{z^2+1}{2}\left(\frac{\ln(1-z)}{1-z}\right)_+\right].
\end{aligned} \tag{3.53}$$

The sum of real and virtual corrections at NLO then gives

$$\begin{aligned}
g^{\mu\nu}\hat{W}_{\mu\nu} &= \frac{1}{2\pi}C_F g_s^2 e^2 Q_q^2\Bigg[\frac{3}{2(1-z)_+}+\frac{(z^2+1)\ln z}{1-z} \\
&-(z^2+1)\left(\frac{\ln(1-z)}{1-z}\right)_+ +\left(\frac{9}{2}+\frac{\pi^2}{3}\right)\delta(1-z)+z-3 \\
&+\frac{1}{2C_F}P_{qq}^{(0)}(z)\left(\frac{1}{\epsilon}-\ln\left(\frac{Q^2}{4\pi\mu^2}\right)-\gamma_E-1\right)\Bigg],
\end{aligned} \tag{3.54}$$

where the leading order quark-to-quark splitting function $P_{qq}^{(0)}$ is identified as

$$P_{qq}^{(0)}(z) = C_F\left(\frac{2(z^2+1)}{(1-z)_+}+3\delta(1-z)\right). \tag{3.55}$$

The normalization of $P_{qq}^{(0)}$ has an extra factor of 2 in accordance with the convention in [35, 36].

The evaluation of $\hat{p}^\mu\hat{p}^\nu\hat{W}_{\mu\nu}$ is much simpler. Among the real and virtual gluon diagrams only Fig. 3.3 (b) contributes while the others vanish due to the appearance of $\hat{\not{p}}\hat{\not{p}} = \hat{p}^2 = 0$ in their traces. Thus

$$\begin{aligned}
\hat{p}^\mu\hat{p}^\nu\hat{W}_{\mu\nu} &= -\frac{1}{2}e^2 Q_q^2\mu^{2\epsilon}g_s^2 C_F\frac{1}{(2\pi)^{n-2}}\int\frac{d^{n-1}r}{2r}\,\mathrm{Tr}\,[\hat{\not{p}}\gamma^\nu(\hat{\not{p}}-\not{r})\hat{\not{p}}\not{p}\hat{\not{p}}(\hat{\not{p}}-\not{r})\gamma_\nu]/(\hat{p}-r)^4 \\
&\times \delta^+((\hat{p}+q-r)^2)
\end{aligned}$$

$$
\begin{aligned}
&= \frac{1}{16} C_F g_s^2 e^2 Q_q^2 Q^2 \mu^{2\epsilon} 2^{4\epsilon} \pi^{-(1-\epsilon)} \frac{1-\epsilon}{\Gamma(1-\epsilon)} \left(\frac{Q^2(1-z)}{z}\right)^{-\epsilon} \int_{-1}^{1} dy (1-y^2)^{-\epsilon} \frac{y+1}{z} \\
&= \frac{1}{8\pi z} C_F g_s^2 e^2 Q_q^2 Q^2. \qquad (3.56)
\end{aligned}
$$

The structure functions can be obtained using Eqs. (3.28),(3.29):

$$
\begin{aligned}
\hat{F_2}^{(1)} &= -\frac{\alpha_s}{2\pi} C_F Q_q^2 z \Bigg[\frac{3}{2(1-z)_+} + \frac{(z^2+1)\ln z}{1-z} \\
&- (z^2+1)\left(\frac{\ln(1-z)}{1-z}\right)_+ + \left(\frac{9}{2} + \frac{\pi^2}{3}\right)\delta(1-z) - 2z - 3 \\
&+ \frac{1}{2C_F} P_{qq}^{(0)}(z) \left(\frac{1}{\epsilon} - \ln\left(\frac{Q^2}{4\pi\mu^2}\right) - \gamma_E\right)\Bigg], \qquad (3.57) \\
\hat{F_L}^{(1)} &= \frac{\alpha_s}{\pi} C_F Q_q^2 z^2. \qquad (3.58)
\end{aligned}
$$

Comparing with the leading-order result Eqs. (3.24), (3.25), a prominent difference is the appearance of a logarithmic Q dependence at NLO in Eq. (3.57), which breaks Bjorken scaling. Moreover, a divergent term (proportional to $1/\epsilon$) due to the collinear emission of a gluon remains in $\hat{F_2}^{(1)}$. The next subsection will show how this divergence is treated in order to give a physical cross section. On the other hand, $\hat{F_L}^{(1)}$ is non-zero but finite at this order. A similar calculation can be carried out for an incoming gluon scattering on the photon (through exchange of a quark). In this case, the collinear splitting of a gluon into a quark pair can be described by the function

$$
P_{qg}^{(0)}(z) = 2T_R(2z^2 - 2z + 1). \qquad (3.59)
$$

3.4. Factorization in DIS

We have seen in the previous sections how to isolate the perturbative part of a DIS cross section and ascribe the detailed information of long distance interaction within a hadron to parton distribution functions. However, the validity of separation between long and short distance interactions has not been justified. For instance, we assumed that the photon interacts with only one incoming parton with its momentum on shell, which is far from obvious. This can be done by a careful analysis of the structure of the S matrix. See for example Ch.13 in [2], where for each diagram, one can isolate the regions of momenta of the particles that give the leading contribution. These regions are called leading regions. It follows from the analysis that the leading regions for DIS process have a typical topology illustrated by the cut-vertex graph in Fig. 3.5[2]. The lower bubble (along with the lines connecting the two bubbles)

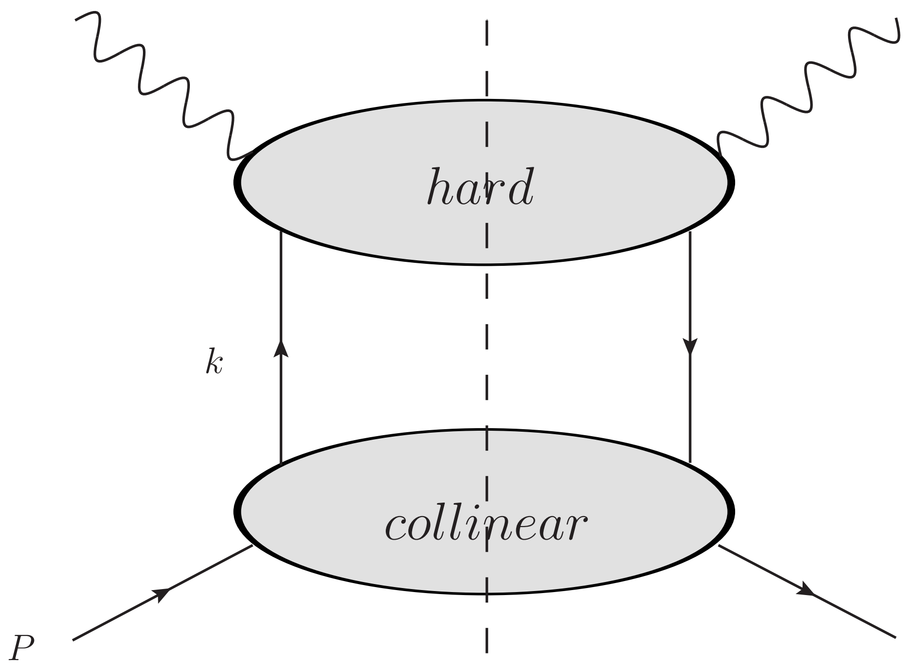

Figure 3.5. Leading regions of deep inelastic scattering.

contains momenta collinear to the incoming proton with low virtuality. The upper bubble represents the hard scattering process in which the virtuality of the particles are of order Q. The hard and collinear regions are connected by one parton line on

[2]Complications with the analysis of DIS leading regions in a gauge theory such as QCD are discussed in detail in [1].

either side of the final-state momentum cut.

To see how factorization of the cross section emerges from quantum field theory, we need a concrete definition for the parton distribution functions. The contribution from the leading-region graph involves integration over the internal momentum k of the intermediate parton connecting the hard and collinear subgraphs. It can be shown that the "small components" k^-, and $\mathbf{k}_T$ can be set to zero with negligible error introduced, where the light-cone coordinates are related to the usual 4-vector notation as

$$\left(V^+, V^-, \mathbf{V_T}\right) \equiv \left(\frac{V^0 + V^3}{\sqrt{2}}, \frac{V^0 - V^3}{\sqrt{2}}, \mathbf{V_T}\right). \tag{3.60}$$

The parton distribution functions are then obtained by integrating the lower part of the graph over these components and picking out the large contribution using γ^+. In light-cone gauge, the quark distribution is defined as

$$f_{q/h}(\zeta) \equiv \int \frac{dy^-}{2\pi} e^{-\zeta p_h^+ y^-} \langle p_h | \bar{\psi}(0, y^-, \mathbf{0}_T) \gamma^+ \psi(0) | p_h \rangle, \tag{3.61}$$

where p_h denotes the momentum of a hadron or a parton. The gluon PDF can be similarly defined.

With this definition, assuming the only important contribution is from the leading region in Fig. 3.5, the DIS structure functions can be written in a factorized form as a convolution of PDFs and hard scattering coefficients

$$F_2(x, Q) = \sum_i \int_x^1 d\zeta C_{2,i}\left(x/\zeta, Q^2/\mu^2, \alpha_s(\mu^2)\right) f_{i/h}(\zeta) + O(m^2/Q^2) \tag{3.62}$$

where the sum is over all parton flavors. m represents the highest virtuality in the collinear part, which is much smaller compared to Q. The long distance information is now all contained in the PDFs, and the coefficients C are infrared safe.

The picture of factorization represented by Fig. 3.5 is not strictly correct for a QCD DIS process. In fact, Fig. 3.5 requires that there is a clear distinction between the virtualities from the two parts of a graph. However, it can be shown that contribution from the intermediate region, e.g. $m^2 \ll k^2 \ll Q^2$, is not power suppressed and thus not negligible. Nevertheless, one can rescue the proof of factorization by reorganizing the structure functions to properly isolate a power-suppressed part [1]. (see also [37]).

In a physical process, k^- and $\mathbf{k}_T$ are constrained by the kinematics of the photon-parton collision. Factorization has removed the constraints on these components. As a consequence, the parton distribution functions need to be renormalized in order to get rid of ultra-violet divergences induced by integration over a region with large transverse momentum. The PDFs obtained through this procedure will depend on a new scale μ_F introduced during renormalization. In practice it is usually convenient to set $\mu_F = \mu_R = Q$, where the renormalization scale $\mu_R \equiv \sqrt{4\pi e^{-\gamma_E}}\mu$. Otherwise perturbation series will contain powers of logarithms of the form $\ln^n(\mu_F/Q)$, or $\ln^n(\mu_R/Q)$, which break down the convergence of calculation. From now on, we use the single notation μ to denote μ_F and μ_R. Now the factorization formula Eq. (3.62) is modified by adding the μ dependence to the PDF part.

A one-loop calculation, using the definition Eq. (3.61) along with an $\overline{MS}$ counter term for renormalization, gives the quark-in-quark distribution [1, 2]

$$f_{q/q}(\zeta, \mu) = \delta(1-\zeta) + \frac{\alpha_S}{4\pi}\frac{S_\epsilon}{(-\epsilon)}P_{qq}^{(0)}(\zeta) + O(\alpha_s^2), \tag{3.63}$$

where $S_\epsilon \equiv 1 + \epsilon(\ln 4\pi - \gamma_E) + O(\epsilon^2)$. The μ dependence is only through α_s. A comparison of the zero order terms on both sides of Eq. (3.62) for a quark target then gives (see Eq. (3.24))

$$C_{2,q}^{(0)}\left(\frac{z}{\zeta}\right) = Q_q^2\delta(1-\frac{z}{\zeta}). \tag{3.64}$$

$C^{(1)}_{2,q}$ is similarly obtained by comparing the first-order terms using Eq. (3.57):

$$C^{(1)}_{2,q}\left(\frac{z}{\zeta},\mu\right) = -\frac{\alpha_s}{2\pi}C_F Q_q^2 z\Bigg[\frac{3}{2(1-z)_+} + \frac{(z^2+1)\ln z}{1-z}$$
$$-(z^2+1)\left(\frac{\ln(1-z)}{1-z}\right)_+ + \left(\frac{9}{2}+\frac{\pi^2}{3}\right)\delta(1-z) - 2z - 3$$
$$-\frac{1}{2C_F}P^{(0)}_{qq}(z)\ln\left(\frac{Q^2}{\mu^2}\right)\Bigg]. \tag{3.65}$$

3.5. Evolution of the PDFs

In reality, the more interesting parton distributions are those in hadrons, rather than partons, since a parton target is not directly probed by the experiments. The partons' momentum distributions in a hadron state are not calculable as is done for the parton-in-parton case, Eq. (3.63), since a hadron state contains long distance interaction between the partons. The corresponding momentum scale results in a strong coupling constant too large for perturbative method to reliably apply. Nonperturbative methods for calculating PDFs have been developed, but so far none is able to reach an accuracy comparable to the experiments. Instead, the nonperturbative PDFs can be determined from experimental data, by knowing that hadron-level cross sections depend on the same infrared-safe coefficient functions that were found from a parton-level calculation in Sec. 3.4. A cross section with a hard momentum scale can be factorized not only in DIS. Similar factorization theorems have been proved for various processes in which the form of the PDFs is universal. An important test of these factorization theorems is to extract the values of PDFs from one process and apply them to others and compare the agreement with the measured cross sections. This is essentially what is done for a global analysis of PDFs by groups such as the CTEQ Collaboration.

One can even go one step further about these PDFs. Just like for the renormalized strong coupling constant, one can derive a renormalization group equation to describe the μ dependence of $f_{i/h}(\zeta,\mu)$, despite that the value of $f_{i/h}(\zeta,\mu)$ at a fixed scale has to be taken from experiment. It is readily proved [1, 37] that the renormalization of the PDFs is carried out by introducing renormalization constants Z_{ij} in the form

$$f_{i/h}(\zeta,\mu) = \sum_j \int_\zeta^1 \frac{dy}{y} Z_{ij}(y,\mu) f_{0j/h}(\frac{\zeta}{y}), \tag{3.66}$$

where $f_{0j/h}$ is expressed by a matrix element such as that in Eq. (3.61), with the field operators being bare fields. This form of the renormalized PDFs ensures that all ultraviolet divergences arising from large transverse momentum integrals are cancelled order by order by the renormalization constants Z_{ij}. The bare parton densities are independent of μ, so that differentiating both sides of the above equation with respect to $\ln\mu$ gives

$$\frac{d}{d\ln\mu} f_{i/h}(\zeta,\mu) = 2\sum_j \int_\zeta^1 \frac{dy}{y} P_{ij}(y) f_{j/h}(\frac{\zeta}{y},\mu), \tag{3.67}$$

where

$$\frac{d}{d\ln\mu} Z_{ij}(y,\mu) = 2\sum_k \int_y^1 \frac{dy'}{y'} P_{ik}(y') Z_{kj}(\frac{y}{y'},\mu). \tag{3.68}$$

Eqs. (3.67) are referred to as the Dokshitzer-Gribov-Lipatov-Altarelli-Parisi (DGLAP) equations [38–41]. They govern the evolution of PDFs with respect to the momentum scale μ. With the help of computer programs, the equations can be solved numerically to the desired accuracy. The evolution kernels P_{ij} that appear in the convolution can be calculated perturbatively as an expansion

$$P_{ij} = P_{ij}^{(0)} + \frac{\alpha_s}{4\pi} P_{ij}^{(1)} + \ldots, \tag{3.69}$$

with the leading order quark-to-quark term given by Eq. (3.55).

Chapter 4

DIS with massive quark production

The calculation of DIS structure functions in the last chapter has assumed that all quark flavors are massless. At NLO we have already seen that collinear singularities associated with varnishing masses of quarks are encountered inevitably. Singularities due to radiation of soft gluons are cancelled between contributions from real and virtual gluon processes. Collinear singularities due to zero mass quarks are ascribed to the internal structure of the target. However, in reality treating all quark flavors as massless is not a good approximation, if at least one quark type has mass comparable to the hard scale Q. In this case, more complicated factorization prescriptions are needed for making accurate predictions. In particular, the previously used "zero-mass" $\overline{MS}$ scheme must be replaced by one that specifies the allocation of not only the divergent terms but also of those with heavy quark mass dependence. It is possible, and even desirable, to allow the allocation of terms to differ at various hard scales, which is reminiscent of the treatment in evolving the strong coupling with various quark flavors discussed in the first chapter. In this chapter we treat the factorization of DIS in a particular scheme, in which we present a method to properly distribute the heavy quark mass dependence at different momentum regions. For this purpose we first review how massive quarks are treated in various factorization schemes.

4.1. Factorization with massive quarks

There are various factorization schemes that retain the heavy quark mass dependence. Among these the fixed flavor-number (FFN) scheme is often adopted when

Q is near the heavy quark threshold [42–47]. Analysis of the leading-power contribution indicates that near the production threshold the leading region contains only light parton lines connecting the hard and collinear parts in a factorized structure function. Therefore FFN scheme keeps all m_h dependence in hard scattering coefficient functions with incoming light partons. The heavy quark is never an active flavor as part of the hadron structure. This scheme gives the dominant contribution near the threshold. The problem with it is at $Q \gg m_h$. A fixed order calculation of light parton initiated processes contains terms proportional to $\ln^n\left(\frac{m_h^2}{Q^2}\right)$. These large logarithms need to be summed to all orders into a heavy parton PDF by DGLAP equations, otherwise the convergence of the perturbation series is ruined.

The sum of the large logarithms through all orders is done in a class of schemes named variable flavor number (VFN) schemes, in which heavy quark PDFs are introduced to sum the log terms as the quark mass threshold is crossed, i.e., a heavy quark is treated as an active flavor above its threshold [48]. Schemes of this class can have different treatment of the heavy quark masses for the light parton initiated process near the thresholds. If the heavy quark masses are dropped completely, the scheme has the name (VFN-) zero-mass (ZM) scheme [49–51]. ZM scheme is reliable when $Q \gg m_h$. Proof of the factorization at this region [37] suggests that the corrections to the factorized cross section have the power suppressed form $(m_h/Q)^p$, where p is a positive number. The corrections can be neglected at large Q. However, setting m_h to zero is no longer valid near the threshold since the error becomes substantial. An illustration of treating the charm quark mass in ZM and FFN schemes at NLO is given by Fig. 4.1, where it is shown that in their respective unreliable regions, both schemes cannot hold to the NLO accuracy.

Because of the above deficiency, recent calculations are usually done in an advanced VFN schemes that keep the mass dependence in hard scattering cross sections

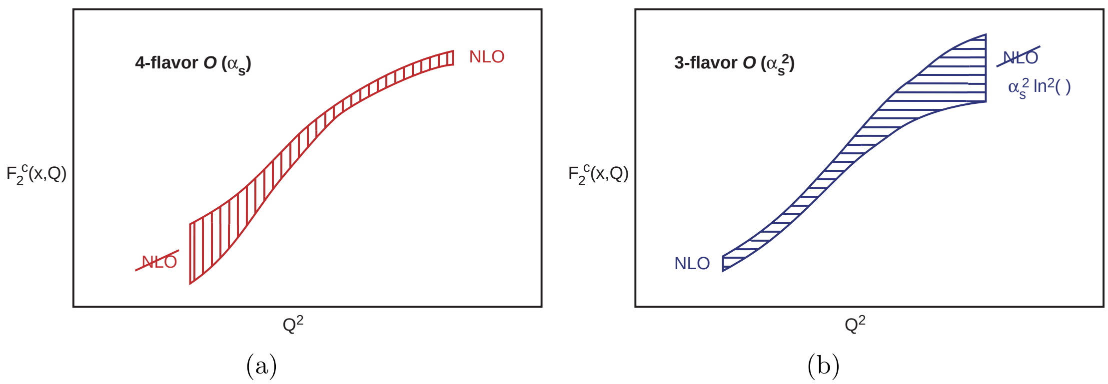

Figure 4.1. From [52]:(a) ZM and (b) FFN treatment of the charm quark mass at NLO.

near the threshold, but turn on heavy-quark PDFs as Q becomes larger. These are so called (VFN-) general mass (GM) schemes [37, 53–60]. They appropriately include the mass effects at both small and large Q, and thus are generally more reliable for performing calculations with heavy quark productions.

The realization of a typical VFN calculation relies on the interplay of three classes of contributions [52]. In literature, the process of heavy quark-photon scattering initiated by a light parton contributes a term in the structure functions which is referred to as the flavor creation (FC) term. A term from heavy quark initiated scattering is called the flavor excitation (FE) term. There is an overlap between the above two since the heavy quark PDF receives contribution from the collinear radiation of the heavy quarks from light partons. This overlapped term is often called the subtraction term since it must be subtracted from the above two terms to avoid double counting. A typical calculation in VFN scheme is realized by including all these terms. Near the threshold region the heavy flavor is mainly produced via $\gamma^* g$ fusion. The contribution from the FE term is canceled by the subtraction term up to high order splitting contribution, which are suppressed at low energy. The cross section is thus sensitive to the mass dependence of the FC term. In contrast, at large Q, the leading contribution of the FC term is from the collinear quark radiation, which is canceled by the subtraction term. The FE term becomes dominant.

The interplay between the above terms at low and high scales is suggestive of the fact that factorization at various regions is done differently for a multiscale process. In a general proof of factorization near the heavy-quark threshold [37], there should be no heavy-quark line connecting the target part and the hard scattering part of a diagram. On the other hand, one has to put in FE contributions in order to obtain a smooth transition to a large Q value, where summation of all order logarithms is needed. As a result, the numerical accuracy at the threshold region relies on the cancellation between FE and the subtraction terms.

In our study we work mainly in a family of schemes founded by Aivazis, Collins, Olness, and Tung (ACOT) [53, 61]. We shall use a scheme called S-ACOT-χ [52, 60]. This is a GM scheme that retains heavy quark mass dependence from the FC contribution. Furthermore, it imposes a "χ" prescription to the approximate FE and subtraction contributions, which amounts to including a mass-dependent correction to integration over the momentum fraction ξ, but neglecting all other mass-dependent terms in the FE coefficient functions. It serves to speed up the cancellation between these two terms near the threshold and to achieve fast convergence. The details of "χ" prescription will be discussed in Sec.4.3.2. So far calculation in S-ACOT-χ scheme have been carried out to NNLO in [62]. There the scheme has shown significant advantage over non-GM schemes.

Meanwhile, the $O(\alpha_s^3)$ correction to DIS coefficient functions have been computed in the zero-mass approximation [63,64]. To promote S-ACOT-χ calculation to N3LO, we need $O(\alpha_s^3)$ massive coefficients, particularly for FC terms. Nonetheless, we can

Factorization schemes	Mass dependence from coefficients	Mass dependence from phase space	Introduce heavy quark PDFs at large Q
FFN	yes	yes	no
ZM	no	no	yes
IM	no	yes	yes
GM	yes	yes	yes

Table 4.1. Properties of various factorization schemes.

account for some mass effects by adopting an intermediate mass (IM) scheme [65], where we use the ZM coefficients for all terms and impose the phase space correction as we do in GM scheme. In Table 4.1 I summarize the properties of the above schemes. Note that heavy quark coefficient functions for light initial partons have been computed to $O(\alpha_s^2)$ in [46,55,66–70]. These results are already used in [62] for a GM calculation. In our work we will use their GM results at $O(\alpha_s^2)$ for a benchmark comparison since they have been proved to be reliable.

In the remainder of this chapter, I present a method to organize DIS structure functions at N3LO according to the flavors of contributing quarks. What we will pursue here is to implement the heavy-quark mass dependence due to the phase space correction to various contributions at the 3-loop level. There are two purposes for this study. First, we wish to classify the DIS structure functions in a useful way that can be applied to both IM scheme and GM scheme at N3LO. Second, at present we are able to obtain numerical results in IM scheme. This will give an estimate on how important the missing mass dependence from coefficient functions are.

We do this in the following sequence: in Sec. 4.2.1, 4.2.2, and 4.2.3 we derive the form of structure functions with full mass dependence; in Sec. 4.2.4 and 4.3.1

we reduce these expressions to ZM forms as all masses are neglected, and discuss how the ZM coefficients are to correspond to those given in the references above; in Sec. 4.3.2 we implement the mass dependence from phase space corrections to the ZM coefficients. To perform the calculation we take the mass dependent coefficients and convolve them with PDFs in the forms derived in Sec. 4.2.3.

4.2. Classification of DIS structure functions

Since kinematics are generally different for various contributing diagrams, it is important to classify all the diagrams before implementing the kinematic constraint. We decompose the structure functions according to the $SU(N_f)$ group structure of PDFs and coefficients. This decomposition is adopted by many calculations of coefficient functions. As will be discussed in Sec. 4.2.4, the zero-mass structure functions in this decomposition take a compact form. Also, the evolution equations of PDFs are decoupled in this decomposition. (see Sec. 4.4)

4.2.1. $SU(N_f)$ Structure

According to the factorization theorem, DIS structure functions can be decomposed as

$$F(x,Q) = \sum_{\substack{i=q,\bar{q} \\ a=g,q,\bar{q}}} \left[C_{i,a} \otimes \Phi_a\right], \tag{4.1}$$

where the momentum distribution of parton a is from a proton. While this decomposition is widely used, other ways of classifying DIS contributions are possible and in some cases useful. We first rewrite this formula by decomposing its quark component in another representation. In the following derivation we omit the convolution operator for simplicity. We will recover it in our final formulae. This can also be thought of as working in Mellin space. We focus on decomposing the quark contributions in

Eq. (4.1). With the help of $SU(N_f)$ generators we can expand both the PDFs and the coefficient functions as

$$\Phi_j = \sum_{\alpha=3,8,15...} \Phi_\alpha (t^\alpha)_{jj} + \Phi_S \hat{I}_{jj} \tag{4.2}$$

$$\sum_i C_{i,j} \equiv C_j = \sum_{\beta=3,8,15...} C_\beta (t^\beta)_{jj} + C_S \hat{I}_{jj} \tag{4.3}$$

where the sums over α and β run over all the diagonal generators of $SU(N_f)$ group (note the values that β takes in the sums of Eqs. (4.2) and (4.3)). t^α here are for $SU(N_f)$. They are not the same as the $SU(3)$ generators in Sec. 2.1. The index i here stands for all the final state indices. In fact we will find contribution from some particular scattering processes with 2 final state indices later. The coefficient of the expansions are given by

$$\Phi_\alpha = 2tr(\hat{\Phi} t^\alpha), \tag{4.4}$$

$$\Phi_S = \frac{1}{N_f} tr(\hat{\Phi}), \tag{4.5}$$

$$C_\beta = 2tr(\hat{C} t^\beta), \tag{4.6}$$

$$C_S = \frac{1}{N_f} tr(\hat{C}) \tag{4.7}$$

where $\hat{\Phi}$ (or $\hat{C}$) is a diagonal matrix with its diagonal element $\hat{\Phi}_{jj}$ being Φ_j (or $\hat{C}_{jj} = C_j$). Then the quark component becomes

$$\sum_{i,j} C_{i,j}\Phi_j = \sum_{\alpha,\beta,j} \Phi_\alpha C_\beta (t^\alpha)_{jj} (t^\beta)_{jj} + \sum_{\alpha,j} \Phi_\alpha C_S (t^\alpha)_{jj} \hat{I}_{jj}$$
$$+ \sum_{\beta,j} \Phi_S C_\beta \hat{I}_{jj} (t^\beta)_{jj} + \sum_j \Phi_S C_S \hat{I}_{jj} \hat{I}_{jj}. \tag{4.8}$$

Since the product of $SU(N_f)$ generators satisfies

$$t^a t^b = \frac{1}{2N_f}\delta_{ab} I_{N_f} + \frac{1}{2}\sum_{c=1}^{N_f^2-1} (if_{abc} + d_{abc}) t^c, \tag{4.9}$$

and for diagonal generators we have

$$\sum_j (t^\alpha)_{jj}(t^\beta)_{jj} = tr(t^\alpha t^\beta), \tag{4.10}$$

the first term of Eq. (4.8) becomes $\frac{1}{2}\sum\limits_\alpha C_\alpha \Phi_\alpha$. Similarly, the cross terms vanish and the last term becomes $N_f C_S \Phi_S$. Therefore we obtain a new decomposition

$$\begin{aligned} \sum_{i,j} C_{i,j}\Phi_j &= \frac{1}{2}\sum_\alpha C_\alpha \Phi_\alpha + N_f C_S \Phi_S, \\ &= \sum_\alpha tr(\hat{C} t^\alpha)\Phi_\alpha + tr(\hat{C})\Phi_S. \end{aligned} \tag{4.11}$$

So to project out the non-singlet contributions one should take the flavor trace of the coefficient matrix with the diagonal generators, and to project out the singlet contributions one should take the trace with unit matrix.

4.2.2. Further classification

To distinguish contributions from different quark flavors, which will generally depend on masses of the quarks, we need to further classify Feynman diagrams of different topologies. In [64, 71], this classification is done according to the flavor structures of Feynman graphs. Depending on the configuration of the quark line/loop to which the photons are attached, the diagrams at three-loop level can belong to one of the five classes. Fig. 4.2 shows representative diagrams of each class, in which the FC_{11} and FC_{11}^g classes are present for the first time at this order. Even more delicate classification is needed when there is different mass dependence between various diagrams within a same flavor class. Due to these considerations, Eq. (4.11) is generalized to

$$\sum_{i,a} C_{i,a}\Phi_a = \sum_{FC,T}\left(\sum_\alpha tr(\hat{C}^{FC,T} t^\alpha)\Phi_\alpha + tr(\hat{C}^{FC,T})\Phi_S + C_g^{FC,T}\Phi_g\right), \tag{4.12}$$

where summation proceeds over various flavor classes, denoted as FC, as well as over contributions with different mass dependence within each given flavor class, indicated by T. The gluon contribution is included, too, to make the expression complete.

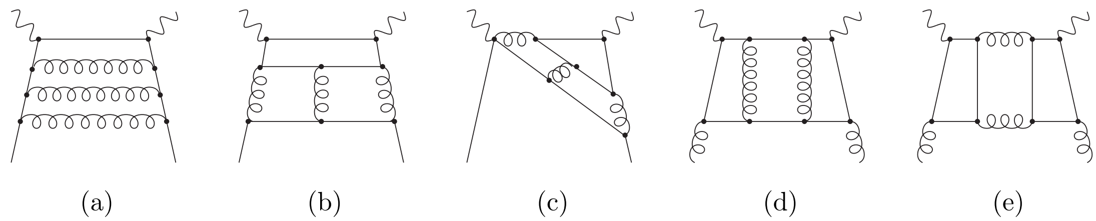

Figure 4.2. Representative three-loop diagrams of the flavor classes (from left to right): FC_2, FC_{02}, FC_{11}, FC_2^g, and FC_{11}^g.

4.2.3. Structure functions for various flavor classes

In a common notation, the electromagnetic charge factor of the photon vertex is conventionally taken out of the coefficient function and included as an extra pre-factor. We follow this convention and derive contribution to Eq. (4.12) from each flavor class. In the discussion below we use N_f to denote the number of initial quark flavors, and use N_{fs} and $\hat{Q}_{fs}$ to denote the number of flavors at the photon vertex and the corresponding charge matrix. The flavor of a possibly produced quark pair in the final state is not included explicitly here, which will be addressed later.

4.2.3.1. FC_2, FC_{02}, and FC_2^g classes

These flavor classes already appear in 2-loop DIS. The non-singlet contribution of FC_2 class is (recall that the elements of the diagonal coefficient matrix $\hat{C}$ are defined in Eq. (4.3))

$$\sum_\alpha tr(\hat{C}^{FC_2} t^\alpha)\Phi_\alpha = \sum_\alpha tr(C^{FC_2}(m_f)\hat{Q}_{fs}^2 t^\alpha)\Phi_\alpha$$
$$= \sum_{i,j}^{N_f} e_i^2 C^{FC_2}(m_i)(\delta_{ij} - \frac{1}{N_f})\Phi^+_{j/p}, \tag{4.13}$$

where the Fiertz identity for t^α

$$t^\alpha_{ik} t^\alpha_{jl} = \frac{1}{2}(\delta_{il}\delta_{kj} - \frac{1}{N_f}\delta_{ik}\delta_{jl}) \tag{4.14}$$

is used. As a convention we factor out the charge of quark at the photon vertex. The singlet contribution in Eq. (4.12) reads

$$\begin{aligned} tr(\hat{C}^{FC_2})\Phi_S &= tr(C^{FC_2}(m_f)\hat{Q}_f^2)\Phi_S \\ &= \sum_{i,j}^{N_f} \frac{1}{N_f} e_i^2 C^{FC_2}(m_i)\Phi^+_{j/p}, \end{aligned} \tag{4.15}$$

So the net contribution of FC_2 class is

$$\begin{aligned} &\sum_\alpha tr(\hat{C}^{FC_2} t^\alpha)\Phi_\alpha + tr(\hat{C}^{FC_2})\Phi_S \\ &= \sum_j^{N_f} e_j^2 C^{FC_2}(m_j)\Phi^+_{j/p}. \end{aligned} \tag{4.16}$$

The non-singlet contribution of FC_{02} class is

$$\begin{aligned} \sum_\alpha tr(\hat{C}^{FC_{02}} t^\alpha)\Phi_\alpha &= \sum_\alpha e_i^2 C^{FC_{02}}(m_i, m_j)(t^\alpha)_{jj}\Phi_\alpha \\ = \sum_i^{N_{fs}} \sum_{j,k}^{N_f} & e_i^2 C^{FC_{02}}(m_i, m_j)(\delta_{jk} - \frac{1}{N_f})\Phi^+_{k/p}. \end{aligned} \tag{4.17}$$

The singlet contribution is

$$\begin{aligned} tr(\hat{C}^{FC_{02}})\Phi_S &= tr(C^{FC_{02}}(m_f)\hat{Q}_{fs}^2)\Phi_S \\ &= \sum_i^{N_{fs}} \sum_{j,k}^{N_f} \frac{1}{N_f} e_i^2 C^{FC_{02}}(m_i, m_j)\Phi^+_{k/p} \end{aligned} \tag{4.18}$$

So the net contribution of this class is

$$\sum_\alpha tr(\hat{C}^{FC_{02}} t^\alpha)\Phi_\alpha + tr(\hat{C}^{FC_{02}})\Phi_S$$

$$= \sum_{i}^{N_{fs}} \sum_{j}^{N_f} e_i^2 C^{FC_{02}}(m_i, m_j) \Phi^+_{j/p}. \tag{4.19}$$

The FC_2^g class has a simpler contribution

$$C_g^{FC_2^g} \Phi_g = tr(C(FC_2^g, m_f) \hat{Q}_f^2) \Phi_g$$
$$= \sum_{i}^{N_{fs}} e_i^2 C(FC_2^g, m_i) \Phi_{g/p}. \tag{4.20}$$

4.2.3.2. FC_{11} and FC_{11}^g classes

In FC_{11} class the flavor number of the open quark line is N_f since it is also the initial flavor. We use N_{fs}^L to denote the quark loop flavor number. The non-singlet contribution to FC_{11} class is

$$\sum_{\alpha} tr(\hat{C}^{FC11} t^{\alpha}) \Phi_{\alpha} = \sum_{\alpha} \sum_{i,j}^{N_f} \sum_{k}^{N_{fs}^L} e_k e_i (t^{\alpha})_{ii} C^{FC11}(m_i, m_k) \times 2(t^{\alpha})_{jj} \Phi^+_{j/p}$$
$$= \sum_{i,j}^{N_f} \sum_{k}^{N_{fs}^L} e_k e_i C^{FC11}(m_i, m_k)(\delta_{ij} - \frac{1}{N_f}) \Phi^+_{j/p}. \tag{4.21}$$

The singlet contribution can be written as

$$tr(\hat{C}^{FC11}) \Phi_S = \sum_{i,j}^{N_f} \sum_{k}^{N_{fs}^L} \frac{1}{N_f} e_k e_i C^{FC11}(m_i, m_k) \Phi^+_{j/p}. \tag{4.22}$$

So the total contribution of the FC_{11} class is

$$\sum_{\alpha} tr(\hat{C}^{FC11} t^{\alpha}) \Phi_{\alpha} + tr(\hat{C}^{FC11}) \Phi_S = \sum_{i,j,k} e_k e_i C(FC_{11}, m_i, m_k) \Phi^+_{j/p} \delta_{ij}$$
$$= \sum_{j}^{N_f} \sum_{k}^{N_{fs}^L} e_k e_j C(FC_{11}, m_j, m_k) \Phi^+_{j/p}. \tag{4.23}$$

The contribution from FC_{11}^g class is simpler.

$$C_g^{FC_{11}^g} \Phi_g = \sum_{i,k}^{N_{fs}^L} e_k e_i C^{FC_{11}^g}(m_i, m_k) \Phi_{g/p}.$$

$$(4.24)$$

Note that gauge-invariance of structure functions is preserved in each flavor class. This is because the flavor classes correspond to various topologies for inserting electroweak vertices. Since the electroweak charges are independent of QCD interactions, the flavor classes are invariant with respect to the SU(3) color gauge.

4.2.4. Massless limit

The N3LO coefficient functions given in [63,64,71] are obtained in the ZM scheme. To carry out a practical calculation with these functions we have to examine the massless limit of all the general results obtained in the last subsection, and define the massless coefficient functions with the same convention (charge factors) as adopted in the above papers. There the coefficient functions are given as non-singlet and singlet components separately. We will also make this distinction here.

In the massless case, all flavors are active, and we will not need to discriminate the flavor number for initial state and that at the photon vertex, or the flavor number at different vertices. We use a single number N_f for the number of flavors. The charge matrix $\hat{Q}_{fs}$ contains N_f diagonal elements in every case. Also note that the coefficient functions has no mass dependence and hence can be taken out of the trace operation. The non-singlet contribution from the FC_2 class is

$$\sum_{\alpha} tr(\hat{C}^{FC_2} t^{\alpha})\Phi_{\alpha} = C^{FC_2} \sum_{\alpha} tr(\hat{Q}_{fs}^2 t^{\alpha})\Phi_{\alpha}, \tag{4.25}$$

where $C^{FC_2} \equiv C^{FC_2}(m_f = 0)$. The non-singlet contribution of the FC_{02} class will be zero because it contains a trace of generators t^{α}, as can be seen in Eq. (4.17). The non-singlet contribution from FC_{11} class in Eq. (4.21) becomes

$$\begin{aligned}
&\sum_\alpha tr(\hat{C}^{FC11}t^\alpha)\Phi_\alpha = C^{FC11}\sum_\alpha tr(\hat{Q}_{fs})tr(\hat{Q}_{fs}t^\alpha)\Phi_\alpha \\
&= C^{FC11}\sum_\alpha \frac{tr(\hat{Q}_{fs})tr(\hat{Q}_{fs}t^\alpha)}{tr(\hat{Q}^2_{fs}t^\alpha)} \times tr(\hat{Q}^2_{fs}t^\alpha)\Phi_\alpha \\
&= N_f fl^{ns}_{11}C^{FC11} \times \sum_\alpha tr(\hat{Q}^2_{fs}t^\alpha)\Phi_\alpha, \qquad (4.26)
\end{aligned}$$

where we have used the fact that

$$\frac{tr(\hat{Q}_{fs}t^\alpha)}{tr(\hat{Q}^2_{fs}t^\alpha)} = 3 \qquad (4.27)$$

holds for all diagonal generators t^α. The factor fl^{ns}_{11} is defined in [64, 71]. The net non-singlet contribution is

$$\begin{aligned}
&\sum_{\alpha,FC} tr(\hat{C}t^\alpha)\Phi_\alpha = [C(FC_2) + N_f fl^{ns}_{11}C(FC_{11})] \times \left[\sum_\alpha tr(\hat{Q}^2_f t^\alpha)\Phi_\alpha\right] \\
&\equiv C_{ns}q_{ns}, \qquad (4.28)
\end{aligned}$$

where $C_{ns} \equiv C(FC_2) + N_f fl^{ns}_{11}C(FC_{11})$ and

$$\begin{aligned}
q_{ns} &= \sum_\alpha tr(\hat{Q}^2_f t^\alpha)\Phi_\alpha = \sum_{i,j,\alpha} e^2_i(t^\alpha)_{ii}\Phi^+_{j/p}2(t^\alpha)_{jj} \\
&= \sum_{i,j} e^2_i(\delta_{ij} - \frac{1}{N_f})\Phi^+_{j/p} \\
&= \sum_{i=1}^{N_f} e^2_i(q_i + q_{\bar{i}} - \frac{1}{N_f}q_s). \qquad (4.29)
\end{aligned}$$

This is the non-singlet quark PDF. Comparing the factors of the coefficient functions in Eq. (4.28) to the parameterizations of coefficient functions given in [63, 64] we are able to identify the functions $C(FC_2)$ and $C(FC_{11})$.

Now we turn to the singlet structure function. In this case one should take the trace of the charge matrices with the unit flavor matrix:

$$tr(\hat{C})\Phi_S = \left[C(FC_2) + \frac{tr(\hat{Q}_f)tr(\hat{Q}_f)}{tr(\hat{Q}^2_f)}C(FC_{11}) + tr(I)C(FC_{02})\right] \times \left[tr(\hat{Q}^2_f)\Phi_S\right]$$

$$= [C(FC_2) + N_f f l_{11}^s C(FC_{11}) + N_f C(FC_{02})] \times tr(\hat{Q}_f^2)\Phi_S$$
$$= \left\langle e^2 \right\rangle C_q q_s, \tag{4.30}$$

where $q_S \equiv N_f \Phi_S$ is introduced to follow the convention in [63, 64, 71]. Again the factors of the coefficient functions are as expected. ($\Phi_S = \frac{1}{N_f} \sum_j^{N_f} \Phi_{j/p}^+$)

For gluon contributions the flavor factors are given by the same references above:

$$C_g \Phi_g = \left[\frac{tr(\hat{Q}_f)^2)}{tr(\hat{Q}_f^2)} C(FC_{11}^g) + C(FC_2^g) \right] \times \left[tr(\hat{Q}_f^2)\Phi_g \right]$$
$$= \left[N_f^2 f l_{11}^g C(FC_{11}^g) + N_f C(FC_2^g) \right] \times \left[\frac{tr(\hat{Q}_f^2)}{N_f} \Phi_g \right]$$
$$= \left\langle e^2 \right\rangle C_g g \tag{4.31}$$

This form has correct factors for coefficient functions and exactly agrees with Eq. (4.32). Combining the results above we recover the massless expression for structure functions given in [63, 64, 71]:

$$x^{-1} F_a = C_{ns} q_{ns} + \left\langle e^2 \right\rangle (C_q q_s + C_g g). \tag{4.32}$$

Note that Eqs. (4.28,4.30,4.31,4.32) are in the same form as in [63, 64]. Therefore we can read off $C(FC_2)$,$C(FC_{02})$,$C(FC_{11})$,$C(FC_2^g)$, and $C(FC_{11}^g)$ from the coefficient functions given in these references.

4.3. Various terms at three loops and the implementation of mass dependence

4.3.1. ZM coefficient functions

The three-loop zero-mass coefficient functions F_2 and F_L are taken from [64] and [63]. In these ZM expressions, contributions from all flavor classes are combined. To implement the mass dependence, these must be broken down to contributions from different classes. A more delicate breakdown is needed if there is a different mass dependence between various diagrams within the same flavor class. We first list the ZM coefficient functions and their breakdown below, then show the corresponding diagrams and discuss their mass implementation. Note here we follow Ref. [63, 64] and use the notation $c_q^n = c_{ns}^n + c_{ps}^n$, i.e., as the sum of non-singlet ("ns") and pure singlet ("ps") contributions. Also we use lowercase notations for functions taken from the above references. The explicit expressions for the ZM coefficient functions are

$$c^{(3)}_{2,\mathrm{ns}} \cong c^{(3),FC_2,T_1}_{2,\mathrm{ns}} + n_f c^{(3),FC_2,T_2}_{2,\mathrm{ns}} + n_f^2 c^{(3),FC_2,T_3}_{2,\mathrm{ns}} + fl_{11}^{\mathrm{ns}}\, n_f c^{(3),FC_{11}}_{2,\mathrm{ns}}, \qquad (4.33)$$

$$\begin{aligned} c^{(3),FC_2,T_1}_{2,\mathrm{ns}}(x) =\; & 512/27\, \mathcal{D}_5 - 5440/27\, \mathcal{D}_4 + 501.099\, \mathcal{D}_3 + 1171.54\, \mathcal{D}_2 - 7328.45\, \mathcal{D}_1 \\ & + 4442.76\, \mathcal{D}_0 - 9170.38\, \delta(x_1) - 512/27\, L_1^5 + 704/3\, L_1^4 - 3368\, L_1^3 \\ & - 2978\, L_1^2 + 18832\, L_1 - 4926 + 7725\, x + 57256\, x^2 + 12898\, x^3 \\ & - 56000\, x_1 L_1^2 - L_0 L_1 (6158 + 1836\, L_0) + 4.719\, x L_0^5 - 775.8\, L_0 \\ & - 899.6\, L_0^2 - 309.1\, L_0^3 - 2932/81\, L_0^4 - 32/27\, L_0^5, \end{aligned} \qquad (4.34)$$

$$c^{(3),FC_2,T_2}_{2,\mathrm{ns}}(x) = 640/81\, \mathcal{D}_4 - 6592/81\, \mathcal{D}_3 + 220.573\, \mathcal{D}_2 + 294.906\, \mathcal{D}_1 - 729.359\, \mathcal{D}_0$$

$$
\begin{aligned}
& + 2574.687\,\delta(x_1) - 640/81\,L_1^4 + 153.5\,L_1^3 - 828.7\,L_1^2 - 501.1\,L_1 + 831.6 \\
& - 6752\,x - 2778\,x^2 + 171.0\,x_1 L_1^4 + L_0 L_1\,(4365 + 716.2\,L_0 - 5983\,L_1) \\
& + 4.102\,x L_0^4 + 275.6\,L_0 + 187.3\,L_0^2 + 12224/243\,L_0^3 + 728/243\,L_0^4\,, \quad (4.35)
\end{aligned}
$$

$$
\begin{aligned}
c_{2,\mathrm{ns}}^{(3),FC_2,T_3}(x) \;=\;& 64/81\,\mathcal{D}_3 - 464/81\,\mathcal{D}_2 + 7.67505\,\mathcal{D}_1 + 1.00830\,\mathcal{D}_0 - 103.2366\,\delta(x_1) \\
& - 64/81\,L_1^3 + 18.21\,L_1^2 - 19.09\,L_1 + 129.2\,x + 102.5\,x^2 + L_0 L_1\,(-96.07 \\
& - 12.46\,L_0 + 85.88\,L_1) - 8.042\,L_0 - 1984/243\,L_0^2 - 368/243\,L_0^3\,, \quad (4.36)
\end{aligned}
$$

$$
\begin{aligned}
c_{2,\mathrm{ns}}^{(3),FC_{11}}(x) \;=\;& \{(126.42 - 50.29\,x - 50.15\,x^2) x_1 - 11.888\,\delta(x_1) - 26.717 - 9.075\,x x_1 L_1 \\
& - x L_0^2 (101.8 + 34.79\,L_0 + 3.070\,L_0^2) + 59.59\,L_0 - 320/81\,L_0^2 (5 + L_0)\,\}\,x\ . \quad (4.37)
\end{aligned}
$$

$$
c_{2,\mathrm{ps}}^{(3)} \;\cong\; n_f c_{2,\mathrm{ps}}^{(3),FC_{02},T_1} + n_f^2 c_{2,\mathrm{ps}}^{(3),FC_{02},T_2} + fl_{11}^{\mathrm{ps}}\, n_f c_{2,\mathrm{ps}}^{(3),FC_{11}}, \qquad (4.38)
$$

$$
\begin{aligned}
c_{2,\mathrm{ps}}^{(3),FC_{02},T_1}(x) \;=\;& (856/81\,L_1^4 - 6032/81\,L_1^3 + 130.57\,L_1^2 - 542\,L_1 + 8501\, - 4714\,x + 61.5\,x^2) \\
& \cdot x_1 + L_0 L_1 (8831\,L_0 + 4162\,x_1) - 15.44\,x L_0^5 + 3333\,x L_0^2 + 1615\,L_0 + 1208\,L_0^2 \\
& - 333.73\,L_0^3 + 4244/81\,L_0^4 - 40/9\,L_0^5 - x^{-1}(2731.82\,x_1 + 414.262\,L_0), \quad (4.39)
\end{aligned}
$$

$$
\begin{aligned}
c_{2,\mathrm{ps}}^{(3),FC_{02},T_2}(x) \;=\;& (-64/81\,L_1^3 + 208/81\,L_1^2 + 23.09\,L_1 - 220.27 + 59.80\,x - 177.6x^2)\,x_1 \\
& - L_0 L_1 (160.3\,L_0 + 135.4\,x_1) - 24.14\,x L_0^3 - 215.4\,x L_0^2 - 209.8\,L_0 - 90.38 L_0^2 \\
& - 3568/243\,L_0^3 - 184/81\,L_0^4 + 40.2426\,x_1 x^{-1}\,, \quad (4.40)
\end{aligned}
$$

$$
\begin{aligned}
c_{2,\mathrm{ps}}^{(3),FC_{11}}(x) \;=\;& \{(126.42 - 50.29\,x - 50.15\,x^2) x_1 - 11.888\,\delta(x_1) - 26.717 - 9.075\,x x_1 L_1 \\
& - x L_0^2 (101.8 + 34.79\,L_0 + 3.070\,L_0^2) + 59.59\,L_0 - 320/81\,L_0^2 (5 + L_0)\,\}\,x\ . \quad (4.41)
\end{aligned}
$$

$$c_{2,\mathrm{g}}^{(3)} \;\cong\; n_f c_{2,\mathrm{g}}^{(3),FC_2^g,T_1} + n_f^2 c_{2,\mathrm{ps}}^{(3),FC_2^g,T_2} + fl_{11}^{\mathrm{g}}\, n_f^2 c_{2,\mathrm{ps}}^{(3),FC_{11}^g}, \qquad (4.42)$$

$$\begin{aligned}
c_{2,\mathrm{g}}^{(3),FC_2^g,T_1}(x) \;=\;& 966/81\, L_1^5 - 1871/18\, L_1^4 + 89.31\, L_1^3 + 979.2\, L_1^2 - 2405\, L_1 + 1372\, x_1 L_1^4 \\
& - 15729 - 310510\, x + 331570\, x^2 - 244150\, xL_0^2 - 253.3\, xL_0^5 \\
& + L_0 L_1 (138230 - 237010\, L_0) - 11860\, L_0 - 700.8\, L_0^2 - 1440\, L_0^3 \\
& + 4961/162\, L_0^4 - 134/9\, L_0^5 - x^{-1}(6362.54 - 932.089\, L_0) \\
& + 0.625\, \delta(x_1)\,, \qquad (4.43)
\end{aligned}$$

$$\begin{aligned}
c_{2,\mathrm{g}}^{(3),FC_2^g,T_1}(x) \;=\;& 131/81\, L_1^4 - 14.72\, L_1^3 + 3.607\, L_1^2 - 226.1\, L_1 + 4.762 - 190\, x - 818.4\, x^2 \\
& - 4019\, xL_0^2 - L_0 L_1 (791.5 + 4646\, L_0) + 739.0\, L_0 + 418.0\, L_0^2 + 104.3\, L_0^3 \\
& + 809/81\, L_0^4 + 12/9\, L_0^5 + 84.423\, x^{-1}\,, \qquad (4.44)
\end{aligned}$$

$$\begin{aligned}
c_{2,\mathrm{g}}^{(3),FC_{11}^g}(x) \;=\;& 3.211\, L_1^2 + 19.04\, xL_1 + 0.623\, x_1 L_1^3 - 64.47\, x + 121.6\, x^2 - 45.82\, x^3 \\
& - xL_0 L_1 (31.68 + 37.24\, L_0) + 11.27\, x^2 L_0^3 - 82.40\, xL_0 - 16.08\, xL_0^2 \\
& + 520/81\, xL_0^3 + 20/27\, xL_0^4 \;. \qquad (4.45)
\end{aligned}$$

$$c_{L,\mathrm{ns}}^{(3)} \;\cong\; c_{L,\mathrm{ns}}^{(3),FC_2,T_1} + n_f c_{L,\mathrm{ns}}^{(3),FC_2,T_2} + n_f^2 c_{L,\mathrm{ns}}^{(3),FC_2,T_3} + fl_{11}^{\mathrm{ns}}\, n_f c_{L,\mathrm{ns}}^{(3),FC_{11}}, \qquad (4.46)$$

$$\begin{aligned}
c_{L,\mathrm{ns}}^{(3),FC_2,T_1}(x) \;=\;& 512/27\, L_1^4 - 177.40\, L_1^3 + 650.6\, L_1^2 - 2729\, L_1 - 2220.5 - 7884\, x \\
& + 4168\, x^2 - (844.7\, L_0 + 517.3\, L_1)\, L_0\, L_1 + (195.6\, L_1 - 125.3)\, x_1\, L_1^3 \\
& + 208.3\, xL_0^3 - 1355.7\, L_0 - 7456/27\, L_0^2 - 1280/81\, L_0^3 + 0.113\, \delta(x_1), \qquad (4.47)
\end{aligned}$$

$$c_{L,\mathrm{ns}}^{(3),FC_2,T_2}(x) = 1024/81\, L_1^3 - 112.35\, L_1^2 + 344.1\, L_1 + 408.4 - 9.345\, x - 919.3\, x^2$$
$$+ (239.7 + 20.63\, L_1)\, x_1\, L_1^2 + (887.3 + 294.5\, L_0 - 59.14\, L_1)\, L_0\, L_1$$
$$- 1792/81\, xL_0^3 + 200.73\, L_0 + 64/3\, L_0^2 + 0.006\, \delta(x_1), \quad (4.48)$$
$$c_{L,\mathrm{ns}}^{(3),FC_2,T_3}(x) = \{3\, xL_1^2 + (6 - 25\, x)\, L_1 - 19 + (317/6 - 12\, \zeta_2)\, x - 6\, xL_0\, L_1 + 6\, x\, \mathrm{Li}_2(x)$$
$$+ 9\, xL_0^2 - (6 - 50\, x)\, L_0\}\, 64/81, \quad (4.49)$$
$$c_{L,\mathrm{ns}}^{(3),FC_{11}}(x) = \{(107.0 + 321.05\, x - 54.62\, x^2)\, x_1 - 26.717 + 9.773\, L_0$$
$$+ (363.8 + 68.32\, L_0)\, xL_0 - 320/81\, L_0^2\, (2 + L_0)\}\, x\ . \quad (4.50)$$

$$c_{L,\mathrm{ps}}^{(3)} \cong n_f c_{L,\mathrm{ps}}^{(3),FC_{02},T_1} + n_f^2 c_{L,\mathrm{ps}}^{(3),FC_{02},T_2} + fl_{11}^{\mathrm{ps}}\, n_f c_{L,\mathrm{ps}}^{(3),FC_{11}}, \quad (4.51)$$

$$c_{L,\mathrm{ps}}^{(3),FC_{02},T_1}(x) = (1568/27\, L_1^3 - 3968/9\, L_1^2 + 5124\, L_1)\, x_1^2 + (2184\, L_0 + 6059\, x_1)\, L_0\, L_1$$
$$- (795.6 + 1036\, x)\, x_1^2 - 143.6\, x_1\, L_0 + 2848/9\, L_0^2 - 1600/27\, L_0^3$$
$$- (885.53\, x_1 + 182.00\, L_0)\, x^{-1}\, x_1, \quad (4.52)$$
$$c_{L,\mathrm{ps}}^{(3),FC_{02},T_2}(x) = (-32/9\, L_1^2 + 29.52\, L_1)\, x_1^2 + (35.18\, L_0 + 73.06\, x_1)\, L_0\, L_1 - 35.24\, xL_0^2$$
$$- (14.16 - 69.84\, x)\, x_1^2 - 69.41\, x_1\, L_0 - 128/9\, L_0^2$$
$$+ 40.239\, x^{-1}\, x_1^2, \quad (4.53)$$
$$c_{L,\mathrm{ps}}^{(3),FC_{11}}(x) = \{(107.0 + 321.05\, x - 54.62\, x^2)\, x_1 - 26.717 + 9.773\, L_0$$
$$+ (363.8 + 68.32\, L_0)\, xL_0 - 320/81\, L_0^2\, (2 + L_0)\}\, x\ . \quad (4.54)$$

$$c_{L,\mathrm{g}}^{(3)} \cong n_f c_{L,\mathrm{g}}^{(3),FC_2^g,T_1} + n_f^2 c_{L,\mathrm{ps}}^{(3),FC_2^g,T_2} + fl_{11}^{\mathrm{g}}\, n_f^2 c_{L,\mathrm{ps}}^{(3),FC_{11}^g}, \quad (4.55)$$

$$
\begin{aligned}
c^{(3),FC^g_2,T_1}_{L,\mathrm{g}}(x) \;=\;& \quad (144\, L_1^4 - 47024/27\, L_1^3 + 6319\, L_1^2 + 53160\, L_1)\; x_1 + 72549\, L_0\, L_1 \\
& + 88238\, L_0^2\, L_1 + (3709 - 33514\; x - 9533\; x^2)\; x_1 + 66773\, x L_0^2 \\
& - 1117\, L_0 + 45.37\, L_0^2 - 5360/27\, L_0^3 - (2044.70\; x_1 \\
& + 409.506\; L_0)\, x^{-1}, \qquad (4.56) \\
c^{(3),FC^g_2,T_2}_{L,\mathrm{g}}(x) \;=\;& \quad (32/3\, L_1^3 - 1216/9\, L_1^2 - 592.3\, L_1 + 1511\, xL_1)\; x_1 + 311.3\, L_0\, L_1 \\
& + 14.24\, L_0^2\, L_1 + (577.3 - 729.0\; x)\; x_1 + 30.78\, x L_0^3 + 366.0\, L_0 \\
& + 1000/9\, L_0^2 + 160/9\, L_0^3 + 88.5037\, x^{-1}\, x_1, \qquad (4.57) \\
c^{(3),FC^g_{11}}_{L,\mathrm{g}}(x) \;=\;& \quad (-0.0105\, L_1^3 + 1.550\, L_1^2 + 19.72\, xL_1 - 66.745\, x + 0.615\, x^2)\; x_1 \\
& + 20/27\, xL_0^4 + (280/81 + 2.260\; x)\, xL_0^3 - (15.40 - 2.201\; x)\; xL_0^2 \\
& - (71.66 - 0.121\; x)\; xL_0\ . \qquad (4.58)
\end{aligned}
$$

4.3.2. Coefficient functions with phase space corrections

Next, we wish to introduce approximate mass dependence into the ZM coefficient functions listed in the previous section. To obtain some guidance, let us briefly review how mass dependence arises in various Feynman diagrams in the GM scheme, to which our current calculation will provide an approximation. DIS cross sections receive contributions from diagrams of various orders. For perturbative calculation to reliably apply, a hard scale represented by Q is required. A perturbative computation of the cross sections using factorization theorem involves convolving a hard scattering factor H with a target factor T. It should be stressed again that strictly speaking H is not the contribution of the graphs with the hard region represented in Fig. 3.5, rather, it is obtained by making the proper approximation to structure functions to eliminate all potential large contributions to correction terms that should be power suppressed. In this notation the factorized structure function is written as [37,62]

$$H \cdot Z \cdot T \equiv \sum_a \int \frac{d^4k}{(2\pi)^4} H_a(q,l) Z_a(l,k,\hat{l}) T_a(k,p), \tag{4.59}$$

where there is a sum over parton flavors and an implicit sum over spin indices, which turns H and T into traces so that the factorization becomes convolution of scalar functions. A projection operator Z is applied between H and T. It serves to approximate the momentum entering the hard part by one collinear to the target momentum with low virtuality. Also it picks out the leading terms in the spin sum. For example, for initial-state quarks Z operator is

$$Z_a(l,k;\widehat{l}) = \frac{1}{4}(2\pi)^4 S_H(\widehat{l})\, S_T\, \delta(l^+ - \widehat{l}^+)\delta(l^- - \widehat{l}^-)\delta^2(\vec{l}_T), \tag{4.60}$$

where $S_H(\widehat{l})$ and $S_T = \gamma^+$ project out the leading spin components and the delta functions select only the large component as the convolution variable and make approximations about the small components. For a quark with negligible mass as compared with Q, it suffices to set

$$\hat{l^\mu} = \hat{p^\mu} = \left(\xi p^+, 0, \vec{0}_T\right). \tag{4.61}$$

Changing the integration variable from l^+ to ξ will then turn the integral in Eq. (4.59) into a convolution over the momentum fraction ξ.

When the massive hard-scattering functions are not fully known, as in our N3LO calculation, the generic structure of Eq. (4.50), and freedom to select the form of $\widehat{l}$ in the Z operator can be employed to approximate mass dependence of the factorized cross sections. To see this let us carefully examine the kinematics of the scattering process. In Eq. (3.62) the integral over ζ is constrained in the range $[x,1]$. The lower bound is obtained by applying momentum conservation of the hard scattering process: $(\hat{p}+q)^2 \geq 0$. The upper bound follows from the requirement that the remnants of the target should have positive energy. However, when the hard and target parts are connected by a heavy quark line, factorization of structure functions removes the kinematic constraint of producing pairs of heavy quarks, because one heavy quark is hidden in the target remnants. This constraint excludes the production of heavy quarks when the CM energy of the hadron-photon system is below the production threshold. As a consequence, the lower bound of the integral becomes $\chi = x\left(1 + (\sum_{fs} m_h)^2/Q^2\right)$. The way to enforce this phase space constraint within the framework of factorization is to set

$$\hat{l^{\mu}} = \left(\xi \frac{p^+}{1 + (\sum_{fs} m_h)^2/Q^2}, 0, \vec{0}_T\right). \tag{4.62}$$

Now we can use this feature to construct approximate coefficient functions in the IM scheme that account for phase space constraints, by writing

$$C_{IM}\left(\hat{x}, m_h\right) = C_{ZM}\left(\hat{\chi}\right) \theta(\chi \leq \xi \leq 1), \tag{4.63}$$

where

$$\chi = x\left(1 + \frac{(\sum_{fs} m_h)^2}{Q^2}\right). \tag{4.64}$$

The sum of fs is over all the massive quarks produced in the final state. In the rest of this section we apply the χ variable to coefficient functions from all the flavor classes. Note that this notation only includes the mass effect from the scattering kinematics, while the mass dependence in the hard scattering coefficients are absent. Furthermore, a generalization of the phase-space constraint(4.64) has also been developed [65], which turn it off when the scattering energy W is much larger than m_h. We now introduce this generalized constraint.

4.3.2.1. Rescaling variable dependence

The phase space constraint(4.64) for FE term is an approximate constraint, which leaves a freedom of tuning it by adjusting the form of the momentum $\hat{l}^{\mu}$ in Eq. (4.60). For a given hard scale Q, threshold suppression due to the phase-space constraint happens at a relatively large x value, where the heavy quark threshold is approached. At this region the mass effect of phase space is important. It has been argued [65] that for small x away from the threshold, it is unnecessary to keep using the χ variable for the FE term. One could generalize the rescaling variable χ to ensure suppression near threshold and recover the scaling variable x away from it. The generalized "rescaling" variable that realizes the smooth transition is given also in Ref. [65] by

$$x = \zeta \left(1 + \zeta^{\lambda} (\sum\nolimits_{fs} m_h)^2 / Q^2\right)^{-1}, \tag{4.65}$$

where the new variable ζ has been shown to satisfy $x < \zeta < \chi$. The parameter λ reflects the extent to which ζ differs from the uniform rescaling χ. $\lambda = 0$ corresponds to the choice $\zeta = \chi$. The transition from χ to x is more rapid as λ becomes larger.

Note that for heavy-flavor production in the FC channel, the kinematics of the hard scattering predicts that we should use χ as the rescaling variable for any x. While this must be enforced in GM scheme calculations, in the IM scheme, we do not have to stick with it because of lack of massive FC coefficients.

The kinematic constraints depend only on the masses of the quarks in a given Feynman diagram. They do not alter classification of flavor classes (FC) that was worked out in Sec. 4.2.3. Once the massive coefficient functions in the FFN scheme are available, we will replace the approximate phase-space constraints in the flavor-creation diagrams by the exact ones in the same way as it has been done in the NNLO GM calculation. We will now list all coefficient functions in the IM scheme, keeping track of their approximate mass dependence in each flavor class.

4.3.3. IM coefficient functions

4.3.3.1. FC_2 class

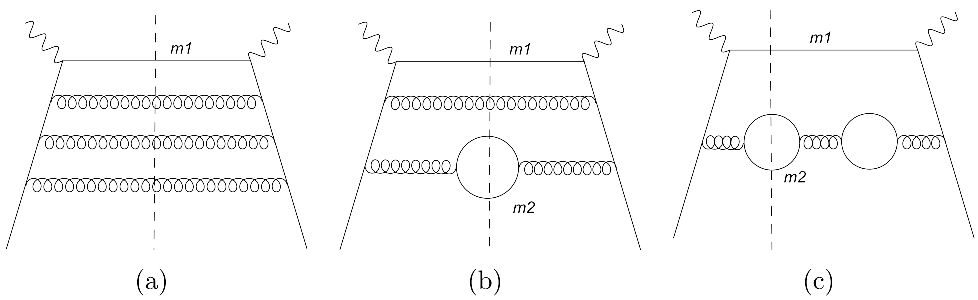

Figure 4.3. Representative diagrams from FC_2 class. (a) T_1 (b) T_2 (c) T_3.

$$C_{a,\text{ns}}^{(3),FC_2,T_1} = c_{a,\text{ns}}^{(3),FC_2,T_1}(\hat{\zeta}(2m_1)), \tag{4.66}$$

$$C_{a,\text{ns}}^{(3),FC_2,T_2} = c_{a,\text{ns}}^{(3),FC_2,T_2}(\hat{\zeta}(2(m_1+m_2))), \tag{4.67}$$

$$C_{a,\text{ns}}^{(3),FC_2,T_3} = n'_f c_{a,\text{ns}}^{(3),FC_2,T_3}(\hat{\zeta}(2(m_1+m_2))). \tag{4.68}$$

where $a = 2, L$. For simplicity, in Eq. (4.68) only the mass of the cut loop is considered. n'_f denotes the number of quark flavors in the uncut quark loop.

When a virtual quark loop appears in a graph, such as the case in Fig. (4.3(c)), a related issue is to consistently include contributions from various quark flavors in the loop. If all quark masses could be neglected, then one could simply set the N_f associated with the loop to be the number of all the quarks known. Unfortunately, this is not our case. We have already seen how $\alpha_s(\mu)$ is evolved when μ runs through the quark masses. Recall that the renormalization equation of $\alpha_s(\mu)$ follows from the scale independence of the bare coupling $g_{s0} = Z_g\mu^\epsilon g_s$. To evolve α_s one varies the number of active quark flavors as μ changes. In a consistent calculation of the hard scattering coefficients, one should also use the same active flavor number in the renormalization constant Z_g to cancel the UV divergences from loop diagrams. Therefore, we count all the flavors with masses below μ in the loop.

4.3.3.2. FC_{02} class

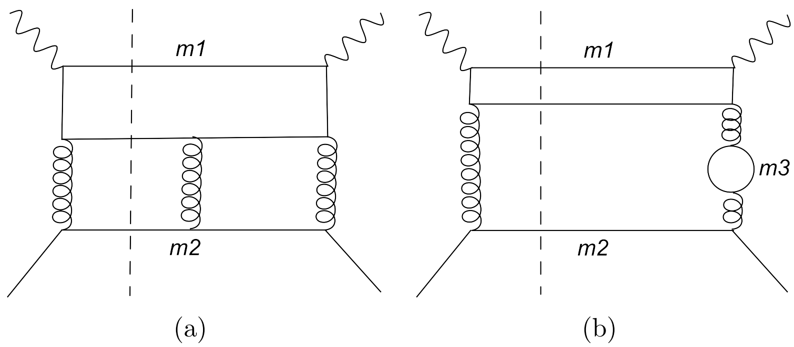

Figure 4.4. Representative diagrams from FC_{02} class. (a) T_1 (b) T_2.

$$C_{a,\mathrm{ps}}^{(3),FC_{02},T_1} = c_{a,\mathrm{ps}}^{(3),FC_{02},T_1}(\hat{\zeta}(2(m_1 + m_2))), \tag{4.69}$$

$$C_{a,\mathrm{ps}}^{(3),FC_{02},T_2} = c_{a,\mathrm{ps}}^{(3),FC_{02},T_2}(\hat{\zeta}(2(m_1 + m_2))). \tag{4.70}$$

In Fig. (4.4(b)) the N_f of the virtual loop is implemented in the same way as in Fig. (4.3(c)). Note that if m_2 is heavy, then this class of diagrams belongs to the FE contribution. While the phase space correction is to be enforced for the production of all quarks, the dependence of the coefficients on m_2 can be consistently neglected along with the contribution from the corresponding subtraction terms. However, the mass dependence on m_1 should be retained.

4.3.3.3. FC_{11} class

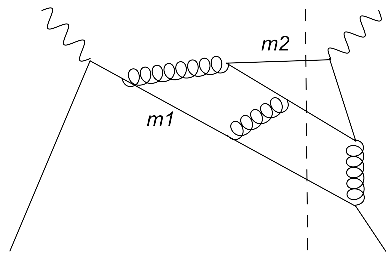

Figure 4.5. Representative diagrams from FC_{11} class.

$$C^{(3),FC_{11}}_{a,\mathrm{ns}} = c^{(3),FC_{11}}_{a,\mathrm{ns}}(\hat{\zeta}(2(m_1+m_2))), \tag{4.71}$$

$$C^{(3),FC_{11}}_{a,\mathrm{ps}} = c^{(3),FC_{11}}_{a,\mathrm{ps}}(\hat{\zeta}(2(m_1+m_2))). \tag{4.72}$$

The massless expression for pure singlet and non-singlet components are the same for FC_{11} class, so we have

$$C^{(3),FC_{11}}_{a,\mathrm{ns}} = C^{(3),FC_{11}}_{a,\mathrm{ps}} = C(FC_{11}, m_1, m_2). \tag{4.73}$$

4.3.3.4. FC^g_2 class

$$C^{(3),FC^g_2,T_1}_{a,\mathrm{g}} = c^{(3),FC^g_2,T_1}_{a,\mathrm{g}}(\hat{\zeta}(2m_1)), \tag{4.74}$$

$$C^{(3),FC^g_2,T_2}_{a,\mathrm{g}} = c^{(3),FC^g_2,T_2}_{a,\mathrm{g}}(\hat{\zeta}(2(m_1+m_2))), \tag{4.75}$$

$$C^{(3),FC^g_2,T_3}_{a,\mathrm{g}} = c^{(3),FC^g_2,T_3}_{a,\mathrm{g}}(\hat{\zeta}(2(m_1+m_2))). \tag{4.76}$$

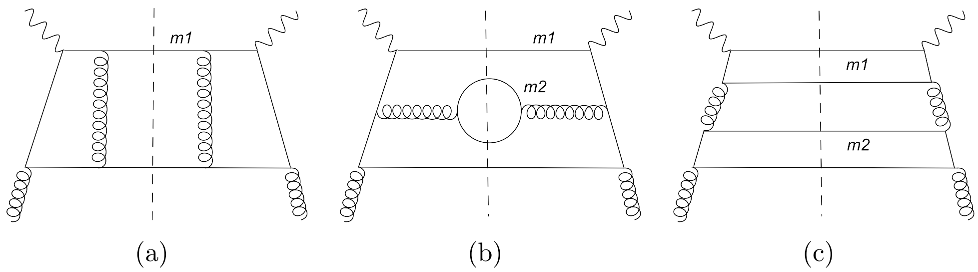

Figure 4.6. Representative diagrams from FC_2^g class. (a) T_1 (b) T_2 (c) T_3.

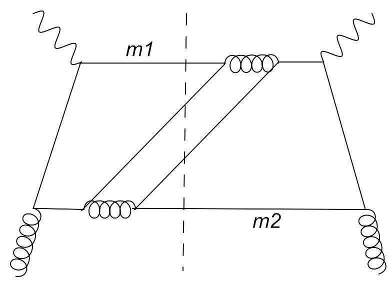

Figure 4.7. Representative diagrams from FC_{11}^g class.

4.3.3.5. FC_{11}^g class

$$C_{a,\mathrm{g}}^{(3),FC_{11}^g} = c_{a,\mathrm{g}}^{(3),FC_{11}^g}(\hat{\zeta}(2(m_1 + m_2))) \tag{4.77}$$

The gluon initiated production of massive quarks belongs to the FC channel. The mass dependence in the coefficients need to be implemented once they are available.

FC_2	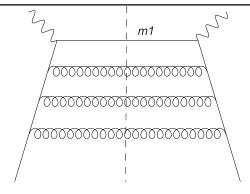	$c_{a,ns}^{FC_2,T_1}(\hat{\zeta}(2m_1))$
	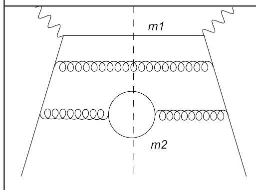	$c_{a,ns}^{FC_2,T_2}(\hat{\zeta}2((m_1+m_2)))$
	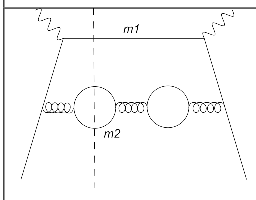	$c_{a,ns}^{FC_2,T_3}(\hat{\zeta}2((m_1+m_2)))$
FC_{02}	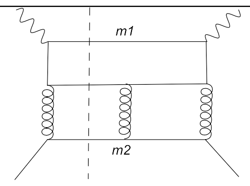	$c_{a,ps}^{FC_{02},T_1}(\hat{\zeta}(2(m_1+m_2)))$
FC_{02}	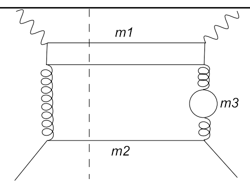	$c_{a,ps}^{FC_{02},T_2}(\hat{\zeta}(2(m_1+m_2)))$
FC_{11}	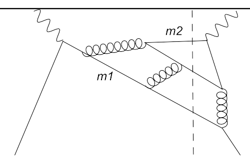	$c_{a,ns}^{FC_{11},T_1}(\hat{\zeta}(2(m_1+m_2)))$ $c_{a,ps}^{FC_{11},T_1}(\hat{\zeta}(2(m_1+m_2)))$

Continued on next page

continued from previous page		
FC_2^g	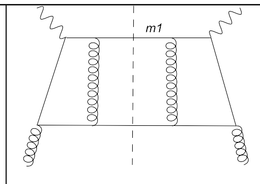	$c_{a,g}^{FC_2^g,T_1}(\hat{\zeta}(2m_1))$
	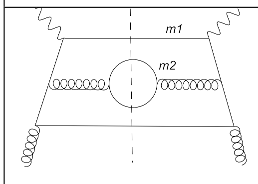	$c_{a,g}^{FC_2^g,T_2}(\hat{\zeta}(2(m_1+m_2)))$
	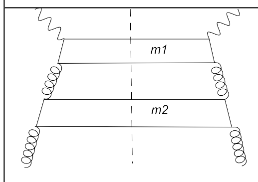	$c_{a,g}^{FC_2^g,T_3}(\hat{\zeta}(2(m_1+m_2)))$
FC_{11}^g	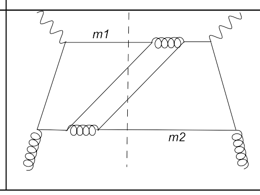	$c_{a,g}^{FC_{11}^g,T_2}(\hat{\zeta}(2(m_1+m_2)))$

Table 4.2: Mass dependence of coefficient functions for various Feynman diagrams

4.4. Scale dependence

So far, the coefficient functions are given at a fixed scale $\mu = Q$. In a perturbative calculation the structure functions computed to all orders are independent of the scale choice, while the coefficient functions and PDFs are not. However, real calculations are done up to some finite order n, in which case the μ dependence of the coefficient functions and PDFs cancel up to one higher order. The uncertainty caused by this residual scale dependence is of the same order as the neglected terms in perturbation series. Generally one would expect the convergence of the scale uncertainty as high order corrections are included. It will become clear that the scale dependent terms are proportional to powers of logarithms of the form $\ln^m(\mu^2/Q^2)$. Therefore the choice

$\mu \sim Q$ is often preferred since it can speed up the convergence of the calculation. Nevertheless, the variation of μ can give an estimation of the magnitude of the high order terms.

As is seen before, the evolution of PDFs are closely related to the splitting functions. Like the hard-scattering coefficients, quark-to-quark splitting functions introduced in Ch. 3 can be decomposed into their NS and PS components,

$$P_{q_i q_k} = P_{\bar{q}_i \bar{q}_k} = \delta_{ik} P^V_{qq} + P^S_{qq}, \tag{4.78}$$

$$P_{q_i \bar{q}_k} = P_{\bar{q}_i q_k} = \delta_{ik} P^V_{q\bar{q}} + P^S_{q\bar{q}}, \tag{4.79}$$

$$P^{\pm}_{NS} \equiv P^V_{qq} \pm P^V_{q\bar{q}}. \tag{4.80}$$

To express the scale dependent terms it is usually convenient to introduce the matrix form of the splitting functions

$$\mathbf{P} \equiv \begin{pmatrix} P_{qq} & P_{qg} \\ P_{gq} & P_{gg} \end{pmatrix}, \tag{4.81}$$

in which the quark-to-quark splitting function is decomposed into a non-singlet and a pure-singlet components as

$$P_{qq} \; = \; P^{+}_{\mathrm{NS}} + P_{\mathrm{PS}}, \tag{4.82}$$

where

$$P_{\mathrm{PS}} \; = \; N_f \left(P^S_{qq} + P^S_{q\bar{q}} \right) \; . \tag{4.83}$$

Other matrix elements are related with the usual splitting functions by

$$P_{qg} \; = \; N_f \, P_{q_i g} \;\; , \quad P_{gq} \; = \; P_{g q_i}. \tag{4.84}$$

The quark-singlet and gluon components of coefficient functions and PDFs can be grouped into vectors

$$\mathbf{C} \equiv \begin{pmatrix} C_s & C_g \end{pmatrix}, \; \mathbf{q} \equiv \begin{pmatrix} q_s \\ g \end{pmatrix}. \tag{4.85}$$

Knowing the coefficient functions at a fixed scale, the expressions for arbitrary μ can be obtained recursively by expanding all the relevant quantities in terms of a_0, which is defined as

$$a_0 \equiv a(\mu = Q), \tag{4.86}$$

$$a(\mu) \equiv \frac{\alpha_s(\mu)}{4\pi}. \tag{4.87}$$

The expansions then read

$$a = A_0 a_0 + A_1 a_0^2 + A_2 a_0^3 + \cdots, \tag{4.88}$$

$$\mathbf{q}_a = \mathbf{q}_a^{(0)} + \mathbf{q}_a^{(1)} a_0 + \mathbf{q}_a^{(2)} a_0^2 + \ldots, \tag{4.89}$$

$$\mathbf{C}_a = \mathbf{D}_a^{(0)} + \mathbf{D}_a^{(1)} a_0 + \mathbf{D}_a^{(2)} a_0^2 + \ldots. \tag{4.90}$$

where all the scale dependence resides in the expansion coefficients. At $\mu = Q$, coefficient functions and PDFs are denoted by

$$\mathbf{q}_a(\mu = Q) \equiv \mathbf{q}_{a,0} = \mathbf{q}_{a,0}^{(0)} + \mathbf{q}_{a,0}^{(1)} a_0 + \mathbf{q}_{a,0}^{(2)} a_0^2 + \ldots, \tag{4.91}$$

$$\mathbf{C}_a(\mu = Q) \equiv \mathbf{C}_{a,0} = \mathbf{D}_{a,0}^{(0)} + \mathbf{D}_{a,0}^{(1)} a_0 + \mathbf{D}_{a,0}^{(2)} a_0^2 + \ldots. \tag{4.92}$$

The evolution of $a(\mu)$ is governed by the beta function

$$\frac{da}{dL} = a(\beta_0 a + \beta_1 a^2 + \ldots), \tag{4.93}$$

where $L \equiv \ln \frac{Q^2}{\mu^2}$. If we plug in Eq. (4.88), we can solve the differential equation for the coefficients A_i order by order and obtain

$$a = a_0 + \beta_0 L a_0^2 + (\beta_0^2 L^2 + \beta_1) a_0^3 + \cdots. \tag{4.94}$$

Similarly, the explicit form of the PDFs can be determined by solving the DGLAP equation in the following form

$$\frac{d\mathbf{q}_a}{dL} = -\mathbf{P} \otimes \mathbf{q}_a. \tag{4.95}$$

To expand RHS we use Eq. (4.89) and

$$\begin{aligned}
\mathbf{P} &= \mathbf{P}^{(0)}a + \mathbf{P}^{(1)}a^2 + \mathbf{P}^{(2)}a^3 + \cdots \qquad (4.96)\\
&= \mathbf{P}^{(0)}a_0 + (\beta_0 L\mathbf{P}^{(0)} + \mathbf{P}^{(1)})a_0^2 + \left[(\beta_0^2 L^2 + \beta_1 L)\mathbf{P}^{(0)} + 2\beta_0 L\mathbf{P}^{(1)} + \mathbf{P}^{(2)}\right] a_0^3 + \cdots \qquad (4.97)
\end{aligned}$$

The first few expansion coefficients of PDFs are found to be

$$\mathbf{q}_a^{(0)} = \mathbf{q}_{a,0}^{(0)}, \qquad (4.98)$$

$$\mathbf{q}_a^{(1)} = -L\mathbf{P}^{(0)} \otimes \mathbf{q}_{a,0}^{(0)} + \mathbf{q}_{a,0}^{(1)}, \qquad (4.99)$$

$$\mathbf{q}_a^{(2)} = \frac{1}{2}(L^2\mathbf{P}^{(0)} \otimes \mathbf{P}^{(0)} - 2L\mathbf{P}^{(1)} - \beta_0 L^2\mathbf{P}^{(0)}) \otimes \mathbf{q}_{a,0}^{(0)} - L\mathbf{P}^{(0)} \otimes \mathbf{q}_{a,0}^{(1)} + \mathbf{q}_{a,0}^{(2)}, \qquad (4.100)$$

$$\begin{aligned}
\mathbf{q}_a^{(3)} = &\left[-\frac{1}{6}L^3\mathbf{P}^{(0)} \otimes \mathbf{P}^{(0)} \otimes \mathbf{P}^{(0)} + \frac{1}{2}\beta_0 L^3\mathbf{P}^{(0)} \otimes \mathbf{P}^{(0)} + L^2\mathbf{P}^{(0)} \otimes \mathbf{P}^{(1)}\right.\\
&\left. - (\frac{1}{3}\beta_0^2 L^3 + \frac{1}{2}\beta_1 L^2)\mathbf{P}^{(0)} - \beta_0 L^2\mathbf{P}^{(1)} - L\mathbf{P}^{(2)}\right] \otimes \mathbf{q}_{a,0}^{(0)}\\
&+ \left(\frac{1}{2}L^2\mathbf{P}^{(0)} \otimes \mathbf{P}^{(0)} - \frac{1}{2}\beta_0 L^2\mathbf{P}^{(0)} - L\mathbf{P}^{(1)}\right) \otimes \mathbf{q}_{a,0}^{(1)} - L\mathbf{P}^{(0)} \otimes \mathbf{q}_{a,0}^{(2)} + \mathbf{q}_{a,0}^{(3)}. \qquad (4.101)
\end{aligned}$$

Now, if we impose scale invariance of the singlet and gluon structure functions

$$\mathbf{C}_a(\mu) \otimes \mathbf{q}_a(\mu) = \mathbf{C}_{a,0} \otimes \mathbf{q}_{a,0} \qquad (4.102)$$

we can obtain $\mathbf{C}_a^{(i)}(\mu)$ for arbitrary μ in terms of $\mathbf{C}_{a,0}^{(i)}$ for $\mu = Q$. Up to third order the coefficients with arbitrary scale are given by

$$\mathbf{C}_a(x, \alpha_s(\mu), L) = \mathbf{c}_a^{(0)}(x) + \sum_{l=1}^{3} a_s^l \left(\mathbf{c}_a^{(l)}(x) + \sum_{m=1}^{l} \mathbf{c}_a^{(l,m)}(x)L^m\right) + \ \ldots\ , \qquad (4.103)$$

with

$$\begin{aligned}
\mathbf{c}_a^{(1,1)} &= \mathbf{c}_a^{(0)} \otimes \mathbf{P}^{(0)},\\
\mathbf{c}_a^{(2,1)} &= \mathbf{c}_a^{(0)} \otimes \mathbf{P}^{(1)} + \mathbf{c}_a^{(1)} \otimes (\mathbf{P}^{(0)} - \beta_0\mathbf{1}),\\
\mathbf{c}_a^{(2,2)} &= \frac{1}{2}\mathbf{c}_a^{(1,1)} \otimes (\mathbf{P}^{(0)} - \beta_0\mathbf{1}),
\end{aligned}$$

$$
\begin{aligned}
\mathbf{c}_a^{(3,1)} &= \mathbf{c}_a^{(0)} \otimes \mathbf{P}^{(2)} + \mathbf{c}_a^{(1)} \otimes (\mathbf{P}^{(1)} - \beta_1 \mathbf{1}) + \mathbf{c}_a^{(2)} \otimes (\mathbf{P}^{(0)} - 2\beta_0 \mathbf{1}), \\
\mathbf{c}_a^{(3,2)} &= \frac{1}{2}\left\{ \mathbf{c}_a^{(1,1)} \otimes (\mathbf{P}^{(1)} - \beta_1 \mathbf{1}) + \mathbf{c}_a^{(2,1)} \otimes (\mathbf{P}^{(0)} - 2\beta_0 \mathbf{1}) \right\}, \\
\mathbf{c}_a^{(3,3)} &= \frac{1}{3}\mathbf{c}_a^{(2,2)} \otimes (\mathbf{P}^{(0)} - 2\beta_0 \mathbf{1}) \ .
\end{aligned} \tag{4.104}
$$

Similar expressions for the non-singlet coefficient functions can also be derived, in which case the evolution of the corresponding non-singlet PDF obeys

$$
\frac{dq_{a,NS}}{dL} = -P_{NS}^{+} \otimes q_{a,NS}. \tag{4.105}
$$

In the following we give the NS and PS components of $\mathbf{c}_a^{(l,m)}$ in terms of scale independent coefficients and splitting functions at N3LO. The non-singlet coefficient functions are

$$
c_{2,q}^{(3,3),NS} = \frac{1}{6}P_{qq}^{(0)} \otimes P_{qq}^{(0)} \otimes P_{qq}^{(0)} - \frac{1}{2}\beta_0 P_{qq}^{(0)} \otimes P_{qq}^{(0)} + \frac{1}{3}\beta_0^2 P_{qq}^{(0)}, \tag{4.106}
$$

$$
\begin{aligned}
c_{2,q}^{(3,2),NS} &= -\frac{1}{3}\beta_0 c_{2,q}^{(1)} \otimes P_{qq}^{(0)} + \frac{1}{2}c_{2,q}^{(1)} \otimes P_{qq}^{(0)} \otimes P_{qq}^{(0)} + P_{qq}^{(1),NS} \otimes P_{qq}^{(0)}, \\
&\quad + \beta_0^2 c_{2,q}^{(1)} - \beta_0 P_{qq}^{(1),NS} - \frac{1}{2}\beta_1 P_{qq}^{(0)},
\end{aligned} \tag{4.107}
$$

$$
c_{2,q}^{(3,1),NS} = c_{2,q}^{(2),NS} \otimes P_{qq}^{(0)} + c_{2,q}^{(1)} \otimes P_{qq}^{(1),NS} - \beta_1 c_{2,q}^{(1)} - 2\beta_0 c_{2,q}^{(2),NS} + P_{qq}^{(2),NS}, \tag{4.108}
$$

$$
c_{L,q}^{(3,3),NS} = 0 \tag{4.109}
$$

$$
c_{L,q}^{(3,2),NS} = -\frac{2}{3}\beta_0 c_{L,q}^{(1)} \otimes P_{qq}^{(0)} + \frac{1}{2}c_{L,q}^{(1)} \otimes P_{qq}^{(0)} \otimes P_{qq}^{(0)} + \beta_0^2 c_{L,q}^{(1)}, \tag{4.110}
$$

$$
c_{L,q}^{(3,1),NS} = c_{L,q}^{(2),NS} \otimes P_{qq}^{(0)} + c_{L,q}^{(1)} \otimes P_{qq}^{(1),NS} - \beta_1 c_{L,q}^{(1)} - 2\beta_0 c_{L,q}^{(2),NS}. \tag{4.111}
$$

where we have used the leading order result $\mathbf{C}_2^{(0)}(x) = (\delta(1-x)\ 0)$ and $\mathbf{C}_L^{(0)}(x) = (0\ 0)$ to simplify the expressions. Note that the non-zero pure-singlet splitting functions start to enter at NNLO. The PS functions are given by

$$
\begin{aligned}
c_{2,q}^{(3,3),PS} &= \frac{1}{6}P_{qg}^{(0)} \otimes P_{gg}^{(0)} \otimes P_{gq}^{(0)} + \frac{1}{6}P_{qq}^{(0)} \otimes P_{qg}^{(0)} \otimes P_{gq}^{(0)} + \frac{1}{6}P_{qg}^{(0)} \otimes P_{gq}^{(0)} \otimes P_{qq}^{(0)}, \\
&\quad - \frac{1}{2}\beta_0 P_{qg}^{(0)} \otimes P_{gq}^{(0)},
\end{aligned} \tag{4.112}
$$

$$c_{2,q}^{(3,2),PS} = \frac{1}{2}c_{2,g}^{(1)} \otimes P_{gq}^{(0)} \otimes P_{qg}^{(0)} + \frac{1}{2}c_{2,g}^{(1)} \otimes P_{gq}^{(0)} \otimes P_{qq}^{(0)} - \frac{2}{3}\beta_0 c_{2,g}^{(1)} \otimes P_{gq}^{(0)} + \frac{1}{2}c_{2,q}^{(1)} \otimes P_{qg}^{(0)} \otimes P_{gq}^{(0)},$$
$$+ \frac{1}{2}P_{qg}^{(1)} \otimes P_{gq}^{(0)} + P_{qq}^{(1),PS} \otimes P_{qq}^{(0)} - \beta_0 P_{qq}^{(1),PS} + \frac{1}{2}P_{qg}^{(0)} \otimes P_{gq}^{(1)}, \tag{4.113}$$
$$c_{2,q}^{(3,1),PS} = c_{2,g}^{(2)} \otimes P_{gq}^{(0)} + c_{2,q}^{(2),PS} \otimes P_{qq}^{(0)} + c_{2,g}^{(1)} \otimes P_{gq}^{(1)} + c_{2,q}^{(1)} \otimes P_{qq}^{(1),PS} - 2\beta_0 c_{2,q}^{(2),PS},$$
$$+ P_{qq}^{(2),PS}, \tag{4.114}$$
$$c_{L,q}^{(3,3),PS} = 0, \tag{4.115}$$
$$c_{L,q}^{(3,2),PS} = \frac{1}{2}c_{L,g}^{(1)} \otimes P_{gq}^{(0)} \otimes P_{qg}^{(0)} + \frac{1}{2}c_{L,g}^{(1)} \otimes P_{gq}^{(0)} \otimes P_{qq}^{(0)} + \frac{1}{2}c_{L,q}^{(1)} \otimes P_{qg}^{(0)} \otimes P_{gq}^{(0)},$$
$$- \frac{2}{3}\beta_0 c_{L,g}^{(1)} \otimes P_{gq}^{(0)}, \tag{4.116}$$
$$c_{L,q}^{(3,1),PS} = c_{L,g}^{(2)} \otimes P_{gq}^{(0)} + c_{L,q}^{(2),PS} \otimes P_{qq}^{(0)} + c_{L,g}^{(1)} \otimes P_{gq}^{(1)} + c_{L,q}^{(1)} \otimes P_{qq}^{(1),PS} - 2\beta_0 c_{L,q}^{(2),PS}. \tag{4.117}$$

The gluon functions are

$$c_{2,g}^{(3,3)} = \frac{1}{6}P_{qg}^{(0)} \otimes P_{gg}^{(0)} \otimes P_{gg}^{(0)} + \frac{1}{6}P_{qq}^{(0)} \otimes P_{qg}^{(0)} \otimes P_{gg}^{(0)} + \frac{1}{6}P_{qg}^{(0)} \otimes P_{gq}^{(0)} \otimes P_{qg}^{(0)},$$
$$+ \frac{1}{6}P_{qq}^{(0)} \otimes P_{qq}^{(0)} \otimes P_{qg}^{(0)} - \frac{1}{2}\beta_0 P_{qg}^{(0)} \otimes P_{gg}^{(0)} - \frac{1}{2}\beta_0 P_{qq}^{(0)} \otimes P_{qg}^{(0)} + \frac{1}{3}\beta_0^2 P_{qg}^{(0)}, \tag{4.118}$$

$$c_{2,g}^{(3,2)} = \frac{1}{2}c_{2,g}^{(1)} \otimes P_{gg}^{(0)} \otimes P_{gg}^{(0)} + \frac{1}{2}c_{2,g}^{(1)} \otimes P_{gq}^{(0)} \otimes P_{qg}^{(0)} + \frac{1}{2}c_{2,q}^{(1)} \otimes P_{qg}^{(0)} \otimes P_{gg}^{(0)},$$
$$+ \frac{1}{2}c_{2,q}^{(1)} \otimes P_{qq}^{(0)} \otimes P_{qg}^{(0)} - \frac{2}{3}\beta_0 c_{2,g}^{(1)} \otimes P_{gg}^{(0)} - \frac{2}{3}\beta_0 c_{2,q}^{(1)} \otimes P_{qg}^{(0)} + \frac{1}{2}P_{qg}^{(0)} \otimes P_{gg}^{(1)},$$
$$+ \frac{1}{2}P_{qg}^{(1)} \otimes P_{gg}^{(0)} + \frac{1}{2}P_{qq}^{(0)} \otimes P_{qg}^{(1)} + \frac{1}{2}P_{qq}^{(1)} \otimes P_{qg}^{(0)} + \beta_0^2 c_{2,q}^{(1)} - \frac{1}{2}\beta_1 P_{qg}^{(0)} - \beta_0 P_{qg}^{(1)}, \tag{4.119}$$

$$c_{2,g}^{(3,1)} = c_{2,g}^{(2)} \otimes P_{gg}^{(0)} + c_{2,q}^{(2)} \otimes P_{qg}^{(0)} + c_{2,g}^{(1)} \otimes P_{gg}^{(1)} + c_{2,q}^{(1)} \otimes P_{qg}^{(1)} - \beta_1 c_{2,g}^{(1)} - 2\beta_0 c_{2,g}^{(2)} + P_{qg}^{(2)}, \tag{4.120}$$

$$c_{L,g}^{(3,3)} = 0, \tag{4.121}$$
$$c_{L,g}^{(3,2)} = \frac{1}{2}c_{L,g}^{(1)} \otimes P_{gg}^{(0)} \otimes P_{gg}^{(0)} + \frac{1}{2}c_{L,g}^{(1)} \otimes P_{gq}^{(0)} \otimes P_{qg}^{(0)} + \frac{1}{2}c_{L,q}^{(1)} \otimes P_{qg}^{(0)} \otimes P_{gg}^{(0)},$$
$$+ \frac{1}{2}c_{L,q}^{(1)} \otimes P_{qq}^{(0)} \otimes P_{qg}^{(0)} - \frac{2}{3}\beta_0 c_{L,g}^{(1)} \otimes P_{gg}^{(0)} - \frac{2}{3}\beta_0 c_{L,q}^{(1)} \otimes P_{qg}^{(0)} + \beta_0^2 c_{L,q}^{(1)}, \tag{4.122}$$

$$c_{L,g}^{(3,1)} = c_{L,g}^{(2)} \otimes P_{gg}^{(0)} + c_{L,q}^{(2)} \otimes P_{qg}^{(0)} + c_{L,g}^{(1)} \otimes P_{gg}^{(1)} + c_{L,q}^{(1)} \otimes P_{qg}^{(1)} - \beta_1 c_{L,g}^{(1)} - 2\beta_0 c_{L,g}^{(2)}. \tag{4.123}$$

Therefore, to compute the scale-dependent terms, one needs the splitting functions as well as coefficients at a fixed scale up to NNLO accuracy. The former can be found in [35,36], and the latter are given in [63,64]. These publications contain both analytical expressions of these functions and their approximate forms obtained by fitting the exact expressions, using much simpler functions in an x range covering the kinematics of current experiments. Since the scale uncertainty is a higher-order effect, it suffices to use the approximate functions to compute the convolutions in the expressions above. Nevertheless, the resulting scale dependent terms at N3LO can be lengthy and contain harmonic polylogarithms [72] of high weights, which would slow down further convolution with PDFs when computing the cross sections. Thus, these parts are also fitted using simpler functions. The expressions for numerical implementation are given in appendix. A

4.5. Numerical results

In this section I present some of the numerical implications of the implementation of the N3LO terms, based on the coefficient functions derived in the previous section. We focus on contributions with charm quarks at HERA, i.e. the most phenomenologically relevant application of our formalism.

4.5.1. μ and λ dependence

In the following discussion we distinguish two definitions of structure functions with heavy quark contributions, F_{2c} and F_{2h}. F_{2c} is an experimentally measured *semi-inclusive* structure function, in which at least one charm quark is observed in the final state. This function is well-defined only when Q is close to the heavy-quark mass m_h; it becomes infrared-unsafe at $Q \gg m_h$. In contrast, F_{2h} includes charm quark contributions only for diagrams where the incoming photon couples to a charm quark directly. F_{2h} cannot be measured on its own, but is well-defined in QCD theory.

We have plotted the x dependence of the semi-inclusive structure function F_{2h} for selected factorization scale choices as well as for selected rescaling variable values near the charm quark threshold region.

Even at N3LO, the IM predictions show larger dependence on the QCD scale μ and rescaling parameter λ in Eq.(4.65), than the numerically stable N2LO GM prediction. This is expected, given the approximate nature of the IM coefficient functions. For example, subfigures (a) and (b) in Fig. 4.8 show scale dependence of NNLO and N3LO predictions in intermediate mass scheme. Here we choose $\lambda = 0.3$ in the rescaling variable for all the IM curves. The factorization scales are taken to be $\mu_F^2 = Q^2, Q^2 + 2m_c^2, Q^2 + 4m_c^2$, for the three curves at each order. Increasing the scale tends to raise the IM curves by a significant amount compared to the GM curves. Though there is a slight decreasing trend of the scale uncertainty as higher order corrections are included, the convergence is much slower than the GM result in (a). The missing mass dependence in IM scheme clearly plays an important role for the production of heavy quarks at a Q value near their threshold. Meanwhile, the scale convergence from NNLO to N3LO is also affected by the evolution of PDFs and the strong coupling α_S, which are evolved only up to NNLO. They give another source of missing scale dependence at N3LO.

Fig. 4.9 shows the effect due to the variation of λ. Subfigure (a) shows the λ dependence of the IM predictions at the fixed factorization scale $\mu_F^2 = Q^2 + 4m_c^2$. The predictions are compared with the GM scheme for F_{2c} and F_{2h}. The difference between these two definitions is due to the contribution from light-quark initiated production of heavy-quark pairs. The plot shows that the difference is essentially not

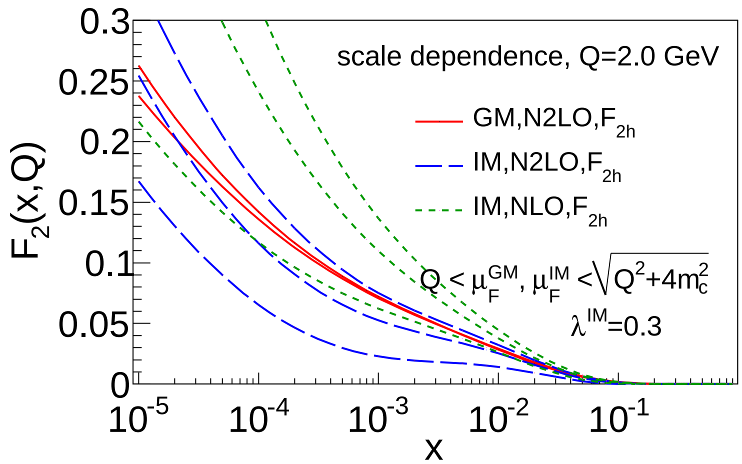

(a)

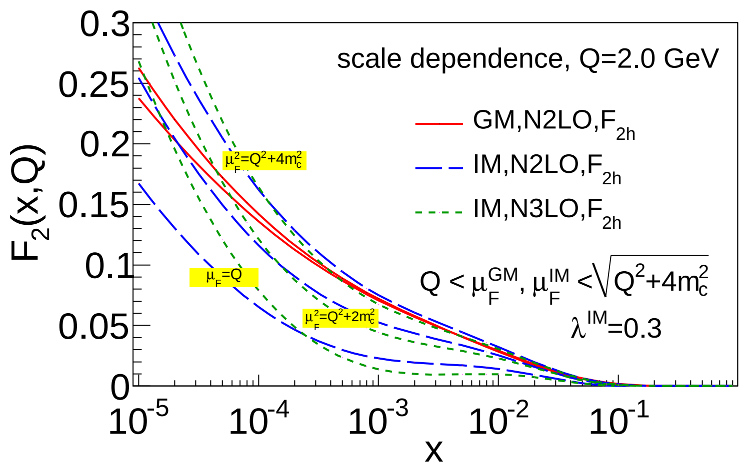

(b)

Figure 4.8. Factorization scale dependence of IM and GM schemes up to NNLO (upper subfigure) and N3LO (lower subfigure).

noticeable. As is shown before, a large value of λ tends to raise the prediction. There is no convergence of the uncertainty due to variation of λ. IM predictions with λ of order 0.2-0.3 are closer to the NNLO GM result than those with $\lambda = 0$. This has been also observed earlier at NLO [65].

4.5.2. Q dependence

The dependence of the structure function F_{2h} on Q is plotted for various schemes and μ and λ values, as shown in Fig. 4.10. In almost the whole Q spectrum the kinematic constraint results in an effect of suppression of the N3LO IM curve, when compared with the N3LO GM curve with the same μ and λ. However, as we have observed previously, we can get the two predictions much closer by setting $\mu = 1.36Q$ and $\lambda = 0.2$. Curves obtained in various VFN schemes tend to converge at large Q, while the FFN curve has a substantial deviation in the same region, as expected. Therefore, the NNLO IM prediction with $\lambda = 0.2$ can be used as a reasonable approximation to the GM prediction at NNLO.

4.6. Conclusions

In this chapter, we have developed a method to systematically classify and organize QCD radiative corrections from heavy quark flavors at N3LO. This is the first study of inclusive DIS with the heavy-quark mass effect from the $O(\alpha_s^3)$ corrections in the S-ACOT-χ scheme. The mass effect is relevant for the measurements at the LHC such as Higgs production and W and Z productions. The results are useful for calculations in both general-mass scheme and intermediate mass scheme. The numerical implementation is at present for IM scheme using the zero-mass coefficient functions computed by Vermaseren, Vogt, and Moch [63,64]. The programming of the IM implementation is integrated into the CTEQ fitting code for future use. Once the

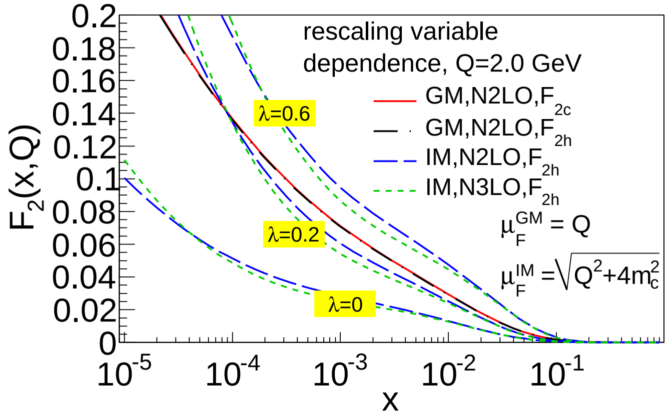

Figure 4.9. Rescaling variable dependence of IM and GM schemes up to N3LO.

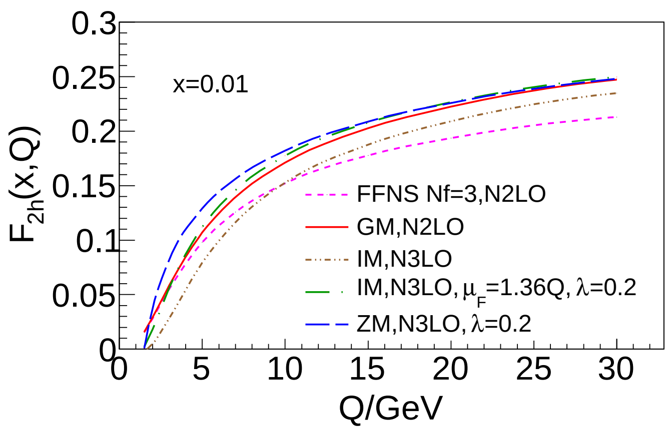

Figure 4.10. Q dependence of FFN, ZM, IM, and GM schemes up to N3LO.

three-loop massive coefficient functions for flavor-creation channels are published, we will be able to use them and our framework to realize an N3LO factorization in GM scheme with the full mass dependence. For numerical purpose we have also computed the three-loop ZM coefficients at an arbitrary factorization scale (Appendix A). The parameterization of these functions have not been given explicitly in previous works.

In our numerical calculations, we have found that the IM structure function converges to the ZM scheme calculation at large Q, as expected. However, near the heavy quark production threshold, both IM and ZM schemes cannot give reliable predictions due to missing of mass dependence from coefficient functions. In particular, the factorization scale uncertainty of the IM scheme does not converge from NLO to N3LO calculations. The uncertainty due to variation of the rescaling variable λ shows the same pattern. These observations tell us that the high order corrections in IM scheme are not reliably small near the heavy quark threshold. Combining them with lower order calculation in IM or GM schemes will not improve the accuracy of the calculation. Nevertheless, we have found that we can vary the scale μ together with λ in IM scheme to mimic the reliable prediction from the GM scheme. The preferred values over the range 1.5GeV$< Q <$30GeV are found approximately to be $\mu = 1.36Q$ and $\lambda = 0.2$.

Chapter 5

TMD FACTORIZATION

QCD factorization methods utilizing transverse-momentum-dependent (TMD) parton distributions and fragmentation functions provide a powerful framework for describing multiscale observables in high-energy hadron interactions. Production of Drell-Yan lepton-antilepton pairs in Z/γ^* boson production in hadron-hadron collisions is one basic process in which TMD factorization is applied. In this chapter, we present a detailed analysis of the factorization for Drell-Yan production of vector bosons at hadron colliders, and examine the issue with evolution of the cross section at small transverse momentum where nonperturbative contribution to the cross section becomes important[1]. We first review the factorization of Drell-Yan process in various cases, then we extend a popular formalism of TMD factorization to perform a phenomenological study using data from hadron colliders.

5.1. Factorization in Drell-Yan process

In Drell-Yan process $h_A(p_A)h_B(p_B) \to l\bar{l}(q)X$, the produced vector boson with momentum q^μ decays into a pair of leptons. As long as $Q \equiv \sqrt{q^2}$ is sufficiently larger than the infrared QCD scale Λ, the leading contribution to the cross section comes from the region of the form in Fig. 5.1, where the vector boson decay belongs to the hard part of the diagram. The cross section of this process then reads

$$\frac{d\sigma}{dQ^2} = \sum_{a,b} \int d\xi_A d\xi_B f_{a/A}(\xi_A) f_{b/B}(\xi_B) \frac{d\hat{\sigma}}{dQ^2} + \text{power suppressed terms} \tag{5.1}$$

[1]The discussion here is mostly from a work by M. Guzzi, P. Nadolsky, and B. Wang [73]

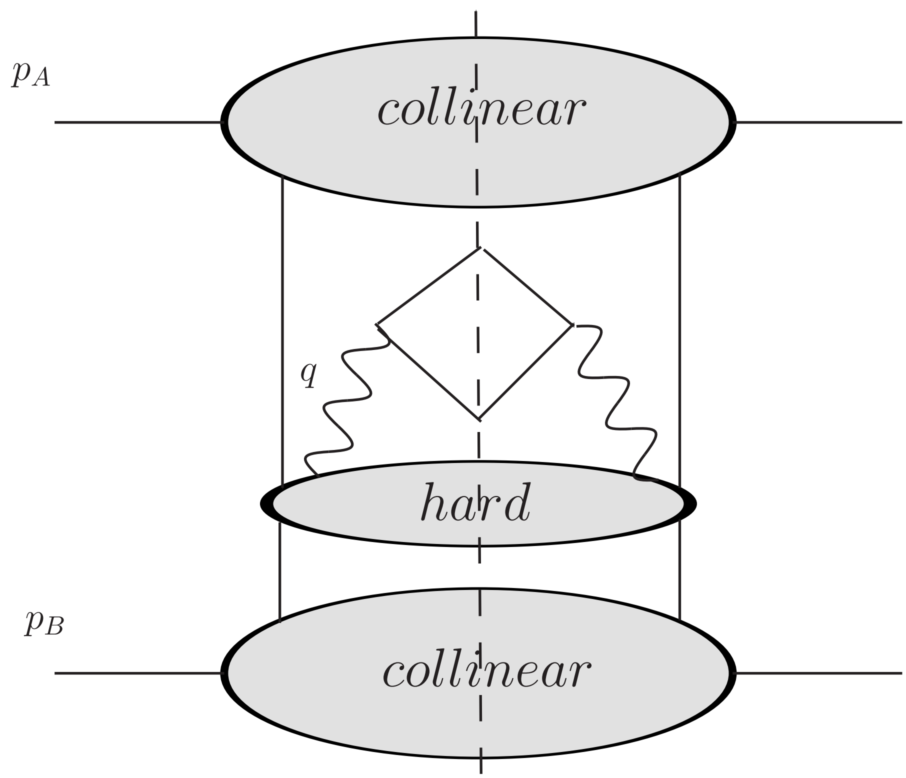

Figure 5.1. Leading region of Drell-Yan process when the transverse momentum of the lepton pair is large or not observed.

where $d\hat{\sigma}/dQ^2$ represents the cross section of the parton level process in the center of Fig. 5.1. This factorization formula works equally well for differential cross sections with respect to other kinematic variables of the vector boson such as the rapidity y, and lepton angular variables. It also works for distributions in transverse momentum Q_T with a value comparable to the hard scale Q. However, this is no longer the case if the phase space contains multiple momentum scales that are well separated. For instance, if one carries out to a fixed order $O(\alpha_s^n)$ a perturbative calculation of the distribution of the vector boson's transverse momentum Q_T, using (collinear) factorization similar to Eq. 5.1, the resulting cross section contains large logarithms up to $\alpha_s^n \ln^{2n-1}(Q_T^2/Q^2)$. Therefore, the perturbation series fails to converge and the cross section blows up as $Q_T/Q \to 0$, which is not supported by data from experiment. People seek to develop a more intricate factorization procedure to separate factors that depend on various scales. The proper evolution of these factors resums the large log terms to all orders and results in a convergent cross section. Such a factorization/resummation formalism has first been developed in the classical papers by Collins, Soper, and Sterman (CSS) [1, 15–18] . The pictorial description of factorization at small Q_T is shown in Fig. 5.2, where a soft factor S is separated from the lepton-vector boson vertex and contains the all order sum of the large logarithms.

An important distinction of factorization in Fig. 5.2 from the collinear factorization in Fig. 5.1 is that the latter fails to include the contribution from radiated soft gluons with small transverse momenta of order Q_T, while the former accounts for this contribution by enforcing the conservation of transverse momenta and using transverse momentum dependent (TMD) distributions for the partons. The cross section takes the form

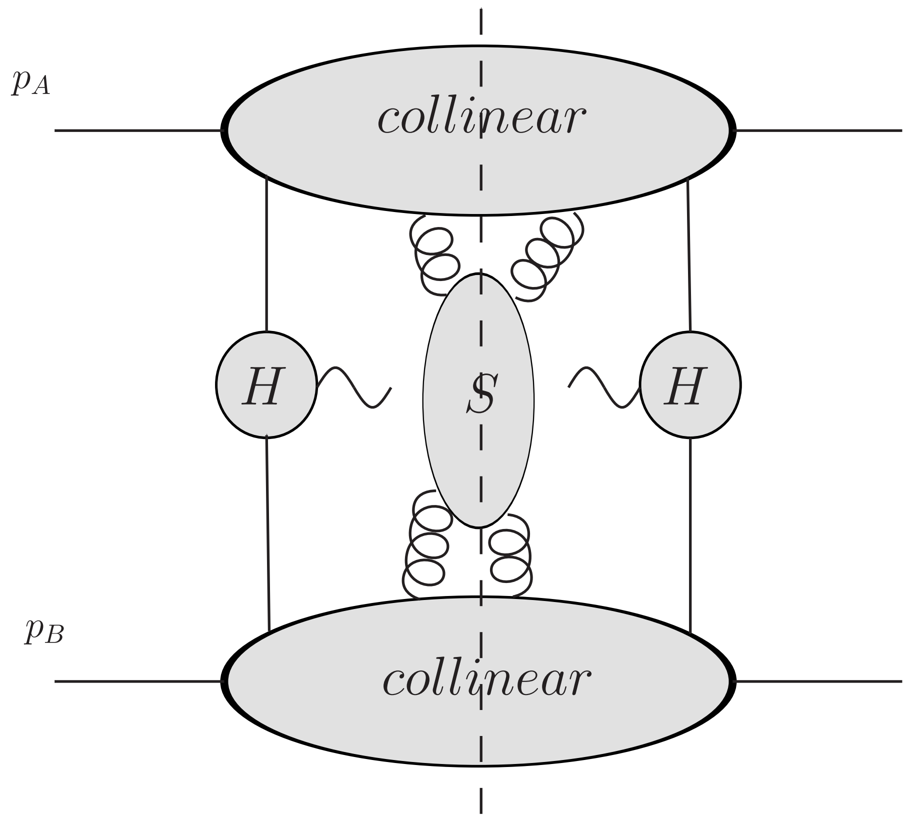

Figure 5.2. Leading region of Drell-Yan process for small transverse momentum of the lepton pair .

$$\frac{d\sigma}{dQ^2 dy dQ_T} = \sum_{a,b} H_{a,b}(Q^2) \int d\mathbf{k}_{AT} d\mathbf{k}_{BT} d\mathbf{k}_{ST} P_{a/A}(\mathbf{k}_{AT}) P_{b/B}(\mathbf{k}_{BT}) S(\mathbf{k}_{ST})$$
$$\times\, \delta^2(\mathbf{Q}_T - \mathbf{k}_{AT} - \mathbf{k}_{BT} - \mathbf{k}_{ST}) + \text{power suppressed terms}, \qquad (5.2)$$

where $H_{a,b}$, S, $P_{a/A}$, and $P_{b/B}$ correspond to the hard, soft, and the collinear factors, respectively, in Fig. 5.2, and the transverse momenta of the soft and collinear factors are denoted by $\mathbf{k}_{ST}$, $\mathbf{k}_{AT}$, and $\mathbf{k}_{BT}$.

As we have seen, the Collinear QCD factorization is applicable for describing lepton pairs with Q_T of order of the invariant mass Q of the pair. The respective large-Q_T cross sections have been computed up to two loops in the QCD coupling strength α_s [74–77] and are in reasonable agreement with the data.

But, at small Q_T, all-order resummation of large logarithms $\ln(Q_T/Q)$ needs to be performed [78–80] to obtain sensible cross sections. TMD factorization, such as the CSS formalism, provides a systematic framework for Q_T resummation to all orders in α_s. The resummed cross sections have been computed at various QCD orders in the CSS formalism and kindred approaches [76, 77, 81–90]. In addition to perturbative radiative contributions, the resummed cross sections include a nonperturbative component associated with QCD dynamics at momentum scales below 1 GeV. Understanding of the nonperturbative terms is important for tests of TMD factorization and precision studies of electroweak boson production, including the measurement of W boson mass [91].

Instead of measuring Q_T distributions directly, one can measure the distribution in the angle ϕ^*_η [92] that is closely related to Q_T/Q. The ϕ^*_η distributions have been recently measured both at the Tevatron [21] and Large Hadron Collider [19, 20]. Small experimental errors of the ϕ^*_η measurements (as low as 0.5%) allow one to test the Q_T resummation formalism at an unprecedented level. On the theory side, the small-Q_T resummed form factor for Z boson production has been computed to NNLL/NNLO [93]. We would like to confront precise theoretical predictions implemented in programs LEGACY and RESBOS [94–96] by the new experimental data to obtain quantitative constraints on the nonperturbative contributions.

Such analysis is technically challenging and requires to examine several effects that were negligible in the previous studies of the resummed nonperturbative terms [94,96,97]. The framework for the fitting for Drell-Yan processes in the CSS formalism must be extended to the ϕ^*_η, rather than Q_T, distributions. Nonperturbative effects must be distinguished from comparable modifications by NNLO QCD corrections and NLO electroweak (EW) corrections.

To carry out this study, we modified the Q_T resummation calculation employed in our previous studies to evaluate NNLO QCD (α_s^2) and NLO EW (α_{EW}) perturbative contributions and consider the residual QCD scale dependence associated with higher-order terms. This implementation was utilized to determine the nonperturbative factor from the DØ Run-2 data on the ϕ^*_η distributions.

Our findings shed light on several questions raised in recent studies of TMD factorization [98–110] and soft-collinear-effective (SCET) theory [111–113]. We examine if the ϕ^*_η data corroborate the universal behavior of the resummed nonperturbative terms that is expected from the TMD factorization theorem [18] and was observed in the global analyses of Drell-Yan Q_T distributions at fixed-target and collider energies [96, 97]. We also investigate the rapidity dependence of the nonperturbative terms, which may be indicative of new types of higher-order contributions [114]. It has been argued [77, 88–90, 115] that the evidence for nonperturbative smearing is inconclusive at the NLL+NLO level because of a large scale dependence. To address this point, we fully include the scale dependence in the resummed cross section up to $\mathcal{O}(\alpha_s^2)$, *i.e.* NNLL/NNLO. We argue that the impact of the power-suppressed contributions is generically distinct from the scale dependence: the nonperturbative effects can be distinguished from the NNLO scale uncertainties.

A significant nonperturbative component that we find is consistent with a universal quadratic (Gaussian) power-suppressed contribution of the magnitude corroborated in 2005 [97]. The DØ data are precise enough and may be able to distinguish between the Gaussian and alternative nonperturbative functions that have been recently proposed [116].

The current chapter documents this analysis in detail and is organized as follows. Section 5.2 reviews the relation between the ϕ_η^* angle and transverse momentum Q_T in the Collins-Soper-Sterman notations (Sec. 5.2.1), general structure of the resummed cross section and estimation of NNLO contributions and their scale dependence (Secs. 5.2.2, 5.2.3, 5.2.4), nonperturbative model (Sec. 5.2.5), matching of the small-Q_T and large-Q_T terms (Sec. 5.2.6) and photon radiation (Sec. 5.2.7). Next, in Sec. 5.3, the size of the nonperturbative contributions is estimated by a χ^2 analysis of the DØ data in three bins of vector boson rapidity (y_Z), by applying two different methods to examine the scale dependence of the resummed cross section. By using the constraining power of this data set, we suggest a Gaussian smearing factor suitable for W and Z production, and we give an estimate at 68% C.L. for the leading parameter of the NP functional form. We provide the user with several sets of grids of theory predictions for phenomenological applications based on CT10 NNLO [117] PDF eigenvector grids and for scans of the nonperturbative smearing function and estimates of its uncertainty in future measurements.

5.2. Overview of the resummation method

5.2.1. Relation between Q_T and ϕ^*_η variables

The CSS resummation formalism predicts fully differential distributions in electroweak boson production, including decay of heavy bosons. While the original formulation of the CSS formalism deals with resummation of logarithms dependent on the boson's transverse momentum Q_T, it can be readily extended to resum angular variables of decay particles. One such variable is the azimuthal angle separation $\Delta\varphi$ of the leptons in the lab frame, which approaches π (back-to-back production of leptons in the transverse plane) when $Q_T \to 0$. Consequently, the region $\Delta\varphi \to \pi$ is sensitive to small-Q_T resummation [95].

Recently, an angular variable ϕ^*_η was proposed in [92] that has an experimental advantage compared to Q_T and $\Delta\varphi$. The ϕ^*_η variable is not affected by the experimental resolution on the magnitudes of the leptons' (transverse) momenta that limits the accuracy of the Q_T measurement. Soft and collinear resummation for the ϕ^*_η distribution can be worked out either analytically [88–90, 115] or numerically by integrating the resummed Q_T distribution over the leptons' phase space.

To describe decays of massive bosons, the CSS formalism [95] usually operates with the lepton polar angle θ_{CS} and azimuthal angle φ_{CS} in the Collins-Soper (CS) reference frame [118]. The CS frame is a rest frame of the vector boson in which the z axis bisects the angle formed by the momenta $\vec{p}_1$ and -$\vec{p}_2$ of the incident quark and antiquark. In the CS frame, the decay leptons escape back-to-back ($\vec{l}_1 + \vec{l}_2 = 0$), and the electron's and positron's 4-momenta are

$$l_1^\mu|_{\text{CS frame}} = (Q/2)\left\{1, \cos\varphi_{CS}\sin\theta_{CS}, \sin\varphi_{CS}\sin\theta_{CS}, \cos\theta_{CS}\right\}, \qquad (5.3)$$

and

$$l_2^\mu|_{\text{CS frame}} = (Q/2)\left\{1, -\cos\varphi_{CS}\sin\theta_{CS}, -\sin\varphi_{CS}\sin\theta_{CS}, -\cos\theta_{CS}\right\}. \qquad (5.4)$$

On the other hand, the angular variable ϕ^*_η is defined in a different frame ("η frame"), in which the leptons escape θ^*_η and $\pi - \theta^*_\eta$ with respect to the incident beams direction. The η frame is related to the lab frame by a boost $\beta = \tanh((\eta_1 + \eta_2)/2)$ along the incident beam direction, where η_1 and η_2 are the pseudorapidities of l^- and l^+ in the lab frame. The frame coincides with the CS frame when $Q_T = 0$. Knowing the polar angle θ^*_η in the η frame and the difference $\Delta\varphi = \varphi_1 - \varphi_2$ of the lepton's azimuthal angles in the transverse plane to the beam direction, one defines

$$\phi^*_\eta = \tan(\phi_{acop}/2)\sin\theta^*_\eta \qquad (5.5)$$

in terms of the acoplanarity angle $\phi_{acop} = \pi - \Delta\varphi$. We write $\cos\theta^*_\eta$ as a function of the lepton momenta in the lab frame as

$$\cos\theta^*_\eta = \tanh\left(\frac{\eta_1 - \eta_2}{2}\right) = \frac{\sqrt{l_1^+ l_2^-} - \sqrt{l_1^- l_2^+}}{\sqrt{l_1^+ l_2^-} + \sqrt{l_1^- l_2^+}} = \frac{f(\cos\theta_{CS}) - f(-\cos\theta_{CS})}{f(\cos\theta_{CS}) + f(-\cos\theta_{CS})}, \qquad (5.6)$$

where $l^\pm_{1,2} = (l^0_{1,2} \pm l^z_{1,2})/\sqrt{2}$,

$$f(\cos\theta_{CS}) \equiv \sqrt{M_T^2 + 2M_T Q\cos\theta_{CS} + Q^2\cos^2\theta_{CS} - Q_T^2\sin^2\theta_{CS}\cos^2\varphi_{CS}}, \qquad (5.7)$$

and $M_T^2 = Q^2 + Q_T^2$. We also write $\cos\Delta\varphi$ as

$$\cos\Delta\varphi = (Q_T^2 - Q^2\sin^2\theta_{CS} - Q_T^2\sin^2\theta_{CS}\cos^2\varphi_{CS})$$

$$\times[(Q^2 \sin^2\theta_{CS} + Q_T^2 \sin^2\theta_{CS} \cos^2\varphi_{CS} + Q_T^2)^2 - 4M_T^2 Q_T^2 \sin^2\theta_{CS} \cos^2\varphi_{CS}]^{-\frac{1}{2}}. \quad (5.8)$$

In the limit $Q_T \to 0$, ϕ_η^* simplifies to

$$\phi_\eta^* \approx (Q_T/Q) \sin\varphi_{CS}, \quad (5.9)$$

since $\tan(\phi_{acop}/2) = \sqrt{(1+\cos\Delta\varphi)/(1-\cos\Delta\varphi)}$, and

$$\theta_\eta^* \to \theta_{CS}, \qquad \cos\Delta\varphi \to -1 + 2\left(\frac{Q_T}{Q}\frac{\sin\varphi_{CS}}{\sin\theta_{CS}}\right)^2. \quad (5.10)$$

Measurement of ϕ_η^* thus directly probes Q_T/Q.[2]

Relations like these can analytically express the ϕ_η^* distribution in terms of the Q_T distribution, but in practice it is easier to compute the ϕ_η^* distribution by Monte-Carlo integration in ResBos code. In this case, the interval of small Q_T/Q maps onto the region of small ϕ_η^* values. For example, in Z production at $Q \approx M_Z$, the range $10^{-3} \le \phi_\eta^* \le 0.5$ radians corresponds to $0.1 \lesssim Q_T \lesssim 50$ GeV.

5.2.2. General structure of the resummed cross section

The resummed cross sections that we present are based on the calculation in [81, 94–96] with added higher-order radiative contributions (Secs. 5.2.3, 5.2.4) and a modified nonperturbative model (Sec. 5.2.5). We write the fully differential cross section for Z boson production and decay as

[2]The asymptotic relation between ϕ_η^* and Q_T/Q can alternatively be obtained by introducing the component a_T of $\vec{Q}_T$ along the thrust axis $\hat{n} = (\vec{l}_{1,T} - \vec{l}_{2,T})/|\vec{l}_{1,T} - \vec{l}_{2,T}|$, where $\vec{l}_{1,T}$ and $\vec{l}_{2,T}$ are the transverse momenta of e^- and e^+, and identifying $a_T = Q_T \sin\varphi_{CS}$ at $Q_T \to 0$ [89, 90, 92, 119].

$$\frac{d\sigma\left(h_1 h_2 \to (Z \to \ell\bar{\ell})X\right)}{dQ^2\ dy_Z\ dQ_T^2\ d\cos\theta_{CS}\ d\varphi_{CS}} = \sum_{\alpha=-1}^{4} F_\alpha\left(Q, Q_T, y\right) A_\alpha\left(\theta_{CS}, \varphi_{CS}\right) \tag{5.11}$$

in terms of the structure functions $F_\alpha(Q, Q_T, y_Z)$ and angular functions $A_\alpha(\theta_{CS}, \varphi_{CS})$. The variables Q, Q_T, and y_Z correspond to the invariant mass, transverse momentum, and rapidity of the boson in the lab frame; θ_{CS} and φ_{CS} are the lepton decay angles in the CS frame. Among the structure functions F_α, two (associated with the angular functions $A_{-1} = 1 + \cos^2\theta_{CS}$ and $A_3 = 2\cos\theta_{CS}$) include resummation of soft and collinear logarithms in the small-Q_T limit. For such functions, we write

$$F_\alpha(Q, Q_T, y_Z) = W_\alpha(Q, Q_T, y_Z; C_1/b, C_2Q, C_3/b) + Y_\alpha(Q, Q_T, y_Z; C_4Q), \tag{5.12}$$

where

$$W_\alpha(Q, Q_T, y_Z) = \int \frac{d^2b}{4\pi^2}\, e^{i\vec{Q}_T\cdot\vec{b}} \sum_{j=u,d,s...} \widetilde{W}_{\alpha,j}(b, Q, y_Z) \tag{5.13}$$

is introduced to resum small-Q_T logarithms to all orders in α_s. The W term depends on several auxiliary QCD scales C_1/b, C_2Q, and C_3/b with constant coefficients $C_{1,2,3} \approx 1$ that emerge from the solution of differential equations describing renormalization and gauge invariance of Q_T distributions [1,15]. $Y_\alpha(Q, Q_T, y_Z; C_4Q)$ is a part of the non-singular remainder, or "the Y term". It depends on a factorization and renormalization momentum scale C_4Q.

The Fourier-Bessel integral over the transverse position b in the W term in Eq. (5.13) acquires contributions from the region of small transverse positions $0 \le b \lesssim 1$ GeV^{-1}, where the form factor can be approximated in perturbative QCD, and the region

$b \gtrsim 1$ GeV^{-1}, where the perturbative expansion in the QCD coupling $\alpha_s(1/b)$ breaks down, and nonperturbative methods are necessitated. In Z boson production, the small-b perturbative contribution dominates the Fourier-Bessel integral for any Q_T value [80, 97, 120]. At Q_T below 5 GeV, the production rate is also mildly sensitive to the behavior in the $b > 0.5$ GeV^{-1} interval, where the full expression for $\widetilde{W}_{\alpha,j}(b,Q)$ is yet unknown.

The constraining of the non-perturbative factor is deteriorated by various uncertainties from theory and from experiment. To determine the acceptable large-b forms of $\widetilde{W}_{\alpha,j}(b,Q)$ by comparison to the latest Z boson data, we need to update the leading-power contribution to $\widetilde{W}_{\alpha,j}(b,Q,y_Z)$ computable in perturbative QCD, denoted by $\widetilde{W}^{pert}_{\alpha,j}(b,Q,y_Z)$, by considering additional QCD and electromagnetic corrections and dependence on QCD factorization scales. In particular, scale dependence in the perturbative form factor $\widetilde{W}^{pert}$ may smear sensitivity to the nonperturbative factor [76, 88, 93, 115]. We will review the perturbative contributions in the next two subsections.

5.2.3. Perturbative coefficients for canonical scales

For a particular "canonical" combination of the scale parameters, the perturbative contributions simplify; the resummed form factor at $b \ll 1$ GeV^{-1} takes the form

$$\begin{aligned}\widetilde{W}^{pert}_{\alpha,j}(b,Q,y_Z) &= \sum_{j=u,d,s\ldots} \left|H_{\alpha,j}(Q,\Omega,Q)\right|^2 \exp\left[-S(b,Q)\right] \\ &\times \sum_{a=g,q,\bar{q}} \left[\mathcal{C}_{ja}\otimes f_{a/h_1}\right](\chi_1,\mu_F) \sum_{b=g,q,\bar{q}} \left[\mathcal{C}_{\bar{j}b}\otimes f_{b/h_2}\right](\chi_2,\mu_F) \quad (5.14)\end{aligned}$$

in terms of a $2 \to 2$ hard part $|H_{\alpha,j}(Q,\Omega,Q)|^2$, Sudakov integral

$$S(b,Q)=\int_{b_0^2/b^2}^{Q^2}\frac{d\bar{\mu}^2}{\bar{\mu}^2}\left[A(\bar{\mu})\,\ln\left(\frac{Q^2}{\bar{\mu}^2}\right)+B(\bar{\mu})\right], \tag{5.15}$$

and convolutions $\left[\mathcal{C}_{j/a}\otimes f_{a/h}\right]$ of Wilson coefficient functions $\mathcal{C}_{j/a}$ and PDFs $f_{a/h}$ for a parton a inside the initial-state hadron h. The convolution integral is defined by

$$\left[\mathcal{C}_{ja}\otimes f_{a/h}\right](\chi,\mu_F)=\int_x^1\frac{d\xi}{\xi}\mathcal{C}_{ja}\left(\frac{\chi}{\xi},\mu_F\right)f_{a/h}(\xi,\mu_F). \tag{5.16}$$

In Eq. (5.16) the convolution depends on the momentum fractions $\chi_{1,2}$ that reduce to $x_{1,2}^{(0)}\equiv(Q/\sqrt{s})e^{\pm yz}$ in the limit $Q_T^2/Q^2\to 0$, as explained in Sec. 5.2.6, as well as on the factorization scale $\mu_F=b_0/b$. Some scales are proportional to the constant $b_0=2e^{-\gamma_E}=1.123...$, where $\gamma_E=0.577...$ is the Euler-Mascheroni constant.

The functions $H_{\alpha,j}$, A, B, and C can be expanded as a series in the QCD coupling strength,

$$H_{\alpha,j}(\alpha_s(\bar{\mu}))=1+\sum_{n=1}^{\infty}\left(\frac{\alpha_s(\bar{\mu})}{\pi}\right)^n H_{\alpha,j}^{(n)}\,,\qquad A(\alpha_s(\bar{\mu}))=\sum_{n=1}^{\infty}\left(\frac{\alpha_s(\bar{\mu})}{\pi}\right)^n A^{(n)}\,,\text{etc.} \tag{5.17}$$

Some perturbative contributions can be moved between the hard function $H_{\alpha,j}$ and Sudakov exponential depending on the resummation scheme [84]. In the Collins-Soper-Sterman (CSS) resummation scheme, $H_{\alpha,j}(\alpha_s)=1$ to all α_s orders. In the Catani-De Florian-Grazzini (CFG) resummation scheme, $H_{\alpha,j}(\alpha_s)$ includes hard virtual contributions starting at $\mathcal{O}(\alpha_s)$, while the Sudakov exponential depends only on the type of the initial-state particle (quark or gluon) that radiates soft emissions. In Drell-Yan production, differences between the CSS and CFG schemes are small, below 1% in the kinematic region explored. We carry out the analysis in the CSS scheme, but the nonperturbative function that we obtain can be readily used with the CFG scheme.

The functions A and B for the canonical choice of scales are evaluated up to $\mathcal{O}(\alpha_s^3)$ and $\mathcal{O}(\alpha_s^2)$ respectively, using their known perturbative coefficients [35, 121–125]. The three-loop coefficient $A^{(3)}$ provided in [35] is included, but has a weak effect on the cross section (3% at $Q_T \approx 2$ GeV). The coefficient $A^{(3)}$ has been also derived within the soft-collinear effective theory [126], and a somewhat different expression was obtained. We do not use the SCET expression for $A^{(3)}$, as the SCET representation for $\widetilde{W}^{pert}$ contains an extra scale-dependent term already at order α_s that is absent in the expansion in the CSS or CFG resummation schemes. The additional term arises from the "collinear anomaly" generated by breaking of the symmetry of the SCET Lagrangian by regulators of loop integrals [126–129]. It does not appear in the expansion of $\widetilde{W}^{pert}$ in the CSS scheme, suggesting that the resummation scheme of the SCET derivation is different, and consequently the perturbative Sudakov coefficients are different, too. In any case, $A^{(3)}$ has inappreciable influence on the conclusions.

The Wilson coefficient functions $\mathcal{C}^{(i)}$ are computed exactly up to $\mathcal{O}(\alpha_s)$ and approximately to $\mathcal{O}(\alpha_s^2)$. Most of our numerical results were obtained with the $\mathcal{O}(\alpha_s^2)$ approximation for the Wilson coefficient before the exact $\mathcal{O}(\alpha_s^2)$ result were published [76, 77, 93]. This expression is constructed by using a numerical approximation for the canonical part of the Wilson coefficient at $\mathcal{O}(\alpha_s^2)$ and exact expression for its dependence on soft scales. Our *a posteriori* comparison shows the approximation to be close to the exact expression, cf. the next subsection.

The Y contribution in Eq. (5.13) is defined as the difference between the fixed-order perturbative Q_T distribution calculation and the asymptotic distribution obtained by expanding the perturbative part $\widetilde{W}^{pert}$ up to the same order. It is given by

$$Y_\alpha(Q_T, Q, y_Z) = \int \frac{d\xi_1}{\xi_1} \int \frac{d\xi_2}{\xi_2} \sum_{n=1}^{\infty} \left[\frac{\alpha_s(C_4 Q)}{\pi}\right]^n \times$$
$$f_{a/h_1}(\xi_1, C_4 Q)\ R^{(n)}_{\alpha,ab}\left(Q_T, Q, y_Z; \xi_1, \xi_2, C_4 Q\right)\ f_{b/h_2}(\xi_2, C_4 Q), \tag{5.18}$$

where the functions $R^{(n)}_{\alpha,ab}$ are integrable when $Q_T \to 0$, and their explicit expressions for all contributing α to $\mathcal{O}(\alpha_s)$ can be found in [17,95]. The $O(\alpha_s^2)$ contribution to the dominant structure function Y_{-1} is included using the calculation in [74,120]. $O(\alpha_s^2)$ corrections to the other structure functions in the Y term are essentially negligible in the small-Q_T region of our fit.

5.2.4. Perturbative coefficients for arbitrary scales

The resummed form factor in Eq. (5.14) can be generalized to allow variations in the arbitrary factorization scales arising in the solution of Collins-Soper differential equations. At small b, the scale-dependent expression takes the form

$$\begin{aligned}\widetilde{W}^{pert}_{\alpha,j} &= \sum_{j=u,d,s\ldots} \left|H_{\alpha,j}(Q,\Omega,C_2 Q)\right|^2 \exp\left[-\int_{C_1^2/b^2}^{C_2^2 Q^2} \frac{d\bar{\mu}^2}{\bar{\mu}^2} A(\bar{\mu};C_1)\ \ln\left(\frac{C_2^2 Q^2}{\bar{\mu}^2}\right) + B(\bar{\mu};C_1,C_2)\right] \\ &\times \sum_{a=g,q,\bar{q}} \left[\mathcal{C}_{ja}\otimes f_{a/h_1}\right]\left(\chi_1, \frac{C_1}{C_2}, \frac{C_3}{b}\right) \sum_{b=g,q,\bar{q}} \left[\mathcal{C}_{\bar{j}b}\otimes f_{b/h_2}\right]\left(\chi_2, \frac{C_1}{C_2}, \frac{C_3}{b}\right),\end{aligned} \tag{5.19}$$

where the coefficients $C_1 = b\bar{\mu}$ and $C_2 = \bar{\mu}/Q$ are associated with the lower and upper integration limits in Eq. (5.19), while $\mu_F = C_3/b$ is the factorization scale at which Wilson coefficient functions are evaluated. The "canonical" representation adopted in Eq. (5.14) corresponds to $C_1 = C_3 = b_0$ and $C_2 = 1$. For the rest of the discussion, we use the same scale $C_2 Q$ to compute the hard function $H_{\alpha,j}$ and the Y term, *i.e.* set $C_4 = C_2$.

The perturbative coefficients $A^{(n)}$, $B^{(n)}$, and $C^{(n)}$ are generally dependent on the scale coefficients, but the full form factor $\widetilde{W}^{pert}$ is independent when expanded to a fixed order in α_s. We can therefore reconstruct the perturbative coefficients order-by-order for arbitrary C_1, C_2, C_3 if we know the canonical values of the coefficients, indicated by the superscript "(c)".

By truncating the series at $\mathcal{O}(\alpha_s^2)$, we must have

$$\widetilde{W}(b, Q, C_1, C_2, C_3)|_{\mathcal{O}(\alpha_s^2)} = \widetilde{W}(b, Q, C_1 = C_3 = b_0, C_2 = 1)|_{\mathcal{O}(\alpha_s^2)}. \tag{5.20}$$

Making a series expansion on both sides of Eq. (5.20), we find the following relations by equating the coefficients in front of each power of $\log(b^2Q^2)$:

$$A^{(1)}(C_1) = A^{(1,c)}; \tag{5.21}$$

$$A^{(2)}(C_1) = A^{(2,c)} - A^{(1,c)}\beta_0 \ln\frac{b_0}{C_1}; \tag{5.22}$$

$$A^{(3)}(C_1) = A^{(3,c)} - 2A^{(2,c)}\beta_0 \ln\frac{b_0}{C_1} - \frac{A^{(1,c)}}{2}\beta_1 \ln\frac{b_0}{C_1} + A^{(1,c)}\beta_0^2\left(\ln\frac{b_0}{C_1}\right)^2 \tag{5.23}$$

$$B^{(1)}(C_1, C_2) = B^{(1,c)} - A^{(1,c)} \ln\frac{b_0^2C_2^2}{C_1^2}; \tag{5.24}$$

$$\begin{aligned} B^{(2)}(C_1, C_2) &= B^{(2,c)} - A^{(2,c)} \ln\frac{b_0^2C_2^2}{C_1^2} \\ &+ \beta_0\left[A^{(1,c)}\ln^2\frac{b_0}{C_1} + B^{(1,c)}\ln C_2 - A^{(1,c)}\ln^2 C_2\right]; \end{aligned} \tag{5.25}$$

$$\begin{aligned} \mathcal{C}_{ja}^{(1)}\left(\xi, \frac{C_1}{C_2}, C_3\right) &= \mathcal{C}_{ja}^{(1,c)}(\xi) + \delta_{ja}\delta(1-\xi)\left\{\frac{B^{(1,c)}}{2}\ln\frac{b_0^2C_2^2}{C_1^2} - \frac{A^{(1,c)}}{4}\left(\ln\frac{b_0^2C_2^2}{C_1^2}\right)^2\right\} \\ &- P_{ja}^{(1)}(x)\ln\frac{\mu_F b}{b_0}; \end{aligned} \tag{5.26}$$

$$\mathcal{C}_{ja}^{(2)}\left(\xi, \frac{C_1}{C_2}, C_3\right) = \mathcal{C}_{ja}^{(2,c)}(\xi) + \delta_{ja}\delta(1-\xi)L^{(2)}(C_1, C_2)$$

$$
\begin{aligned}
&+ \quad \left\{ \frac{\beta_0}{2} \mathcal{C}_{jb}^{(1,c)}(\xi) - [\mathcal{C}_{jb}^{(1,c)} \otimes P_{ba}^{(1)}](\xi) - P_{ja}^{(2)}(\xi) \right\} \ln \frac{\mu_F b}{b_0} \\
&+ \quad \frac{1}{2} [P_{jb}^{(1)} \otimes P_{ba}^{(1)}](\xi) \ln^2 \frac{\mu_F b}{b_0}.
\end{aligned} \tag{5.27}
$$

Here the beta-function coefficients for N_c colors and N_f flavors are $\beta_0 = (11N_c - 2N_f)/6$, $\beta_1 = (17N_c^2 - 5N_c N_f - 3C_F N_f)/6$, $C_F = (N_c^2 - 1)/(2N_c)$. $P_{ja}^{(n)}(\xi)$ is a splitting function of order n. The term $L^{(2)}(C_1, C_2)$ in $\mathcal{C}_{ja}^{(2)}$ realizes the exact dependence on the *soft* scale constants C_1 and C_2:

$$
\begin{aligned}
& L^{(2)}(C_1, C_2) \equiv \frac{1}{32} (A^{(1,c)})^2 \log^4 \left(\frac{b_0^2 C_2^2}{C_1^2} \right) \\
- \quad & \frac{1}{8} A^{(1,c)} \beta_0 \log \left(\frac{b^2 \mu_F^2}{b_0^2} \right) \log^2 \left(\frac{b_0^2 C_2^2}{C_1^2} \right) - \frac{1}{8} A^{(1,c)} B^{(1,c)} \log^3 \left(\frac{b_0^2 C_2^2}{C_1^2} \right) \\
- \quad & \frac{1}{24} A^{(1,c)} \beta_0 \log^3 \left(\frac{b_0^2 C_2^2}{C_1^2} \right) - \frac{1}{4} A^{(1,c)} \delta\mathcal{C}_{1c} \log^2 \left(\frac{b_0^2 C_2^2}{C_1^2} \right) \\
- \quad & \frac{1}{4} A^{(2,c)} \log^2 \left(\frac{b_0^2 C_2^2}{C_1^2} \right) + \frac{1}{4} \beta_0 B^{(1,c)} \log \left(\frac{b^2 \mu_F^2}{b_0^2} \right) \log \left(\frac{b_0^2 C_2^2}{C_1^2} \right) \\
+ \quad & \frac{1}{8} (B^{(1,c)})^2 \log^2 \left(\frac{b_0^2 C_2^2}{C_1^2} \right) + \frac{1}{8} \beta_0 B^{(1,c)} \log^2 \left(\frac{b_0^2 C_2^2}{C_1^2} \right) \\
+ \quad & \frac{1}{2} B^{(1,c)} \delta\mathcal{C}_{1c} \log \left(\frac{b_0^2 C_2^2}{C_1^2} \right) + \frac{1}{2} B^{(2,c)} \log \left(\frac{b_0^2 C_2^2}{C_1^2} \right).
\end{aligned} \tag{5.28}
$$

The dependence on C_3 is small already at $\mathcal{O}(\alpha_s)$. The canonical coefficients in the CSS scheme are [95]

$$
\begin{aligned}
& A^{(1,c)} = C_F; \qquad B^{(1,c)} = -\frac{3}{2} C_F; \qquad A^{(2,c)} = C_F \left[\left(\frac{67}{36} - \frac{\pi^2}{12} \right) C_A - \frac{5}{18} N_f \right]; \\
& B^{(2,c)} = C_F^2 \left(\frac{\pi^2}{4} - \frac{3}{16} - 3\zeta_3 \right) + C_A C_F \left(\frac{11}{36} \pi^2 - \frac{193}{48} + \frac{3}{2} \zeta_3 \right) + \frac{1}{2} C_F N_f \left(-\frac{\pi^2}{9} + \frac{17}{12} \right),
\end{aligned} \tag{5.29}
$$

and $\delta\mathcal{C}^{(1,c)} = -\ln^2(C_1/(b_0 C_2) e^{-3/4}) + \pi^2/4 - 23/16$.

The expression for $\mathcal{C}_{ja}^{(2)}(\xi, C_1/C_2, C_3)$ in Eq. (5.27) is more complex than for the other coefficients. From the fixed-order NNLO calculation [130] we know that the contribution $\mathcal{C}_{ja}^{(2)}$ is small in magnitude (2-3% of the cross section) in Z production and does not vary strongly with y_Z [75], hence has weak dependence on ξ. Its importance is further reduced in the computation of the *normalized* ϕ_η^* distributions that we will work with.

Knowing this, we approximate $\mathcal{C}_{ja}^{(2)}(\xi, C_1/C_2, C_3)$ as

$$\mathcal{C}_{ja}^{(2)}(\xi, C_1/C_2, C_3) \approx \left\{ \langle \delta\mathcal{C}^{(2,c)} \rangle + L^{(2)}(C_1, C_2) \right\} \delta(1-\xi)\,\delta_{ja}, \tag{5.30}$$

where $\langle \delta\mathcal{C}^{(2,c)} \rangle$ denotes the average value of the Wilson coefficient in Z production for the canonical scale combination and $L^{(2)}(C_1, C_2)$ is the same as in Eq.(5.28). It is estimated from the requirement that the resummed cross section reproduces the fixed-order prediction for the computation of the invariant mass distribution, which is known since a long time [131] and was evaluated in our analysis by the computer code CANDIA [132,133] [3]. The second term in Eq. (5.30) realizes the exact dependence on *soft* scale constants C_1 and C_2. The ξ dependence of $\mathcal{C}_{ja}^{(2)}(\xi, C_1/C_2, C_3)$ is neglected in this approximation. The C_3 dependence is included to $\mathcal{O}(\alpha_s)$ and is of the same order as the $\mathcal{O}(\alpha_s^2)$ dependence on C_1 and C_2.

The part $\delta\mathcal{C}_{ja}^{(2,c)}$ of $\mathcal{C}_{ja}^{(2,c)}$ proportional to $\delta_{ja}\delta(1-\xi)$ can be determined from the calculation in [93] as

$$\begin{aligned}
\delta\mathcal{C}_{qq,c}^{(2)} &= C_A C_F \left(\frac{59}{18}\zeta_3 - \frac{1535}{192} + \frac{215}{216}\pi^2 - \frac{\pi^4}{240} \right) + \frac{1}{4} C_F^2 \left(-15\zeta_3 + \frac{511}{16} - \frac{67\pi^2}{12} + \frac{17}{45}\pi^4 \right) \\
&- \frac{1}{16}\left(\pi^2 - 8\right)^2 C_F^2 + \frac{1}{864} C_F N_f \left(192\zeta_3 + 1143 - 152\pi^2 \right),
\end{aligned} \tag{5.31}$$

[3] Other computer codes are also publicly available at this purpose: DYNNLO [76,86] and VRAP [75].

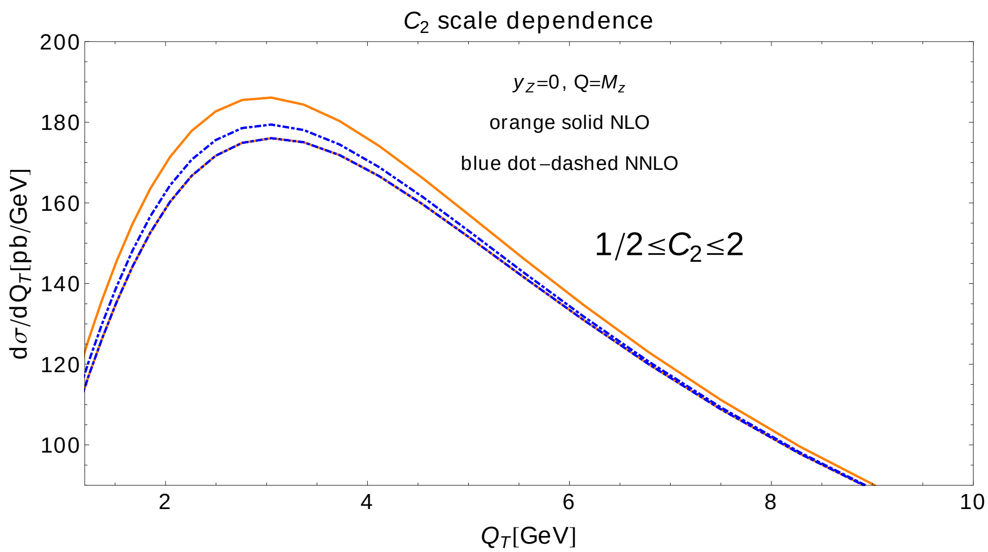

Figure 5.3. Dependence of Z boson Q_T distribution on the scale parameter C_2 at $\mathcal{O}(\alpha_s^2)$ and $\mathcal{O}(\alpha_s)$.

where $\zeta_3 = 1.20206...$, $C_F = (N_C^2 - 1)/(2N_C)$, $C_A = N_C$. Using the following relation in the CFG formalism:

$$H_{\alpha,j}^{DY} = 1 + \frac{\alpha_s(Q)}{\pi} H^{DY(1)} + \frac{\alpha_s^2(Q)}{\pi^2} H^{DY(2)} + \dots, \tag{5.32}$$

one can estimate that the impact on H_q^{DY} due to the inclusion of the $\mathcal{O}(\alpha_s^2)$ virtual corrections $H_q^{DY(2)}$ at $Q \approx M_Z$ is about 2%. This correction is of the same order as the magnitude of the effect of about 1% from the averaged coefficient $\langle \delta\mathcal{C}^{(2,c)} \rangle$ in our calculation. This approximation is valid in the kinematic region of W/Z production. The full expression for $\mathcal{C}_{ja}^{(2,c)}(\xi)$ can be implemented in the future numerical work when the experimental errors further decrease.

The effect of the inclusion of scale-dependent terms at $\mathcal{O}(\alpha_s^2)$ is illustrated in Fig. 5.3 for the Q_T differential cross section for Tevatron Z production at the central rapidity $y_Z = 0$ and $Q = M_Z$. The orange solid band is the $\mathcal{O}(\alpha_s)$ uncertainty obtained by variations of C_2 in the range $0.5 - 2$, while the blue dot-dashed band is the same uncertainty evaluated at $\mathcal{O}(\alpha_s^2)$. The sensitivity of the cross section to C_2 is clearly reduced upon the inclusion of the $\mathcal{O}(\alpha_s^2)$ contribution.

5.2.5. Nonperturbative resummed contributions

Our fit to the ϕ_η^* will adopt a simple flexible convention [97] for $\widetilde{W}_\alpha(b, Q)$ at $b \gtrsim 1$ GeV^{-1} that can emulate a variety of functional forms arising in detailed non-perturbative models [82, 108, 109, 111, 134–138].

The convention is motivated by the observation that, given the strong suppression of the deeply nonperturbative large-b region in Z boson production, only contributions from the transition region of b of about 1 GeV^{-1} are non-negligible compared to the perturbative contribution from $b < 1$ GeV^{-1}. In the transition region, $\widetilde{W}(b, Q)$ can be reasonably approximated by the extrapolated leading-power, or perturbative, part $\widetilde{W}^{pert}(b, Q)$, and the nonperturbative smearing factor $\widetilde{W}^{NP}(b, Q)$:

$$\widetilde{W}_{\alpha,j}(b, Q, y_Z) = \widetilde{W}_{\alpha,j}^{pert}(b_*, Q, y_Z)\widetilde{W}^{NP}(b, Q, y_Z). \tag{5.33}$$

When b is large, the slow b dependence in $\widetilde{W}_{\alpha,j}^{pert}(b_*, Q)$ can be neglected, compared to the rapidly changing $\widetilde{W}_{NP}(b, Q)$. The latter contribution captures the effect of the powerlike contributions proportional to b^p with $p > 0$ that alter the large-b tail of $\widetilde{W}(b, Q)$ in a different way compared to $\widetilde{W}^{pert}(b, Q)$. The powerlike contributions suppress the rate only at Q_T below 2-3 GeV, while the leading-power term and its scale dependence affect a broader interval of Q_T values (see representative figures in

Ref. [115]). The nonperturbative suppression results in a characteristic shift of the peak in the $d\sigma/dQ_T$ distribution, which is distinct from the scale dependence.

To avoid divergence due to the Landau pole in $\alpha_s(\overline{\mu})$ at $\overline{\mu} \to 0$, we redefine the scales of order $1/b$ in $\widetilde{W}^{pert}(b, Q)$ according to the b_* prescription [16,17] dependent on two parameters [97]. In the Sudakov exponential, the lower limit $(C_1/b)^2$ is replaced by $\left(C_1/b_*(b, b_{max})\right)^2$, with

$$b_*(b, b_{max}) \equiv \frac{b}{\sqrt{1 + (b/b_{max})^2}}, \tag{5.34}$$

where b_{max} is set to 1.5 GeV^{-1} in [97]. To avoid evaluating the PDFs $f_{a/h}(\xi, \mu_F)$ at a factorization scale μ_F below the initial PDF scale $\mu_{ini} \approx 1$ GeV, we choose $\mu_F = C_3/b_*(b, C_3/\mu_{ini})$; it is larger than μ_{ini} for any b. This prescription is preferred by the global fit to Drell-Yan Q_T data, where it both preserves the exact perturbative expansion for $\widetilde{W}^{pert}$ at $b < 1$ GeV^{-1} and improves the agreement with the data.

In a broad range of Q values in the Drell-Yan process, the behavior of experimentally observed Q_T distributions is described by [96, 97]

$$\widetilde{W}^{NP}(b, Q) = \exp\left[-b^2\left(a_1 + a_2 \ln\left(\frac{Q}{2\,Q_0}\right) + a_3 \ln\left(\frac{x_1^{(0)} x_2^{(0)}}{0.01}\right)\right)\right], \tag{5.35}$$

with $x_{1,2}^{(0)} = \frac{Q}{\sqrt{s}} e^{\pm y}$, free parameters $a_1,\ a_2,\ a_3$, and a fixed dimensional parameter $Q_0 =$ 1.6 GeV. The b^2 dependence characterizes the leading power-suppressed contribution [134] that can be resolved with the available data. The $\ln(Q)$ dependence is predicted by the Collins-Soper evolution equation [15]. The higher-order power-suppressed contributions proportional to b^4, etc. cannot be reliably distinguished in the fit from the b^2 term. Although linear contributions proportional to b may also arise from long-distance dynamics [139], they have been empirically disfavored in a global Q_T

fit [96].

In the vicinity of Q around M_Z, Eq. (5.35) reduces to

$$\widetilde{W}^{NP}\left(b, Q \approx M_Z\right) = \exp\left[-b^2 a_Z\right] \tag{5.36}$$

with

$$a_Z = a_1 + a_2 \ln\left(\frac{M_Z}{2\ Q_0}\right) + a_3 \ln\left(\frac{M_Z^2}{0.01\ s}\right). \tag{5.37}$$

One of the essential applications of CSS resummation formalism concerns the measurement of W boson mass in hadron-hadron collisions. The current most precise W mass measurements obtained by the DØ and CDF collaborations at the Tevatron [140, 141] quote a total error of about 20 MeV, with the bulk of it (approximately 90%) associated with three theoretical sources: PDFs uncertainty (of order 10 MeV according to [142]), EW corrections, and the model of $\widetilde{W}_{NP}(b, Q)$ in production of W bosons. The last source of uncertainty appears because the W mass measurements are sensitive to the shape of the cross section in the low-Q_T region.

Once a_Z is determined from Z/γ^* boson production, it is easy to predict $\widetilde{W}^{NP}$ in W boson production at the same $\sqrt{s}$:

$$\widetilde{W}^{NP}\left(b, Q \approx M_W\right) = \exp\left[-b^2 a_W\right], \tag{5.38}$$

where

$$a_W = a_Z + a_2 \ln\left(\frac{M_W}{M_Z}\right) + a_3 \ln\left(\frac{M_W^2}{M_Z^2}\right). \tag{5.39}$$

For $b_{max} = 1.5$ GeV^{-1}, one finds $a_2 = 0.17 \pm 0.03$ GeV^2 and $a_3 = -0.03 \pm 0.02$ GeV^2 [97], where the error estimate includes the scale dependence. The log terms proportional to a_2 and a_3 are small in Eq. (5.39), so that it is safe to assume $a_W \approx a_Z$ in central-rapidity measurements at the same $\sqrt{s}$.

If Q is substantially different from M_Z, or if predictions for the LHC are made, the a_2 and a_3 contributions cannot be neglected. The nonperturbative coefficient becomes

$$a(Q, \sqrt{s}) = a_Z(1.96 \text{ TeV}) + a_2 \ln\left(\frac{Q}{M_Z}\right) + a_3 \ln\left(\frac{Q^2}{M_Z^2} \frac{s}{(1.96 \text{ TeV})^2}\right). \tag{5.40}$$

5.2.6. Matching the W and Y terms

By examining the mapping of Q_T distributions on ϕ_η^* distributions discussed in Sec. 5.2.1, we can identify three regions with distinct QCD dynamics: the resummation region $\phi_\eta^* \lesssim 0.1$ rad, where the W term dominates; the intermediate (matching) region $0.1 \lesssim \phi_\eta^* \lesssim 0.5$ rad; and the perturbative region $\phi_\eta^* \gtrsim 0.5$ rad, where the $W+Y$ term approaches the fixed-order (FO) contribution. As ϕ_η^* increases in the intermediate region, the $W+Y$ term eventually becomes smaller than the FO term at $\phi_\eta^* \equiv \phi_{switch}(Q, y_Z)$. The final cross section is taken to be equal to the $W+Y$ term at $\phi_\eta^* < \phi_{switch}$ and FO term at $\phi_\eta^* \geq \phi_{switch}$ [95].

The position of the switching point is subject to some variations dependent on the shapes of the W term and its asymptotic expansion at not too small $\phi_\eta^* \propto Q_T/Q$, *i.e.* away from the $Q_T^2/Q^2 \to 0$ limit where the W term is uniquely defined. These variations have almost no effect on the fit of the nonperturbative function in the resummation region ϕ_η^*. They originate from the possibility of including additional terms of order Q_T^2/Q^2 in the longitudinal momentum fractions $\chi_{1,2}$ in the W term and its asymptotic expansion. These terms vanish at $Q_T^2/Q^2 \to 0$, but they can be numerically important or even desirable in the intermediate region, where they may improve agreement between the $W + Y$ and FO terms.

At intermediate Q_T/Q, radiation of a Z boson and semi-hard jets requires sufficient center-of-mass energy of incident partons, or large enough partonic momentum fractions ξ_1 and ξ_2. For example, the FO hadronic cross section is written as

$$\frac{d\sigma}{dQ^2 dy_Z dQ_T^2} = \sum_{a,b} \int_0^1 d\xi_1 \int_0^1 d\xi_2 \frac{d\hat{\sigma}}{dQ^2 dy_Z dQ_T^2} f_{a/A}(\xi_1) f_{b/B}(\xi_2)$$
$$\equiv \int_{\bar{\xi}_1}^1 d\xi_1 \int_{\bar{\xi}_2}^1 d\xi_2 h(\xi_1, \xi_2)\, \delta \left[\left(\frac{\xi_1}{x_1} - 1 \right) \left(\frac{\xi_2}{x_2} - 1 \right) - \frac{Q_T^2}{M_T^2} \right], \tag{5.41}$$

where $h(\xi_1, \xi_2)$ contains the hard-scattering matrix element and PDFs, and $M_T = \sqrt{Q^2 + Q_T^2}$. The energy constraint from the δ-function imposes the following boundaries on the partonic momentum fractions: $\xi_1 = x_1 + (Q_T^2/s)/(\xi_2 - x_2)$; $\bar{\xi}_1 = [x_1 + (Q_T^2/s)/(1 - x_2)] \leq \xi_1 \leq 1$; $\bar{\xi}_2 \equiv [x_2 + (Q_T^2/s)/(1 - x_1)] \leq \xi_2 \leq 1$, with $x_{1,2} = \frac{M_T}{\sqrt{s}} e^{\pm y}$.

These boundaries are absent in the W and asymptotic contributions, which depend on convolutions of Wilson coefficient functions and PDFs,

$$\left[C_{j,a} \otimes f_{a/h_i} \right] (\chi_i, \mu_F) = \int_{\chi_i}^1 \frac{d\xi_i}{\xi_i} C_{j,a} \left(\frac{\chi_i}{\xi_i}, \mu_F b, C_1, C_2, C_3 \right) f_{a/h_i}(\xi_i, \mu_F) \tag{5.42}$$

for $i = 1$ or 2. The variables χ_i satisfy $\chi_{1,2} \to x_{1,2}^{(0)} \equiv (Q/\sqrt{s}) e^{\pm y}$ and cannot exceed $\bar{\xi}_{1,2}$. Thus, for non-negligible Q_T^2/Q^2, the W and asymptotic term may include contributions from the unphysical momentum fractions $\xi_i \leq \bar{\xi}_i$, and ideally one should include kinematically important Q_T^2/Q^2 contributions into $\chi_{1,2}$ to bring them as close to $\bar{\xi}_{1,2}$ as possible.[4]

[4] The logic here follows a general argument for matching of the resummed contribution onto the fixed-order result that applies in other areas, such as the treatment of PDFs for heavy quarks in DIS

As the procedure for including the Q_T^2/Q^2 corrections in the W term is not unique, we explored several of them. We find that either $\chi_{1,2} = x_{1,2}^{(0)} = (Q/\sqrt{s})e^{\pm y}$ or $\chi_{1,2} = x_{1,2} = (M_T/\sqrt{s})e^{\pm y}$ results in the comparable agreement with the ϕ_η^* data from DØ and ATLAS 7 TeV. These prescriptions are designated as the "kinematical corrections of type 0" and "type 1", or kc_0 and kc_1, in our numerical outputs.

In contrast, some alternative choices produce worse agreement with the examined data, such as $\chi_{1,2} = \bar{\xi}_{1,2} = ((M_T + Q_T)/\sqrt{s})e^{\pm y}$ designated as kc_2. Furthermore, the kc_1 prescription improves matching compared to kc_0 at $\sqrt{s} = 14$ TeV, corresponding to scattering at smaller x. We use the kc_1 matching as the default prescription in the subsequent comparisons.

5.2.7. Photon radiative contributions

Our resummed calculations include both Z-mediated and photon-mediated contributions to production of Drell-Yan pairs, as well as their interference. Electroweak radiative contributions have been extensively studied in Z boson [143–146] and W boson production [147–152]. The dominant NLO electroweak contribution is associated with final-state radiation of photons. To compare the DØ data to the ResBos prediction without the NLO electroweak correction, we correct the fitted data to the Born level for final-state leptons by subtracting the NLO EM correction obtained bin-by-bin by the Photos code [153]. This correction is essential for the agreement of ResBos theory and data. However, since the photon-mediated and final-state photon radiation contributions are relatively small, in the first approximation we can treat them as a linear perturbation and evaluate for a fixed combination of the

in a general-mass variable number scheme [52,62]. Matching is stabilized by constructing resummed coefficient functions that comply with the energy-momentum conservation in the exact fixed-order contribution.

nonperturbative and scale parameters taken either from the BLNY or our best-fit parametrizations.

5.2.8. Numerical accuracy

Given the complexity of the resummation calculation, we expect several sources of random numerical errors that may compete with the accuracy of the most precise ϕ_η^* data points, which are of order 0.5% of the respective central cross sections. The numerical errors may arise from the parametrizations of PDFs, integration, and interpolation at various stages of the analysis. They can be treated as independent and uncorrelated and primarily result in higher-than-normal values of the figure-of-merit function χ^2 when not explicitly included in the estimates. In comparison, the variations due to a_Z or $C_{1,2,3}$ parameters are of order a few percent and correlated across the ϕ_η^* spectrum.

5.3. Numerical results

5.3.1. General features

In this section we determine a_Z from the distribution $(1/\sigma)\ d\sigma/d\phi_\eta^*$ measured by DØ [21] that is normalized to the total cross section σ in the measured Q and y range. These data are given in three bins of Z boson rapidity y_Z. In the first two, $|y_Z| \leq 1$ and $1 \leq |y_Z| \leq 2$, the $(1/\sigma)\ d\sigma/d\phi_\eta^*$ distribution is measured separately for electrons and muons at $N_{pt} = 29$ points of ϕ_η^*. In the third bin, $|y_Z| \geq 2$, only electrons are measured at 25 points of ϕ_η^*. The first two y_Z bins provide substantial new constraints. The third bin has larger statistical errors and reduced discriminating power.

All predictions are obtained by using CT10 NNLO PDFs [117]. Predictions based on MSTW'08 NNLO PDF sets [154] were also computed and did not show significant

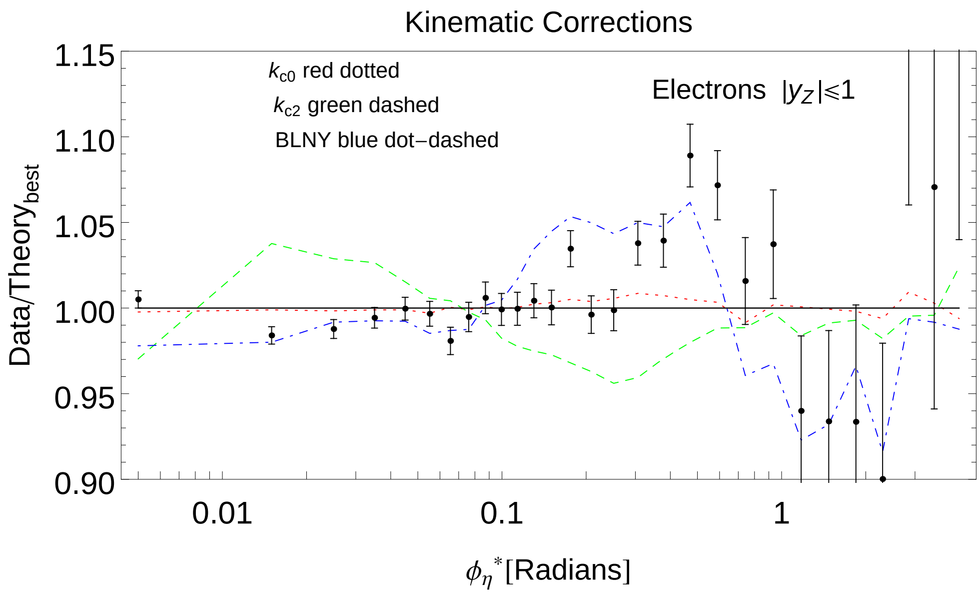

Figure 5.4. The ratios to the central theoretical prediction of the DØ electron data at $|y_Z| \leq 1$ and alternative theoretical predictions. The central prediction is computed assuming $C_1 = C_3 = 2b_0$, $C_2 = 1/2$, $a_Z = 1.1$ GeV^2, and kinematical correction 1. Theory predictions based on alternative kinematical corrections (0 and 2) and BLNY nonperturbative parametrization are also shown.

difference with CT10 NNLO predictions.

From the previous section, the resummed cross sections depend on the perturbative scales, power-suppressed contributions, and choice of subleading kinematic terms. It is possible to identify an optimal combination of these factors that results in a good description of the DØ data across the full ϕ^*_η range. In particular, the large-Q_T/large-ϕ^*_η data generally prefer the factorization scale of order $Q/2$ or even less in the fixed-order piece. At small-Q_T/small-ϕ^*_η, the scale parameter C_3 in the range $1.5b_0 - 2b_0$ is slightly more preferable. To illustrate properties of the ϕ^*_η distributions, we compute the resummed cross sections using a combination $C_1 = C_3 = 2\ b_0$,

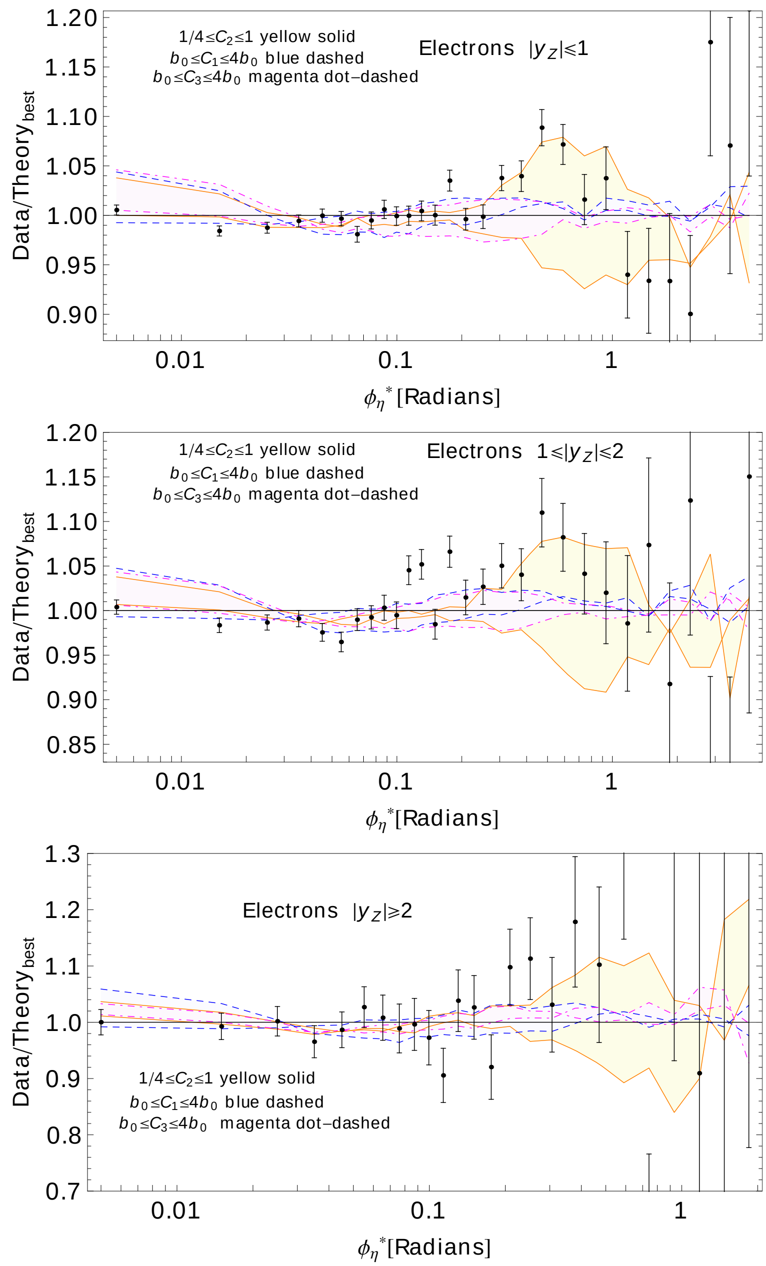

Figure 5.5. Electrons: scale variation due to $C_{1,2,3}$ at small ϕ^*_η.

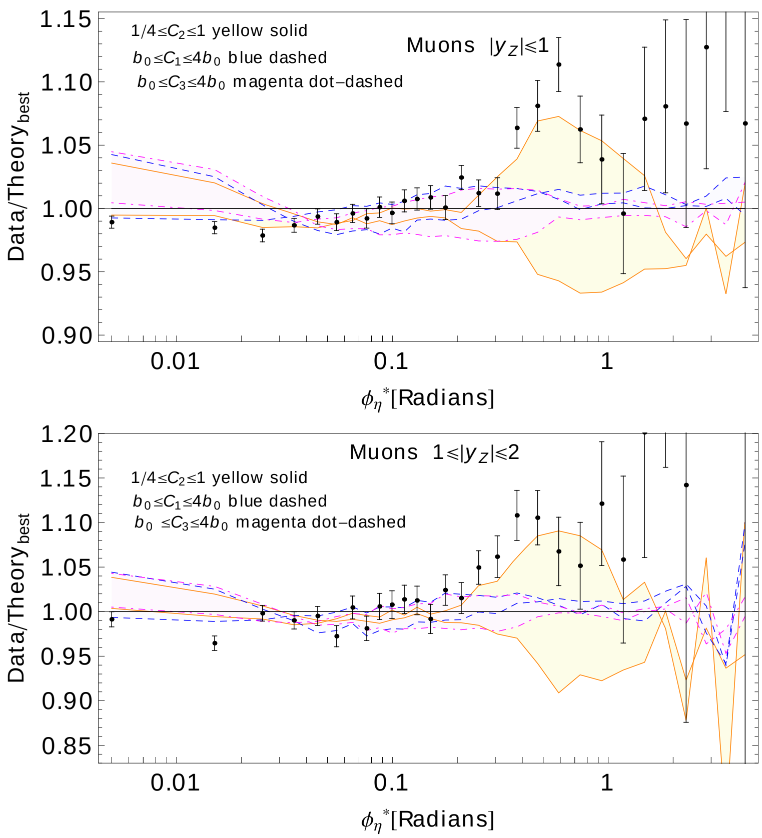

Figure 5.6. Same as above but for the muons.

$C_2 = Q/2$, and $a_Z = 1.1$ GeV^2 that is close to the best-fit solution. The difference between the best-fit solution and the prediction based on these round-off values will be discussed in Sec. 5.3.2.

A comparison of the prediction with these choices to the DØ data for $|y_Z| \leq 1$ and a few other predictions is presented in Fig. 5.4. The new parametrization provides better description of the data at $0.1 \leq \phi_\eta^* \leq 1$ than the superimposed prediction utilizing the BLNY parametrization [96] of $\widetilde{W}^{NP}$. Consequently, it results in a better χ^2 than the ResBos prediction used in the DØ analysis [21], which used the CTEQ6.6 NLO PDFs, BLNY $\widetilde{W}_{NP}$, and canonical choice of $C_{1,2,3}$.

We also compare predictions for three types (0, 1, 2) of the kinematical (matching) correction discussed in Sec. 5.2.6. For the selected combination of scale parameters, the type-0 and 1 kinematical corrections provide a nearly identical prediction. The type-0 and type-1 corrections can differ by 2-3% for other scales. Type 2 is generally disfavored, so that we assume the type-1 correction for the rest of the analysis.

A prediction with the same theoretical parameters, as well as for variations in QCD scales in the ranges $1/4 \leq C_2 \leq 1$ and $b_0 \leq C_{1,3} \leq 4b_0$, are compared to the data for electron production in Fig. 5.5 and muon production in Fig. 5.6. Here we show all rapidity bins both for electron and muon samples. The ratios of the DØ data to ResBos theory with the optimal parameters are indicated by black circles. Yellow solid, blue dashed, and magenta dot-dashed bands represent variations in theory due to C_2, C_1, and C_3, respectively, all normalized to the best-fit prediction. Again, the agreement with ResBos observed in these figures is better than in [21]. Figs. 5.5 and 5.6 demonstrate that the theoretical uncertainty at small ϕ_η^* is dominated by variations of C_1 and C_3. The bands of scale uncertainty are reduced significantly for $0.04 \leq \phi_\eta^* \leq 0.1$ upon the inclusion of $\mathcal{O}(\alpha_s^2)$ scale dependence, as has been discussed in Sec. 5.2.4.

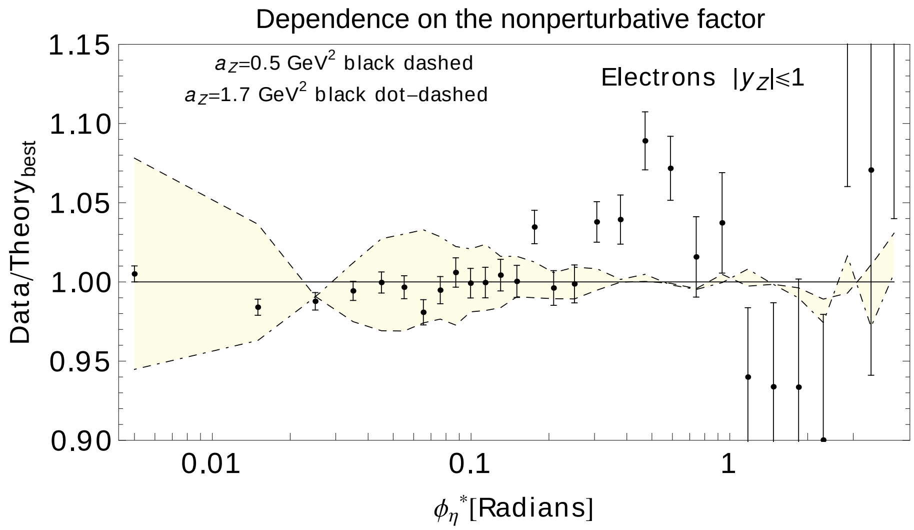

Figure 5.7. Dependence on the nonperturbative parameter a_Z for electrons with $|y_Z| \leq 1$.

The scale variations can be compared to the dependence on a_Z and kinematic correction in Fig. 5.7, which result in a distinctly different patterns of variation in $d\sigma/d\phi_\eta^*$. In particular, while the perturbative scale coefficients C_1, C_2, C_3 produce a slowly changing variation across most of the measured ϕ_η^* range, the increase in a_Z produces a distinct variation that suppresses the rate at $\phi_\eta^* \lesssim 0.02$ and increases it at $0.02 \lesssim \phi_\eta^* \lesssim 0.5$, with the rate above 0.5 essentially unaffected.

It is therefore possible to separate the scale dependence from the a_Z dependence if we restrict the attention to ϕ_η^* below and around $\phi_\eta^* = 0.1$. To this aim we consider only the first 12 bins of ϕ_η^*, starting from the smallest value, for each value of rapidity. Extending the fitted range above $\phi_\eta^* \geq 0.1$ has a minimal effect on a_Z.

5.3.2. Detailed analysis

We pursue two approaches for the examination of the low-ϕ_η^* region. In method I, we study dependence on a_Z assuming fixed resummation scales corresponding to half-integer scale parameters, such as $C_1/b_0 = C_3/b_0 = 1, C_2 = 1/2$ or $C_1/b_0 = C_3/b_0 = 2, C_2 = 1/2$. In this method, the goodness-of-fit function χ^2 is minimized with respect to a_Z for select combinations of fixed scale parameters. We find that a χ^2 minimum with respect to a_Z exists in these cases, but, given the outstanding precision of the ϕ_η^* data, the best-fit χ^2/N_{pt} remains relatively high, of order 2-3. This is partly due to the numerical noise discussed in Sec.5.2.8.

The χ^2 function can be further reduced by allowing arbitrary $C_{1,2,3}$ parameters, in particular, by taking C_2 to be *below* $1/2$. In this context, one has to decide on the acceptable range of variations in $C_{1,2,3}$, *i.e.* the resummation scales.

As computations for multiple combinations of a_Z and $C_{1,2,3}$ parameters would be prohibitively CPU-extensive, in method II we first consider a fixed scale combination indicated by $\{\bar{C}_1, \bar{C}_2, \bar{C}_3\}$ and implement a linearized model for small deviations of the scale parameters from $\bar{C}_{1,2,3}$. The central combination $\bar{C}_{1,2,3}$, namely $\bar{C}_1 = \bar{C}_3 = 2b_0$, $\bar{C}_2 = 1/2$, produces good agreement with the data, although not as good as completely free $C_{1,2,3}$. The linearized model is explained in Sec. 5.3.2.2. It provides a fast estimate of small correlated changes in the ϕ_η^* shape of the kind shown in Figs. 5.5 and 5.6.

The χ^2 function is sampled at discrete a_Z values in the interval $a_Z = [0.1 : 3.5]$ GeV^2 and reconstructed between the sampling nodes by using polynomial interpolation. When the scale variations are allowed, the dependence of χ^2 on a_Z is asymmetric and very different from a quadratic one.

To account for the asymmetry of the distributions, we quote the central value $\overline{a}_Z$ that minimizes $\chi^2(a_Z)$ and the 68% confidence level (C.L.) uncertainty. The probability density function $\mathcal{P}(a_Z)$ for a_Z in a sample with N points is taken to

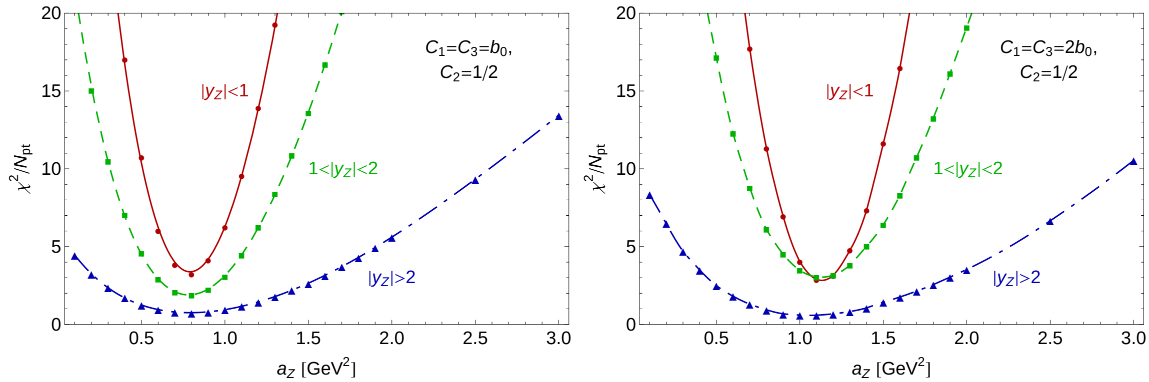

Figure 5.8. χ^2/N_{pt} as a function of a_Z with fixed $C_{1,2,3}$.

follow a chi-squared distribution with N degrees of freedom,

$$\mathcal{P}(a_Z) = \mathcal{P}_\chi(N, \chi^2(a_Z)) = \frac{(\chi^2)^{N/2-1} \exp\left(-\chi^2/2\right)}{\Gamma(N/2)\; 2^{N/2}}. \tag{5.43}$$

With this, we determine the 68% C.L. intervals $[a_{Z,min},\ a_{Z,max}]$, where $a_{Z,min}$ and $a_{Z,max}$ are defined implicitly by

$$0.16 = \frac{\int_0^{a_{Z,min}} \mathcal{P}(a_Z)\; da_Z}{\int_0^{+\infty} \mathcal{P}(a_Z)\; da_Z}\,, \qquad 0.84 = \frac{\int_0^{a_{Z,max}} \mathcal{P}(a_Z)\; da_Z}{\int_0^{+\infty} \mathcal{P}(a_Z)\; da_Z}\,. \tag{5.44}$$

For an asymmetric distribution as in method II, the central value $\overline{a}_Z$ does not coincide with the middle of the 68% C.L. interval or the mean a_Z given by the first moment of the $\mathcal{P}(a_Z)$ distribution.

5.3.2.1. *Method I: minimization with fixed scale parameters*

In method I a_Z is determined from the DØ data by minimization of a function

Fit results for $\phi_\eta^* \leq 0.1$			
	N_{pt}	χ^2_{min}/N_{pt}	$\overline{a}_Z \pm \delta a_Z$ (GeV^2)
$\lvert y_Z \rvert \leq 1, \quad e+\mu$	24	3.24	$0.79^{+0.2}_{-0.03}$
		2.83	1.14 ± 0.08
$1 \leq \lvert y_Z \rvert \leq 2, \quad e+\mu$	24	1.87	0.79 ± 0.05
		3.03	$1.12^{+0.14}_{-0.13}$
$\lvert y_Z \rvert \geq 2, \quad e$	12	0.74	$0.8^{+0.03}_{-0.05}$
		0.58	$1.04^{+0.18}_{-0.16}$
All y_Z bins,	60	2.19	0.79 ± 0.03
weighted average		2.46	1.12 ± 0.07

Table 5.1. The best-fit χ^2/N_{pt}, central value and 68% C.L. intervals for a_Z with fixed $C_{1,2,3} = \{b_0,\ 1/2,\ b_0\}$ (upper lines) and $\{2b_0,\ 1/2,\ 2b_0\}$ (lower lines).

$$\chi^2(a_Z) = \sum_{i=1}^{N_{pt}} \left(\frac{D_i - \bar{T}_i(a_Z)}{s_i} \right)^2, \tag{5.45}$$

where D_i are the data points; $\bar{T}_i(a_Z)$ are the theoretical predictions for fixed scale parameters $\{\bar{C}_1, \bar{C}_2, \bar{C}_3\}$; s_i are the uncorrelated experimental uncertainties; and N_{pt} is the number of points.

The dependence of χ^2 on a_Z in three rapidity bins for two combinations of $\bar{C}_{1,2,3}$ is illustrated in Fig. 5.8, and the corresponding best-fit parameters are listed in Table 5.1. Electrons and muons are combined in the first two bins of rapidity, $|y_Z| \leq 1$ and $1 \leq |y_Z| \leq 2$. In both cases, the χ^2 behavior is close to parabolic. The locations of the χ^2 minima are consistent in all three bins. However, the quality of the fit is unacceptable in the first two bins that have the smallest experimental errors, with $\chi^2/N_{pt} \approx 3$. On the other hand, the agreement is very good ($\chi^2/N_{pt} < 1$) in the third bin, which has larger errors.

The weighted averages over all three bins are $\bar{a}_{Z,\text{all y}} = 0.79 \pm 0.03$ and 1.12 ± 0.07 GeV^2 for the two scale combinations. The location of the minimum is distinct from zero in both cases, but its dependence on the scale parameters warrants further investigation that we will now perform.

5.3.2.2. Method II: computation with scale-parameter shifts

To simplify the minimization when the scale parameters are varied, we introduce a linearized approximation for the covariance matrix of the type adopted for evaluating correlated systematic effects in PDF fits [155, 156]. For each scale parameter C_α, $\alpha = 1, 2, 3$, we define a nuisance parameter $\lambda_\alpha \equiv \log_2(C_\alpha/\bar{C}_\alpha)$ and compute the finite-difference derivatives of theory cross sections

$$\beta_{i\alpha} \equiv \frac{T_i(a_Z, \lambda_\alpha = +1) - T_i(a_Z, \lambda_\alpha = -1)}{2}, \qquad \alpha = 1, 2, 3; \quad i = 1, \ldots, N_{pt} \tag{5.46}$$

over the interval $\lambda_\alpha = \pm 1$ corresponding to $\bar{C}_\alpha/2 \leq C_\alpha \leq 2\bar{C}_\alpha$. Variations of λ_α introduce correlated shifts in theory cross sections $T_i(a_Z, C_{1,2,3})$ with respect to the fixed-scale theory cross sections $T_i(a_Z, \bar{C}_{1,2,3}) \equiv \bar{T}_i(a_Z)$. We can reasonably assume that the probability distribution over each λ_α is similar to a Gaussian one with a central value of 0 and half-width σ_λ, taken to be the same for all λ_α. The goodness-of-fit function is then defined as

$$\chi^2(a_Z, \lambda_{1,2,3}) = \sum_{i=1}^{N_{pt}} \left(\frac{D_i - \bar{T}_i(a_Z) - \sum_{\alpha=1}^{3} \beta_{\alpha i}\lambda_\alpha}{s_i} \right)^2 + \sum_{\alpha=1}^{3} \frac{\lambda_\alpha^2}{\sigma_\lambda^2}. \tag{5.47}$$

The minimum with respect to λ_α can be found algebraically for every a_Z as [155]

$$\min \chi^2 = \chi^2(a_Z, \bar{\lambda}_\alpha) = \sum_{i,j}^{N_{pt}} (D_i - \bar{T}_i(a_Z))(\mathrm{cov}^{-1})_{ij}(D_j - \bar{T}_j(a_Z)), \tag{5.48}$$

containing the inverse of the covariance matrix,

$$(\mathrm{cov}^{-1})_{ij} = \left[\frac{\delta_{ij}}{s_i^2} - \sum_{\alpha,\beta=1}^{3} \frac{\beta_{i,\alpha}}{s_i^2} \mathcal{A}_{\alpha\beta}^{-1} \frac{\beta_{j,\beta}}{s_j^2} \right], \tag{5.49}$$

and a matrix $\mathcal{A}$ given by

$$\mathcal{A}_{\oslash\odot} = \sigma_\lambda^2 \delta_{\alpha\beta} + \sum_{k=1}^{N_{pt}} \frac{\beta_{k,\alpha}\beta_{k,\beta}}{s_k^2}. \tag{5.50}$$

Eq. (5.48) is essentially the standard χ^2 function based on the covariance matrix in the presence of the correlated shifts. For every a_Z, the nuisance parameters $\bar{\lambda}_\alpha$ that realize the χ^2 minimum are also known,

$$\bar{\lambda}_\alpha(a_Z) = \sum_{i=1}^{N_{pt}} \frac{D_i - \bar{T}_i(a_Z)}{s_i} \sum_{\delta=1}^{3} \mathcal{A}^{-1}_{\alpha\delta} \frac{\beta_{i,\delta}}{s_i}. \tag{5.51}$$

Based on this representation for χ^2 (designated as "fitting method II"), we explored the impact of the scale dependence on the constraint on a_Z. Even if the scales are varied, data prefer a nonzero nonperturbative Gaussian smearing of about the same magnitude as in method I.

In the simplest possible case, the $C_{1,2,3}$ parameters are independent of the rapidity or other kinematic parameters and shared by all e and μ bins. In this case, variations of the scale parameters reduce χ^2/N_{pt} to about 1.3, *i.e.* the fit is better than for the fixed scale combinations discussed above. We focus on the case when the central scale parameters are $\bar{C}_1 = \bar{C}_3 = 2\ b_0, C_2 = 1/2$, although the conclusions remain the same for other choices.

The plots of χ^2/N_{pt} vs. a_Z and optimal C_1/b_0, C_2, C_3/b_0 vs. a_Z, derived from the optimal λ_α parameters in Eq. (5.51), are shown in Fig. 5.9. The χ^2 dependence on a_Z becomes asymmetric when the scale shifts are allowed, with the large-a_Z branch being flattened out in contrast to the small-a_Z one that remains steeply growing. From the right inset, we see that the optimal C_1 and C_3 are monotonously increasing and decreasing as functions of a_Z, respectively. In the vicinity of the minimum, C_1 and C_3 are of about the same magnitude at $(1.2 - 1.5)b_0$. Very small or large a_Z can be obtained only by taking C_1 and C_3 to be uncomfortably far from unity. In contrast, the optimal C_2 parameter is generally in the range 0.3-0.5 and has weaker dependence on a_Z.

Fit results for $\phi^*_\eta \leq 0.1$				
C_1,C_2, C_3 are shared by all y_Z bins				
	N_{pt}	χ^2_{min}/N_{pt}	$\overline{a}_Z \pm \delta a_Z$ (GeV^2)	Best-fit $C_{1,2,3}$
All y_Z bins	60	1.29	$0.82^{+0.34}_{-0.12}$	1.4, 0.33, 1.23
		1.31	$0.82^{+0.22}_{-0.11}$	1.42, 0.33, 1.23
C_1,C_2, C_3 are independent in each y_Z bin				
	N_{pt}	χ^2_{min}/N_{pt}	$\overline{a}_Z \pm \delta a_Z$ (GeV^2)	Best-fit $C_{1,2,3}$
$\lvert y_Z \rvert \leq 1, \quad e+\mu$	24	1.0	$0.56^{+0.95}_{-0.02}$	0.21, 0.18, 7.56
		1.16	$0.85^{+0.3}_{-0.15}$	1.47, 0.3, 1.46
$1 \leq \lvert y_Z \rvert \leq 2, \quad e+\mu$	24	1.48	$1.22^{+0.27}_{-0.36}$	18, 0.58,0.1
		1.70	$0.79^{+0.2}_{-0.1}$	1.69, 0.37, 0.77
$\lvert y_Z \rvert \geq 2, \quad e$	12	-	-	-
		0.59	$0.99^{+0.99}_{-0.31}$	1.74, 0.48, 2.12
Weighted average	60		0.97 ± 0.25	
of all bins			0.82 ± 0.12	

Table 5.2. The best-fit χ^2/N_{pt}, central value and 68% C.L. intervals for a_Z, and best-fit $C_{1,2,3}$ for $1/\sigma_\lambda = 0$ (upper rows in each section) and 1 (lower rows).

The values of χ^2/N_{pt}, a_Z, and $C_{1,2,3}$ parameters at the minimum are reported in the upper portion of Table 5.1. When the $C_{1,2,3}$ parameters are shared by all bins, the fit is relatively insensitive to the confidence level assigned to the variations $\lambda_\alpha \pm 1$, controlled by the parameter σ_λ in Eq. (5.47). In Table 5.1, the upper rows in each section correspond to the fit without a constraint on the λ parameters, *i.e.*, for $1/\sigma_\lambda = 0$. The lower rows are for assigning a 68% probability to the $-1 \leq \lambda_\alpha \leq 1$ intervals, corresponding to $1/\sigma_\lambda = 1$.

For the shared $C_{1,2,3}$, the outcomes of the fits with $1/\sigma_\lambda = 0$ and 1 are very similar, apart from the uncertainty on the a_Z parameter, which is increased when the λ_α variations are totally free. [The asymmetric 68% C.L. uncertainties are computed according to Eq. (5.44)].

In contrast, when the scale parameters are taken to be independent in each y_Z bin (but still shared between the electron and muon samples), only the case of $\sigma_\lambda = 1$ results in an acceptable fit in all three y_Z bins. The best-fit parameters for this case are listed in the lower part of Table 5.2. When the scale shifts were arbitrary ($1/\sigma_\lambda = 0$, upper lines), the fits were underconstrained and produced inconsistent a_Z values and large scale shifts in all three bins, especially in the third bin that is not shown for this reason. On the other hand, for $\sigma_\lambda = 1$ (lower lines), the three fits converged well and rendered compatible a_Z values. The χ^2/N_{pt} vs. a_Z dependence for this case is illustrated in Fig. 5.10, where the minima are neatly aligned in the three bins. The fit to the second bin is generally worse than for the other two, suggesting possible rapidity dependence of a_Z. The scale dependence in each bin is qualitatively similar to that in the right inset of Fig. 5.9.

Even when $C_{1,2,3}$ are independent in each y_Z bin, by averaging the a_Z values over three bins, we obtain the $\bar{a}_Z = 0.8 - 0.9$ GeV^2 in the last section of Table 5.2 that is essentially the same as in the case when $C_{1,2,3}$ are shared by all bins. The findings in

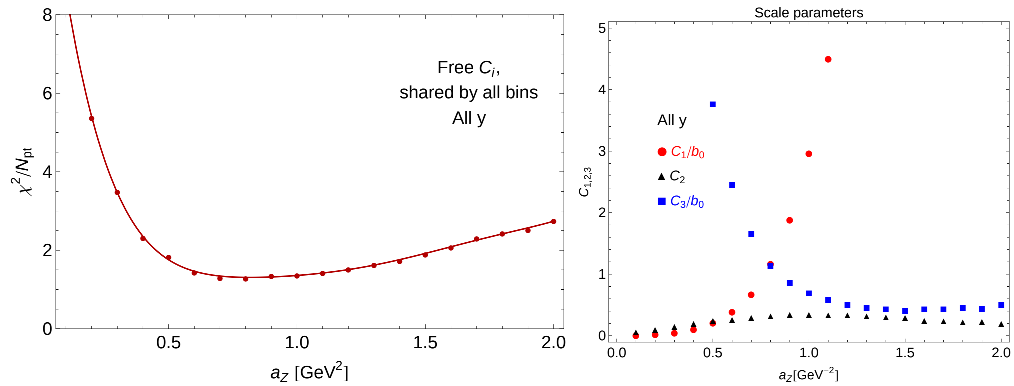

Figure 5.9. χ^2/N_{pt} and scale parameters as a function of a_Z for $\bar{C}_1 = \bar{C}_3 = 2\ b_0, \bar{C}_2 = 1/2$. The scale parameters are shared across three y_Z bins.

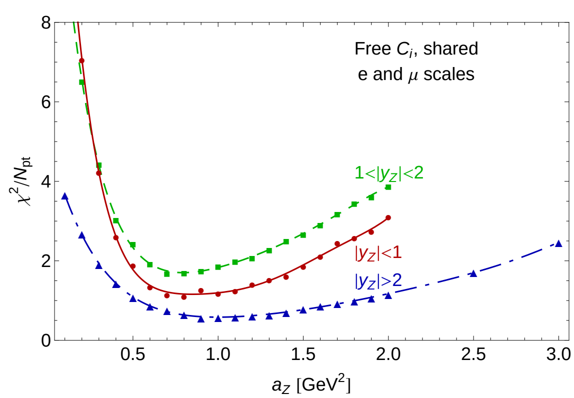

Figure 5.10. χ^2/N_{pt} as a function of a_Z for $\bar{C}_1 = \bar{C}_3 = 2\ b_0, \bar{C}_2 = 1/2$. The scale parameters are independent in each y_Z bin.

Tables 5.1 and 5.2 are recapitulated in Fig. 5.11, showing the 68% C.L. intervals in the fits with fixed $C_{1,2,3} = b_0, 1/2, b_0$ and $2b_0, 1/2, 2b_0$, as well as the fit with varied $C_{1,2,3}$ and $\sigma_\lambda = 1$. All fits consistently yield a_Z values that are at least 5σ from zero.

5.4. Implications for the W mass measurement and LHC

The previous sections demonstrated that the ϕ_η^* distributions in Z/γ^* production are sensitive to several QCD effects. Depending on the ϕ_η^* range, hard or soft QCD emissions can be studied. The nonperturbative power corrections in QCD can be determined at $\phi_\eta^* \leq 0.1$, provided the dependence on resummation scales is controlled.

To distinguish between various contributing effects, new developments in the Collins-Soper-Sterman resummation formalism were necessitated. The computer code ResBos includes all such effects relevant for computation of resummed differential distributions of lepton pairs. New components of the theoretical framework implemented in ResBos were reviewed in Sec. 5.2. In the large-ϕ_η^* region dominated by hard emissions, the two-loop fixed-order contributions implemented in ResBos show good agreement with the DØ data when the renormalization/factorization scale $C_4 Q$ for hard emissions is set to be close to $Q/2$.[5]

In the resummed W piece dominating at small ϕ_η^*, we include 2-loop perturbative coefficients in the resummed W term by using the exact formulas for the $\mathcal{A}$ and $\mathcal{B}$ coefficients and a numerical estimate for the small $\mathcal{O}(\alpha_s^2)$ contribution $\delta C^{(2)}$ to the Wilson coefficient functions. We also fully include up to $\mathcal{O}(\alpha_s^2)$ the dependence on resummation scale parameters C_1 and C_2, see Secs. 5.2.3 and 5.2.4. Matching corrections and final-state electroweak contributions were implemented and investigated in order to understand their non-negligible impact on the cross sections. Finally, we

[5]In this region, a three-loop correction must be computed in the future to reach NNLO accuracy in α_s.

implemented a form factor $\widetilde{W}_{NP}(b,Q)$ describing soft nonperturbative emissions at transverse positions $b \gtrsim 1$ GeV^{-1} in the context of a two-parameter b_* model [97], cf. Sec. 5.2.5.

With this setup, we performed a study of the small-ϕ^*_η region at the DØ Run-2 with the goal to determine the range of plausible nonperturbative contributions. We found that, to describe Drell-Yan dilepton production with the invariant mass $70 \leq Q \leq 110$ GeV, it suffices to use a simplified nonperturbative form factor that retains only a leading power correction, $\widetilde{W}_{NP}(b, Q = M_Z) = \exp\left(-b^2 a_Z\right)$. The power correction modifies the shape of $d\sigma/d\phi^*_\eta$ in a pattern distinct from variations due to the dependence on the resummation scales C_1/b, C_2Q, and C_3/b in the leading-power term $\widetilde{W}^{pert}$, see Figs. 5.5, 5.6, and 5.7. For various fixed combinations of scale parameters $C_{1,2,3}$, or when the scale parameters were varied, the fits require nonzero a_Z values that were summarized in Tables 5.1 and 5.2. For example, when the variations in the scales $C_{1,2,3}$ were incorporated as shared free parameters in all rapidity bins using a correlation matrix, we obtained $a_Z = 0.82^{+0.22}_{-0.11}$ GeV^2 at 68% C.L., cf. Table 5.2, consistently with other tried methods. The estimate of the 68% C.L. uncertainty including the scale dependence indicates clear preference for a non-zero a_Z, without appreciable rapidity dependence.

The magnitude of a_Z depends on the resummation scales, but allowing the scales to vary increases the probability for having larger, not smaller a_Z. The best-fit a_Z is also correlated with b_{max}, which controls the upper boundary of the b range where the exact perturbative approximation for $\widetilde{W}^{pert}(b, Q, y_Z)$ is used. Using $b_{max} = 1.5$ GeV^{-1} in this study, we obtain $a(b, Q) \approx 0.8$ GeV^2 at $Q = M_Z$, which is consistent with the value obtained with the other $\widetilde{W}_{NP}$ forms maximally preserving the perturbative contribution [97,136–138]. The dependence on b_{max} weakens at b_{max} above 1 GeV^{-1}, and even larger a_Z values are preferred for b_{max} below 1 GeV^{-1}, cf. Fig. 2 in [97].

The fitted data was corrected for the effects of final-state NLO QED radiation. In the fitted region $\phi_\eta^* < 0.1$, the uncertainty due to the matching of the resummed and finite-order terms was shown to be negligible.

The nonperturbative form factor at other $\sqrt{s}$ and Q values can be predicted using the relations in Sec. 5.2.5. This is possible because the dominant part of $\widetilde{W}_{NP}$ is associated with the soft factor $\exp\left(-S(b,Q)\right)$ which does not depend on $\sqrt{s}$ or the types of the incident hadrons. It is argued in Sec. 5.2.5 that the $\widetilde{W}_{NP}$ factors are identical within the 68% C.L. error in central-rapidity Z and W production at the same $\sqrt{s}$. The same a_Z value that we determined can be readily applied to predict W boson differential distributions at the Tevatron Run-2, or, with appropriate modifications proportional to $\ln(Q)$ and $\ln(s)$, in other kinematical ranges, cf. Eq. (5.40).

The resummation calculation employed in this analysis can be reproduced using the ResBos-P code [157] and input tables [158] available at the "Q_T resummation portal at Michigan State University". The central input tables are provided for $a_Z = 1.12 \pm 0.07$ GeV^2, $C_1 = C_3 = 2b_0$, $C_2 = 1/2$, and central CT10 NNLO PDF. In addition, the distribution includes ResBos tables corresponding to the best-fit resummed parameters and CT10 NNLO PDF eigenvector sets. Finally, for a detailed exploration of the low-ϕ_η^* region, the distribution includes tables for a_Z in the interval $0.5 - 1.7$ GeV^2 with step 0.1 GeV^2 using the central PDF, and, to study scale dependence, 7 ResBos grids for the central $a_{Z,central} = 1.12$ GeV^2, and the scale parameters $C_1 = b_0, 4b_0$, $C_2 = 1/4, 1$, and $C_3 = b_0, 4b_0$.

As an example of a phenomenological application, Fig. 5.12 compares the ResBos predictions with the ATLAS data [19, 20] on Drell-Yan pair production near the Z boson resonance peak at $\sqrt{s} = 7$ TeV. The figure shows ratios of data to theory cross sections. The left subfigure shows the Q_T distribution for $35 - 40$ pb^{-1}, compared to the ResBos prediction with $a_Z = 1.1$GeV^2, $C_1 = C_3 = 2\ b_0, C_2 = 1/2$. The

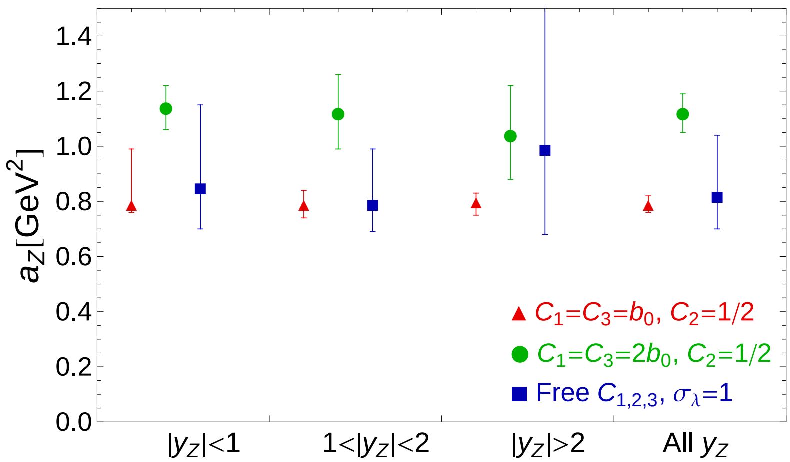

Figure 5.11. 68% C.L. ranges for a_Z in individual y_Z bins and in all bins.

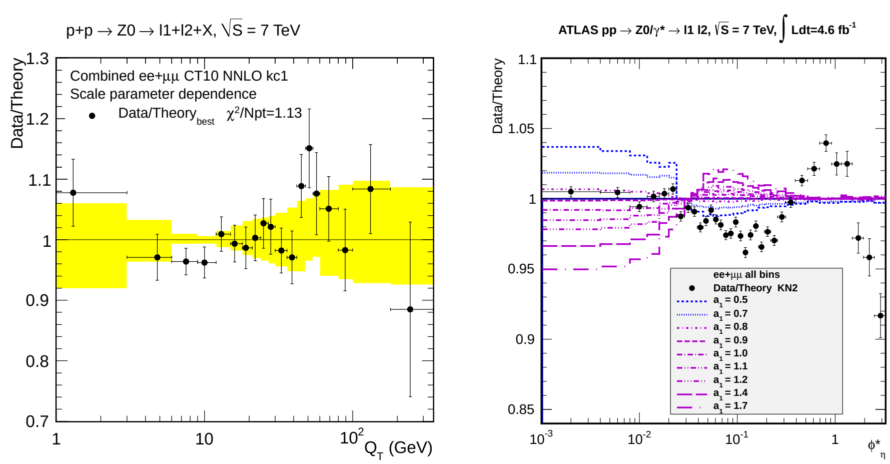

Figure 5.12. Data vs. theory ratios for the Q_T distribution by ATLAS 7 TeV, $35-40$ pb^{-1} [19] and ϕ^*_η distribution ATLAS 7 TeV, 4.6 fb^{-1} [20]

yellow band indicates variations in the cross section due to the scales in the range $C_1 = b_0, 4b_0$, $C_2 = 1/4, 1$, and $C_3 = b_0, 4b_0$. In the case of Q_T distribution, we obtain good agreement between theory and data and in the intermediate/small Q_T region the theoretical uncertainty due to $C_{1,2,3}$ scale parameters is reduced compared to the study of Ref. [88].

The right subfigure shows the ratio of the more recent ϕ^*_η distribution to the central theory prediction based on our default parametrization at much higher level of accuracy. Here, a ResBos prediction based on the BLNY parametrization has shown better agreement with the data than other available codes and was used for event simulation during the ATLAS analysis. A comparable, although somewhat worse agreement is realized by the GNW parametrization, which was not used at any stage by ATLAS. The right subfigure shows several curves for the default $C_{1,2,3}$ choice and a_Z in the range $0.5 - 1.7$ GeV^2. It is clear that the ATLAS ϕ^*_η data is sensitive to a_Z as well as b_{max} and can possibly discriminate subleading power contributions to the nonperturbative form factor $\widetilde{W}_{NP}(b, Q)$ proportional to b^4 and beyond. We provide sets of updated ResBos grids for the LHC kinematics that can be used for future improvements in the nonperturbative model.

5.5. Nonperturbative resummed contributions at low Q

As presented above, the data from Tevatron and the LHC have put better constraints on the nonperturbative parameterizations of the resummed cross section in CSS resummation formalism. However, one needs to be cautious to use the same parameterization for a lower Q region, as in this case the cross section receives more contribution from the large b region where the nonperturbative factor becomes important, and therefore is more sensitive to the form of the parameterization. The trend is clearly shown in Fig. 5.13 where the b-space cross section multiplied by b is plotted as a function of b at $Q = m_Z$ and $Q = 11$ GeV. The uncertainty caused by variation of b_{max} increases substantially as Q decreases. This shows that simply extending the high Q fit to small Q may turn out to be unsuccessful.

A recent study Ref. [159] suggests that the quadratic form of Eqs. (5.35) can be modified to reduce the b_{max} dependence. The modification satisfies general properties of the a_2 term in the small and large b limits (see Eq.(79) of that reference for the explicit form for the proposed parameterization). The effect is reflected in the evolution kernel $\tilde{K}(b, \mu)$ [1] of the TMD distributions. The desired property that $\tilde{K}(b, \mu)$ approaches a constant at large b is clearly shown in Fig. 5.14. At small b the quadratic behavior of the nonperturbative parameterization is recovered as expected. The full consequence of this new parameterization is under an on-going study by D. Clark, P. Nadolsky, T. Rogers, N. Sato, and B. Wang.

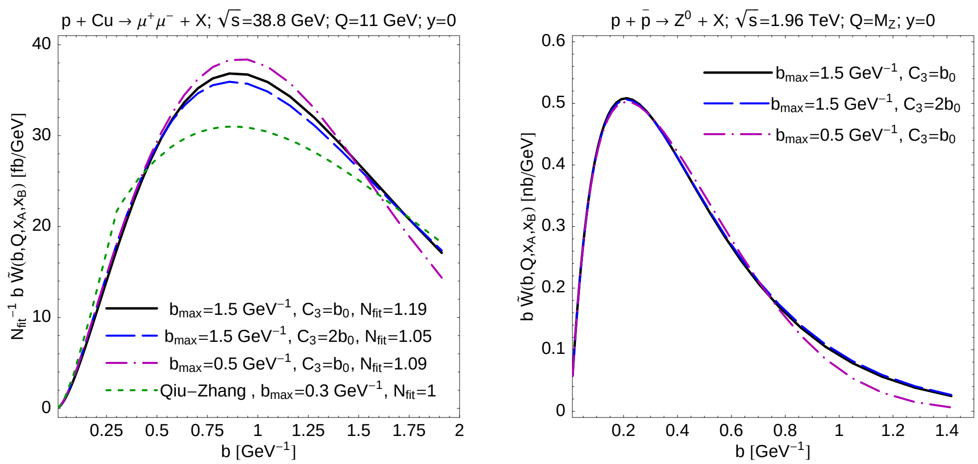

Figure 5.13. From [97]: the best-fit form factors $b\tilde{W}(b)$ in (a) Tevatron Run-2 Z boson production; (b) E605 experiment.

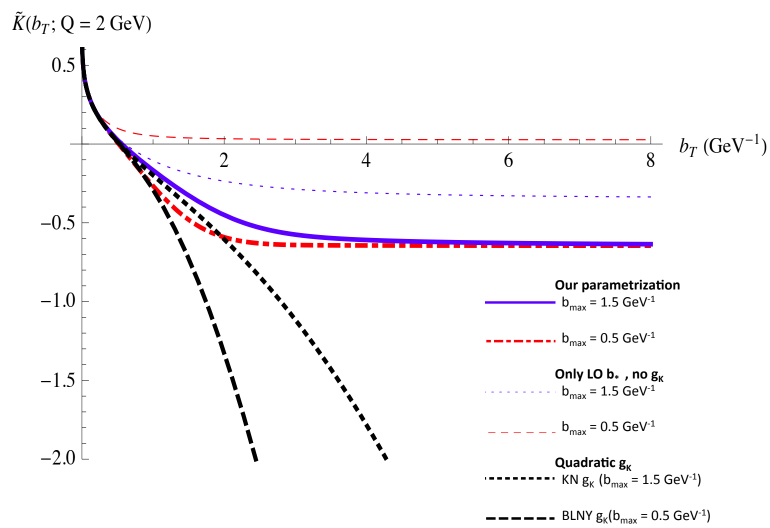

Figure 5.14. From [159]: different nonperturbative parameterizations for $\tilde{K}(b,\mu)$ at $Q = 2$ GeV.

5.6. Conclusions

In our analysis we have shown that a significant nonperturbative Gaussian smearing is necessary to describe features of the low ϕ_η^* spectrum. A non-zero NP function is present even if all the perturbative scale parameters of the CSS formalism are varied. Values of a_Z smaller than 0.5 GeV^2 are disfavored by the fit to the recent DØ data, as demonstrated in Sec. 5.3. Therefore, the small-Q_T/small-ϕ_η^* spectrum cannot be fully described by employing perturbative scale variations only. The constraining power of ϕ_η^* differential distribution data allows us to estimate the size of these nonperturbative effects. The parameterization of the nonperturbative factor could be different for low Q processes such as semi-inclusive DIS at the ep collider HERA. Further studies are needed to reconcile our result with low Q fits.

Concluding, ResBos is a valuable tool for investigations at low transverse momentum regions at colliders. It will be of particular interest to explore the constraining power of the new forthcoming LHC data for Z and W production at a variety of $\sqrt{s}$, boson's invariant masses, and rapidities. Precise measurements of hadronic cross sections at small Q_T will verify the TMD formalism for QCD factorization and shed light on the nonperturbative QCD dynamics.

Chapter 6

Summary and Conclusion

In this thesis, I present two studies applying QCD factorization theorems to important hadronic processes. In the study of DIS with massive quark contributions, I've developed a framework for implementation of DIS factorization in a general-mass scheme and intermediate mass scheme. Approximate analytic expressions for structure functions with mass dependence are derived for all classes of QCD radiative contributions at N3LO. The general results I obtain account for dependences on heavy-flavor masses arising both from hard scattering coefficients and from phase-space constraints. This derivation not only enables an immediate calculation of DIS structure functions in intermediate mass scheme using N3LO zero-mass coefficient functions, it also ensures a full implementation in general-mass scheme once the corresponding massive coefficients are published. Meanwhile, I've programmed the N3LO IM calculation into the CTEQ fitting package and used it to obtain numerical results. When compared with the GM prediction near the heavy quark threshold, IM scheme shows a much slower convergence and is less stable when the factorization scale μ or the rescaling variable λ are varied. This behavior indicates that the convergence of IM scheme is not satisfactory unless the missing mass dependence from the coefficient functions is implemented to obtain a GM result. However, I have found that increasing μ or λ from their default values ($\mu = Q$, $\lambda = 0$) tends to bring the IM prediction close to the GM prediction. In the Q and x range we have explored, the preferred combination of μ and λ is $\lambda \approx 0.2$ and $\mu \approx 1.5Q$.

In the other study I and my collaborators extended the CSS resummation formalism to the distribution of a transverse-momentum-dependent variable ϕ^*_η, which has been measured precisely at the hadron colliders LHC and Tevatron. After making several advancements that substantially improve the theory prediction, our calculation reaches an accuracy at which the nonperturbative contribution to the resummed cross section at small ϕ^*_η is unambiguously constrained by the data. In our fits to transverse momentum distributions in inclusive Z boson production at the Tevatron, positive values of a_Z above 0.5 GeV^2 are strongly preferred, even after the uncertainty due to variations of perturbative scales are included by the fits. This study gives conclusive evidence that the nonperturbative smearing at small ϕ^*_η must be included in order to obtain sensible description of the Q_T distributions in the Tevatron vector boson production. This work is done by M. Guzzi, P. Nadolsky, and myself. In this work, I've derived the relation between the kinematic variable ϕ^*_η and Q_T, and explored various prescriptions for matching the resummed contribution onto the fixed-order result, and found the best candidate that has been used by our fittings. I also contributed to the development of the resummation code ResBos and adopted it for calculations of vector boson production in LHC nuclear-nuclear scattering documented in [160].

Appendix A

Factorization scale dependent DIS coefficients at N3LO in ZM approximation

In this appendix I collect explicit parameterizations of the scale-dependent parts of N3LO zero-mass coefficient functions in Eqs. (4.106) to (4.123). These expressions are obtained by fitting to the corresponding coefficients in the above equations using elementary functions to speed up numerical calculation. The abbreviations used in these functions follow the convention in Ref. [64], where

$$x_1 = 1 - x,\ L_0 = \ln x,\ L_1 = \ln x_1,\ D_k = [L_1^k/x_1]_+ \tag{A.1}$$

More compact expressions can be further obtained by optimizing the the set of elementary functions used in the fits. However, the results here are sufficient to achieve desirable accuracy and speed in our numerical calculation. With an error of 0.1% or less the non-zero coefficients are given by

$$\begin{aligned}
c_{2,q}^{(3,3),NS} =& 308.55\delta(1-x) - 101.66D_0 - 199.11D_1 + 75.852D_2 + 148.24 - 139.11x \\
& - 6.7296x^2 - 0.32885x^3 + 33.842L_0 + 1.5424L_0^2 - 0.00092756L_0^3 \\
& + 0.067578xL_0^5 + 274.96L_1 + 250.85L_0L_1 - 37.83x_1L_0L_1 + 74.512L_0^2L_1 \\
& + 13.72L_0^3L_1 + 1.3355L_0^4L_1 + 0.14154L_0^5L_1 - 75.852L_1^2 + 21.358x_1L_1^2 \\
& - 7.4233L_0L_1^2 - 0.000010418L_1^3 + 1.2416L_0L_1^3 + 0.093976L_0L_1^4 + 0.00351L_0L_1^5 \\
& + N_f(-29.819\delta(1-x) - 11.852D_0 + 18.963D_1 + 1.1852 + 10.667x \\
& + 7.1111L_0 + 7.1111xL_0 - (9.4815L_0)/x_1 - 9.4815L_1 - 9.4815xL_1)
\end{aligned}$$

$$+ N_f^2(0.59259\delta(1-x) + 0.79012D_0 - 0.39506 - 0.39506x), \tag{A.2}$$

$$\begin{aligned}
c_{2,q}^{(3,2),NS} =& -3136.8\delta(1-x) + 1993.9D_0 + 363.65D_1 - 704D_2 + 151.7D_3 \\
& - 2225.1 + 488.49x + 486.69x^2 - 83.463x^3 - 481.39L_0 \\
& - 111.7L_0^2 - 4.7637L_0^3 - 5.7988xL_0^5 - 2267.6L_1 - 2850.1L_0L_1 \\
& + 985.17x_1L_0L_1 - 516.67L_0^2L_1 - 88.271L_0^3L_1 - 7.2046L_0^4L_1 - 5.7366L_0^5L_1 \\
& + 1253.8L_1^2 - 394.29x_1L_1^2 + 496.05L_0L_1^2 - 151.71L_1^3 - 40.285L_0L_1^3 \\
& + 4.6966L_0L_1^4 + 0.29938L_0L_1^5 + N_f(458.24\delta(1-x) - 28.9D_0 - 162.77D_1 \\
& + 42.667D_2 + 78.21 - 308.93x + 1.3006x^2 - 0.78035x^3 \\
& + 74.036L_0 + 8.2812L_0^2 - 0.00032616L_0^3 + 0.57989xL_0^5 + 307.37L_1 \\
& + 242.52L_0L_1 - 9.9832x_1L_0L_1 + 91.021L_0^2L_1 + 18.229L_0^3L_1 + 1.762L_0^4L_1 \\
& + 0.66393L_0^5L_1 - 42.666L_1^2 - 6.8392x_1L_1^2 - 17.458L_0L_1^2 + 0.000021119L_1^3 \\
& + 1.2188L_0L_1^3 + 0.070134L_0L_1^4 + 0.0010968L_0L_1^5) + N_f^2(-13.428\delta(1-x) \\
& - 5.7284D_0 + 2.3704D_1 + 3.1605 + 6.716x + 2.3704L_0 + 2.3704xL_0 \\
& + 2.3704xL_0 - (4.7407L_0)/x_1 - 1.1852L_1 - 1.1852xL_1),
\end{aligned} \tag{A.3}$$

$$\begin{aligned}
c_{2,q}^{(3,1),NS} =& 9909.8\delta(1-x) - 3466.1D_0 + 1475.3D_1 + 1012.6D_2 - 692.15D_3 \\
& + 94.815D_4 - 1.3022e5 - 1.6888e6x + 4.9762e6x^2 + 1.5383e6x^3 \\
& - 39109L_0 - 3820.2L_0^2 - 116.17L_0^3 - 1.2286e5xL_0^5 + 1.2579e6L_1 \\
& - 1.2349e7L_0L_1 + 9.2416e6x_1L_0L_1 - 2.8764e6L_0^2L_1 - 7.222e5L_0^3L_1 \\
& - 82641L_0^4L_1 - 1.2637e5L_0^5L_1 + 1.2404e5L_1^2 - 1.7743e7x_1L_1^2 \\
& - 2.4192e7L_0L_1^2 + 7056.2L_1^3 - 2.5795e6L_0L_1^3 - 3.0623e5L_0L_1^4
\end{aligned}$$

$$
\begin{aligned}
&- 31762L_0L_1^5 + N_f(-1752.8\delta(1-x) + 314.4D_0 + 163.4D_1 - 229.93D_2 \\
&+ 31.605D_3 - 352.69 - 569.88x + 83.527x^2 + 46.774x^3 - 236.92L_0 \\
&- 114.12L_0^2 - 8.9338L_0^3 - 0.13281xL_0^5 - 1785.9L_1 - 949.61L_0L_1 \\
&+ 84.103x_1L_0L_1 - 77.659L_0^2L_1 - 21.676L_0^3L_1 - 2.0691L_0^4L_1 \\
&- 0.24703L_0^5L_1 + 337.18L_1^2 - 57.32x_1L_1^2 - 151.17L_0L_1^2 - 35.185L_1^3 \\
&- 3.2916L_0L_1^3 - 0.096397L_0L_1^4 - 0.0016913L_0L_1^5) + N_f^2(63.585\delta(1-x) \\
&- 0.79012D_0 - 11.457D_1 + 2.3704D_2 + 6.4081 - 55.287x + 12.039L_0 \\
&- 4.3457xL_0 + (3.9506xL_0)/x_1 + 3.5846L_0^2 - 0.59259xL_0^2 \\
&+ (1.1852xL_0^2)/x_1 + 30.6L_1 + 23.96L_0L_1 + 4.048L_0^2L_1 - 2.276L_1^2),
\end{aligned}
\tag{A.4}
$$

$$
\begin{aligned}
c_{L,q}^{(3,2),NS} =& - 234.67 + 445.9x - 18.963L_0 + 215.7xL_0 + 9.4815xL_0^2 + 75.852L_1 \\
&- 431.41xL_1 + 75.852xL_1^2 + 75.852x(-L_0L_1 - Li_2(x)) + 75.852xLi_2(x) \\
&+ N_f(14.222 - 71.111x - 14.222xL_0 + 28.444xL_1) + 2.3704N_f^2x,
\end{aligned}
\tag{A.5}
$$

$$
\begin{aligned}
c_{L,q}^{(3,1),NS} =& - 0.87467D_0 + 2.9520\delta(1-x) + 1673.2 - 2019.4x - 157.33x^2 - 33.264x^3 \\
&+ 563.89L_0 + 38.908L_0^2 + 0.015289L_0^3 + 3.6906xL_0^5 + 1424.4L_1 \\
&+ 3522L_0L_1 + 247.33x_1L_0L_1 + 1245.9L_0^2L_1 + 131.57L_0^3L_1 + 11.105L_0^4L_1 \\
&+ 4.4232L_0^5L_1 - 542.69L_1^2 - 106.96x_1L_1^2 - 1052.1L_0L_1^2 + 72.64L_1^3 \\
&- 23.271L_0L_1^3 - 2.0821L_0L_1^4 - 0.094305L_0L_1^5 + N_f(-0.21867\delta(1-x) - 201.63 \\
&+ 467.6x - 38.763L_0 + 183.31xL_0 - 0.041333L_0^2 + 49.636xL_0^2 - 45.942L_1 \\
&- 184.1xL_1 - 200.67L_0L_1 + 18.16L_1^2 + 18.963xL_1^2 + 37.926x(-L_0L_1 - Li_2(x)) \\
&+ 47.407xLi_2(x)) + N_f^2(4.7407 - 19.753x - 9.4815xL_0 + 4.7407xL_1),
\end{aligned}
\tag{A.6}
$$

$$
\begin{aligned}
c_{2,q}^{(3,3),PS} =& N_f(128.11 - 78.222/x + 4.46x + 78.222x^2 - 39.111L_0 - (14.222L_0)/x \\
& - 18.963xL_0 + 12.642x^2L_0 + 5.9259L_0^2 - 26.074xL_0^2 + 20.148L_1 \\
& + (26.864L_1)/x - 20.148xL_1 - 26.864x^2L_1 - 40.296Li_2(x) - 40.296xLi_2(x)) \\
& + N_f^2(1.1852 + 1.5802/x - 1.1852x - 1.5802x^2 + 2.3704L_0 + 2.3704xL_0),
\end{aligned}
\tag{A.7}
$$

$$
\begin{aligned}
c_{2,q}^{(3,2),PS} =& N_f(-2577 - 519.71/x + 2452.6x + 670.85x^2 - 27.766x^3 \\
& - 1339.7L_0 - (92.445L_0)/x + 59.722L_0^2 - 20.315L_0^3 - 22.157xL_0^5 \\
& - 0.1809L_1 + 1889.7L_0L_1 - 1064.1L_0^2L_1 + 184.32L_0^3L_1 \\
& + 3.8334L_0^4L_1 - 14.034L_0^5L_1 - 0.011195L_1^2 - 446.79x_1L_1^2 \\
& - 68.801L_0L_1^2 - 0.00023531L_1^3 + 59.064L_0L_1^3 + 4.4548L_0L_1^4 \\
& + 0.15857L_0L_1^5) + N_f^2(-41.481 + 2.3704/x + 27.259x + 11.852x^2 \\
& - 18.963L_0 - 26.074xL_0 + 9.4815x^2L_0 - 7.1111L_0^2 - 7.1111xL_0^2),
\end{aligned}
\tag{A.8}
$$

$$
\begin{aligned}
c_{2,q}^{(3,1),PS} =& N_f(-1.0426e5 - 1327.3/x + 1.0591e5x + 369.04x^2 - 840.12x^3 \\
& - 44264L_0 - (196.19L_0)/x - 6075.8L_0^2 - 678.89L_0^3 + 312.43xL_0^5 \\
& - 27.464L_1 + 38744L_0L_1 - 32525L_0^2L_1 - 2662.1L_0^3L_1 - 1230.9L_0^4L_1 \\
& + 204.25L_0^5L_1 - 1.8507L_1^2 - 2132x_1L_1^2 + 9166.7L_0L_1^2 - 0.042467L_1^3 \\
& + 1744.6L_0L_1^3 + 159.44L_0L_1^4 + 7.4339L_0L_1^5) + N_f^2(-1108.5 \\
& + 2.3109/x + 1420.5x - 350.75x^2 + 36.062x^3 - 187.79L_0 \\
& - (0.00011512L_0)/x + 2.7895L_0^2 + 5.8977L_0^3 - 13.273xL_0^5 \\
& - 0.058827L_1 + 433.38L_0L_1 - 489.15L_0^2L_1 + 111.58L_0^3L_1 + 4.6653L_0^4L_1
\end{aligned}
$$

$$
\begin{aligned}
&- 9.3149 L_0^5 L_1 - 0.0035366 L_1^2 + 22.537 x_1 L_1^2 + 137.96 L_0 L_1^2 \\
&- 0.000071868 L_1^3 + 16.668 L_0 L_1^3 + 1.3545 L_0 L_1^4 + 0.051912 L_0 L_1^5), \qquad \text{(A.9)}
\end{aligned}
$$

$$
\begin{aligned}
c_{L,q}^{(3,2),PS} =& N_f(289.19 - 214.52/x + 92.9x - 471.7x^2 - 71.111 L_0 - (42.667 L_0)/x \\
&+ 298.67 x L_0 - 37.926 x^2 L_0 + 128 x L_0^2 - 184.89 L_1 + (61.63 L_1)/x + 123.26 x^2 L_1 \\
&+ 184.89 x Li_2(x)) + N_f^2(-14.222 + 4.7407/x + 9.4815 x^2 - 14.222 x L_0),
\end{aligned}
\qquad \text{(A.10)}
$$

$$
\begin{aligned}
c_{L,q}^{(3,1),PS} =& N_f(-3314.6 + 102.66/x + 5670.9x - 3197.1x^2 + 738.22x^3 - 1402.1 L_0 \\
&+ (28.442 L_0)/x + 60.877 L_0^2 - 2.6978 L_0^3 - 25.085 x L_0^5 - 724.27 x_1^2 L_1 \\
&+ 4.7652 L_0 L_1 - 915.67 L_0^2 L_1 + 378.68 L_0^3 L_1 + 12.415 L_0^4 L_1 - 16.477 L_0^5 L_1 \\
&- 76.44 x_1^2 L_1^2 + 0.51302 L_0 L_1^2 - 31.596 x_1^2 L_1^3 + 0.018705 L_0 L_1^3 \\
&- 1.6877 x_1^2 L_1^4) + N_f^2(101.54 - 18.962/x - 30.29x + 20.191x^2 \\
&- 25.693x^3 + 37.453 L_0 + 66.843 x L_0 + 18.963 x^2 L_0 + 0.56133 L_0^2 \\
&+ 2.0267 x L_0^2 + 49.698 L_1 - (9.4815 L_1)/x - 49.456 x L_1 + 16.189 x^2 L_1 \\
&- 6.9493 x^3 L_1 - 28.444 x Li_2(x)), \qquad \text{(A.11)}
\end{aligned}
$$

$$
\begin{aligned}
c_{2,g}^{(3,3)} =& N_f(399.05 - 181.33/x - 525.5x + 1149.4x^2 - 24.444 L_0 - (32 L_0)/x \\
&- 686.22 x L_0 + 260.44 x^2 L_0 + 19.852 L_0^2 - 215.7 x L_0^2 + 9.4815 x^2 L_0^2 \\
&- 34.519 L_1 + (78.222 L_1)/x + 675.85 x L_1 - 772.44 x^2 L_1 - 78.815 L_0 L_1 \\
&+ 157.63 x L_0 L_1 - 157.63 x^2 L_0 L_1 + 78.815 L_1^2 - 157.63 x L_1^2 + 157.63 x^2 L_1^2 \\
&- 176 Li_2(x) - 352 x Li_2(x) - 77.037 x^2 Li_2(x)) + N_f^2(-15.259 + 3.358/x
\end{aligned}
$$

$$+ 39.704x - 26.025x^2 - 3.8519L_0 + 13.037xL_0 - 1.7778L_0^2 + 3.5556xL_0^2$$
$$+ 5.037L_1 - 10.074xL_1 + 10.074x^2L_1), \quad \text{(A.12)}$$

$$\begin{aligned}
c_{2,g}^{(3,2)} =& N_f(-57450 - 1228.1/x + 47479x + 10102x^2 + 2427.5x^3 - 17307L_0 \\
&- (208.01L_0)/x - 1354.6L_0^2 - 107.18L_0^3 - 357.75xL_0^5 - 379.06L_1 \\
&+ 35759L_0L_1 - 16867L_0^2L_1 + 4963.8L_0^3L_1 + 180.86L_0^4L_1 - 197.24L_0^5L_1 \\
&- 370.32L_1^2 - 388.72x_1L_1^2 + 5088.3L_0L_1^2 + 132.44L_1^3 + 1330.5L_0L_1^3 \\
&+ 80.9L_0L_1^4 + 2.9889L_0L_1^5) + N_f^2(1344.3 + 3.755/x - 1122.1x \\
&- 247.27x^2 - 14.576x^3 + 446.05L_0 + (0.00012663L_0)/x + 52.883L_0^2 \\
&+ 6.3206L_0^3 + 5.4021xL_0^5 - 32.587L_1 - 846L_0L_1 + 275.42L_0^2L_1 \\
&- 118.79L_0^3L_1 - 5.3802L_0^4L_1 + 2.0534L_0^5L_1 + 9.3333L_1^2 + 194.83x_1L_1^2 \\
&+ 44.656L_0L_1^2 - 9.8797e-6L_1^3 - 22.146L_0L_1^3 - 1.5846L_0L_1^4 - 0.050975L_0L_1^5),
\end{aligned} \quad \text{(A.13)}$$

$$\begin{aligned}
c_{2,g}^{(3,1)} =& N_f(-3.36D_0 + 3.08\delta(1-x) - 2.8815e7 - 48.168/x + 2.848e7x - 1.6448e6x^2 \\
&- 6.4254e5x^3 - 7.7369e6L_0 - (146.04L_0)/x - 7.3547e5L_0^2 - 25503L_0^3 \\
&- 41247xL_0^5 - 7.5335e5L_1 + 2.1693e7L_0L_1 - 4.644e6L_0^2L_1 + 3.3127e6L_0^3L_1 \\
&+ 1.4557e5L_0^4L_1 + 39200L_0^5L_1 - 78297L_1^2 + 9.0347e6x_1L_1^2 + 1.6752e7L_0L_1^2 \\
&- 3920.9L_1^3 + 2.1277e6L_0L_1^3 + 2.3136e5L_0L_1^4 + 21262L_0L_1^5) \\
&+ N_f^2(-0.186667\delta(1-x) + 25577 - 0.058912/x - 27228x + 1573x^2 + 165.3x^3 \\
&+ 9176.9L_0 - (0.0038876L_0)/x + 1339.1L_0^2 + 80.841L_0^3 - 48.032xL_0^5 \\
&+ 19.23L_1 - 9640.5L_0L_1 + 8303.2L_0^2L_1 + 334.28L_0^3L_1 + 267.15L_0^4L_1 \\
&- 33.442L_0^5L_1 - 18.685L_1^2 - 49.197x_1L_1^2 - 2785.1L_0L_1^2 - 3.0983L_1^3
\end{aligned}$$

$$- 399.04L_0L_1^3 - 49.526L_0L_1^4 - 2.3414L_0L_1^5), \tag{A.14}$$

$$\begin{aligned}
c_{L,g}^{(3,2)} =& N_f(269.33 - 498.67/x + 4314x - 7570.7x^2 - 238.22L_0 - (96L_0)/x \\
& + 4085.3xL_0 - 519.11x^2L_0 + 1009.8xL_0^2 - 483.56L_1 + (192L_1)/x - 3315.6xL_1 \\
& + 3607.1x^2L_1 - 576xL_0L_1 + 576x^2L_0L_1 + 576xL_1^2 - 576x^2L_1^2 \\
& + 1543.1xLi_2(x) + 576x^2Li_2(x)) + N_f^2(33.778 + 10.074/x - 200.89x + 157.04x^2 \\
& + 21.333L_0 - 71.111xL_0 - 28.444x^2L_0 - 21.333xL_0^2 + 32xL_1 - 32x^2L_1),
\end{aligned} \tag{A.15}$$

$$\begin{aligned}
c_{L,g}^{(3,1)} =& N_f(1.9209e5 + 193.97/x - 1.6788e5x - 17981x^2 - 6269.8x^3 + 50113L_0 \\
& + (64.016L_0)/x + 5164.1L_0^2 + 156.89L_0^3 + 1100.5xL_0^5 + 30.05L_1 \\
& - 1.0998e5L_0L_1 + 56816L_0^2L_1 - 16132L_0^3L_1 - 546.58L_0^4L_1 + 570.79L_0^5L_1 \\
& + 1.9748L_1^2 + 2045.1x_1L_1^2 - 20527L_0L_1^2 + 0.044221L_1^3 - 4553.1L_0L_1^3 \\
& - 326.95L_0L_1^4 - 13.199L_0L_1^5) + N_f^2(-480.99 - 42.863/x + 886.38x \\
& - 843.69x^2 + 34.592x^3 - 252.14L_0 + 40.032xL_0 - 62.097x^2L_0 - 50.265L_0^2 \\
& + 154.01xL_0^2 - 0.28067L_0^3 + 16.249xL_0^3 + 500.47L_1 - 781.54xL_1 \\
& + 267.18x^2L_1 + 13.899x^3L_1 + 1548xL_0L_1 + 63.16L_1^2 - 95.96xL_1^2 + 32.8x^2L_1^2 \\
& + 774x(-L_0L_1 - Li_2(x)) + 31.88Li_2(x) + 908.15xLi_2(x) + 105.46x^2Li_2(x)),
\end{aligned} \tag{A.16}$$

REFERENCES

[1] J. Collins, Foundations of perturbative QCD (Cambridge University Press, 2013).

[2] G.F. Sterman, An Introduction to quantum field theory (Cambridge University Press, 1993).

[3] M.E. Peskin and D.V. Schroeder, An Introduction to quantum field theory (Addison-Wesley, 1995).

[4] D.J. Gross and F. Wilczek, Phys. Rev. Lett. 30 (1973) 1343.

[5] H.D. Politzer, Phys. Rev. Lett. 30 (1973) 1346.

[6] S. Bethke, Nucl.Phys.Proc.Suppl. 234 (2013) 229, 1210.0325.

[7] T. Kinoshita, J. Math. Phys. 3 (1962) 650.

[8] T.D. Lee and M. Nauenberg, Phys. Rev. 133 (1964) B1549.

[9] G.F. Sterman, QCD and beyond. Proceedings, Theoretical Advanced Study Institute in Elementary Particle Physics, TASI-95, Boulder, USA, June 4-30, 1995, 1995, hep-ph/9606312.

[10] W.K. Tung, Perturbative QCD and the parton structure of the nucleon (Unpublished, 2001).

[11] CTEQ, R. Brock et al., Rev. Mod. Phys. 67 (1995) 157.

[12] S. Dulat et al., Phys. Rev. D89 (2014) 113002, 1310.7601.

[13] S. Dulat et al., (2015), 1506.07443.

[14] P.M. Nadolsky et al., Phys. Rev. D78 (2008) 013004, 0802.0007.

[15] J.C. Collins and D.E. Soper, Nucl.Phys. B193 (1981) 381.

[16] J.C. Collins and D.E. Soper, Nucl.Phys. B197 (1982) 446.

[17] J.C. Collins, D.E. Soper and G.F. Sterman, Nucl.Phys. B250 (1985) 199.

[18] J.C. Collins and A. Metz, Phys.Rev.Lett. 93 (2004) 252001, hep-ph/0408249.

[19] ATLAS Collaboration, G. Aad et al., Phys.Lett. B705 (2011) 415, 1107.2381.

[20] ATLAS Collaboration, G. Aad et al., Phys.Lett. B720 (2013) 32, 1211.6899.

[21] D0 Collaboration, V.M. Abazov et al., Phys.Rev.Lett. 106 (2011) 122001, 1010.0262.

[22] C.N. Yang and R.L. Mills, Phys. Rev. 96 (1954) 191.

[23] F. Jegerlehner, Quantum Chromodynamics and strong interaction physics (Unpublished, 2009).

[24] G. Rodrigo, A. Pich and A. Santamaria, Phys. Lett. B424 (1998) 367, hep-ph/9707474.

[25] K.G. Chetyrkin, J.H. Kuhn and C. Sturm, Nucl. Phys. B744 (2006) 121, hep-ph/0512060.

[26] Y. Schroder and M. Steinhauser, JHEP 01 (2006) 051, hep-ph/0512058.

[27] I.J.R. Aitchison and A.J.G. Hey, Gauge theories in particle physics: A practical introduction. Vol. 1: From relativistic quantum mechanics to QED (, 2003).

[28] R.K. Ellis, W.J. Stirling and B.R. Webber, QCD and collider physics (Cambridge University Press, 1996).

[29] J.D. Bjorken, Phys. Rev. 179 (1969) 1547.

[30] J.D. Bjorken and E.A. Paschos, Phys. Rev. 185 (1969) 1975.

[31] R.P. Feynman, Phys. Rev. Lett. 23 (1969) 1415.

[32] C.G. Callan, Jr. and D.J. Gross, Phys. Rev. Lett. 22 (1969) 156.

[33] G. 't Hooft and M.J.G. Veltman, Nucl. Phys. B44 (1972) 189.

[34] R. Mertig, M. Bohm and A. Denner, Comput.Phys.Commun. 64 (1991) 345.

[35] S. Moch, J. Vermaseren and A. Vogt, Nucl.Phys. B688 (2004) 101, hep-ph/0403192.

[36] A. Vogt, S. Moch and J. Vermaseren, Nucl.Phys. B691 (2004) 129, hep-ph/0404111.

[37] J.C. Collins, Phys.Rev. D58 (1998) 094002, hep-ph/9806259.

[38] V.N. Gribov and L.N. Lipatov, Sov. J. Nucl. Phys. 15 (1972) 438.

[39] L.N. Lipatov, Sov. J. Nucl. Phys. 20 (1975) 94.

[40] Y.L. Dokshitzer, Sov. Phys. JETP 46 (1977) 641.

[41] G. Altarelli and G. Parisi, Nucl. Phys. B126 (1977) 298.

[42] M. Gluck, E. Hoffmann and E. Reya, Z. Phys. C13 (1982) 119.

[43] M. Gluck, R.M. Godbole and E. Reya, Z. Phys. C38 (1988) 441, [Erratum: Z. Phys.C39,590(1988)].

[44] P. Nason, S. Dawson and R.K. Ellis, Nucl. Phys. B327 (1989) 49, [Erratum: Nucl. Phys.B335,260(1990)].

[45] E. Laenen et al., Phys. Lett. B291 (1992) 325.

[46] E. Laenen et al., Nucl. Phys. B392 (1993) 162.

[47] E. Laenen et al., Nucl. Phys. B392 (1993) 229.

[48] J.C. Collins, F. Wilczek and A. Zee, Phys. Rev. D18 (1978) 242.

[49] J. Sanchez Guillen et al., Nucl. Phys. B353 (1991) 337.

[50] W.L. van Neerven and E.B. Zijlstra, Phys. Lett. B272 (1991) 127.

[51] E.B. Zijlstra and W.L. van Neerven, Phys. Lett. B273 (1991) 476.

[52] W.K. Tung, S. Kretzer and C. Schmidt, J.Phys. G28 (2002) 983, hep-ph/0110247.

[53] M.A.G. Aivazis et al., Phys. Rev. D50 (1994) 3102, hep-ph/9312319.

[54] B.A. Kniehl et al., Phys. Lett. B356 (1995) 539, hep-ph/9505410.

[55] M. Buza et al., Eur. Phys. J. C1 (1998) 301, hep-ph/9612398.

[56] R.S. Thorne and R.G. Roberts, Phys. Rev. D57 (1998) 6871, hep-ph/9709442.

[57] R.S. Thorne and R.G. Roberts, Phys. Lett. B421 (1998) 303, hep-ph/9711223.

[58] M. Cacciari, M. Greco and P. Nason, JHEP 05 (1998) 007, hep-ph/9803400.

[59] A. Chuvakin, J. Smith and W.L. van Neerven, Phys. Rev. D61 (2000) 096004, hep-ph/9910250.

[60] M. Kramer, 1, F.I. Olness and D.E. Soper, Phys. Rev. D62 (2000) 096007, hep-ph/0003035.

[61] M.A.G. Aivazis, F.I. Olness and W.K. Tung, Phys. Rev. D50 (1994) 3085, hep-ph/9312318.

[62] M. Guzzi et al., Phys.Rev. D86 (2012) 053005, 1108.5112.

[63] S. Moch, J. Vermaseren and A. Vogt, Phys.Lett. B606 (2005) 123, hep-ph/0411112.

[64] J. Vermaseren, A. Vogt and S. Moch, Nucl.Phys. B724 (2005) 3, hep-ph/0504242.

[65] P.M. Nadolsky and W.K. Tung, Phys.Rev. D79 (2009) 113014, 0903.2667.

[66] S. Riemersma, J. Smith and W.L. van Neerven, Phys. Lett. B347 (1995) 143, hep-ph/9411431.

[67] B.W. Harris and J. Smith, Nucl. Phys. B452 (1995) 109, hep-ph/9503484.

[68] M. Buza et al., Phys. Lett. B411 (1997) 211, hep-ph/9707263.

[69] I. Bierenbaum, J. Blumlein and S. Klein, Nucl. Phys. B780 (2007) 40, hep-ph/0703285.

[70] I. Bierenbaum, J. Blumlein and S. Klein, Phys. Lett. B672 (2009) 401, 0901.0669.

[71] S.A. Larin et al., Nucl. Phys. B492 (1997) 338, hep-ph/9605317.

[72] E. Remiddi and J. Vermaseren, Int.J.Mod.Phys. A15 (2000) 725, hep-ph/9905237.

[73] M. Guzzi, P.M. Nadolsky and B. Wang, Phys. Rev. D90 (2014) 014030, 1309.1393.

[74] P.B. Arnold and M.H. Reno, Nucl.Phys. B319 (1989) 37.

[75] C. Anastasiou et al., Phys.Rev. D69 (2004) 094008, hep-ph/0312266.

[76] S. Catani et al., Phys.Rev.Lett. 103 (2009) 082001, 0903.2120.

[77] G. Bozzi et al., Phys.Lett. B696 (2011) 207, 1007.2351.

[78] Y.L. Dokshitzer, D. Diakonov and S. Troian, Phys.Lett. B79 (1978) 269.

[79] G. Parisi and R. Petronzio, Nucl.Phys. B154 (1979) 427.

[80] G. Curci, M. Greco and Y. Srivastava, Nucl.Phys. B159 (1979) 451.

[81] C. Balazs, J. Qiu and C.P. Yuan, Phys.Lett. B355 (1995) 548, hep-ph/9505203.

[82] R.K. Ellis and S. Veseli, Nucl.Phys. B511 (1998) 649, hep-ph/9706526.

[83] D. de Florian and M. Grazzini, Phys.Rev.Lett. 85 (2000) 4678, hep-ph/0008152.

[84] S. Catani, D. de Florian and M. Grazzini, Nucl.Phys. B596 (2001) 299, hep-ph/0008184.

[85] D. de Florian and M. Grazzini, Nucl.Phys. B616 (2001) 247, hep-ph/0108273.

[86] S. Catani and M. Grazzini, Phys.Rev.Lett. 98 (2007) 222002, hep-ph/0703012.

[87] G. Bozzi et al., Nucl.Phys. B815 (2009) 174, 0812.2862.

[88] A. Banfi et al., Phys.Lett. B715 (2012) 152, 1205.4760.

[89] A. Banfi, M. Dasgupta and S. Marzani, Phys.Lett. B701 (2011) 75, 1102.3594.

[90] A. Banfi, M. Dasgupta and R.M. Duran Delgado, JHEP 0912 (2009) 022, 0909.5327.

[91] P.M. Nadolsky, AIP Conf.Proc. 753 (2005) 158, hep-ph/0412146.

[92] A. Banfi et al., Eur.Phys.J. C71 (2011) 1600, 1009.1580.

[93] S. Catani et al., Eur.Phys.J. C72 (2012) 2195, 1209.0158.

[94] G. Ladinsky and C.P. Yuan, Phys.Rev. D50 (1994) 4239, hep-ph/9311341.

[95] C. Balazs and C.P. Yuan, Phys.Rev. D56 (1997) 5558, hep-ph/9704258.

[96] F. Landry et al., Phys.Rev. D67 (2003) 073016, hep-ph/0212159.

[97] A.V. Konychev and P.M. Nadolsky, Phys.Lett. B633 (2006) 710, hep-ph/0506225.

[98] J.C. Collins and F. Hautmann, Phys.Lett. B472 (2000) 129, hep-ph/9908467.

[99] J.C. Collins and F. Hautmann, JHEP 0103 (2001) 016, hep-ph/0009286.

[100] A. Henneman, D. Boer and P. Mulders, Nucl.Phys. B620 (2002) 331, hep-ph/0104271.

[101] A.V. Belitsky, X. Ji and F. Yuan, Nucl.Phys. B656 (2003) 165, hep-ph/0208038.

[102] D. Boer, P. Mulders and F. Pijlman, Nucl.Phys. B667 (2003) 201, hep-ph/0303034.

[103] J.C. Collins, Acta Phys.Polon. B34 (2003) 3103, hep-ph/0304122.

[104] J. Collins, T. Rogers and A. Stasto, Phys.Rev. D77 (2008) 085009, 0708.2833.

[105] A. Idilbi, X.d. Ji and F. Yuan, Phys.Lett. B625 (2005) 253, hep-ph/0507196.

[106] I. Cherednikov and N. Stefanis, Phys.Rev. D77 (2008) 094001, 0710.1955.

[107] I. Cherednikov and N. Stefanis, Phys.Rev. D80 (2009) 054008, 0904.2727.

[108] M.G. Echevarria, A. Idilbi and I. Scimemi, JHEP 1207 (2012) 002, 1111.4996.

[109] M.G. Echevarria et al., Eur. Phys. J. C73 (2013) 2636, 1208.1281.

[110] S.M. Aybat and T.C. Rogers, Phys.Rev. D83 (2011) 114042, 1101.5057.

[111] T. Becher, M. Neubert and D. Wilhelm, JHEP 1202 (2012) 124, 1109.6027.

[112] S. Mantry and F. Petriello, Phys.Rev. D83 (2011) 053007, 1007.3773.

[113] S. Mantry and F. Petriello, Phys.Rev. D84 (2011) 014030, 1011.0757.

[114] S. Berge et al., Phys.Rev. D72 (2005) 033015, hep-ph/0410375.

[115] A. Banfi et al., JHEP 1201 (2012) 044, 1110.4009.

[116] J. Collins, Int.J.Mod.Phys.Conf.Ser. 25 (2014) 1460001, 1307.2920.

[117] J. Gao et al., Phys.Rev. D89 (2014) 033009, 1302.6246.

[118] J.C. Collins and D.E. Soper, Phys.Rev. D16 (1977) 2219.

[119] A. Banfi, M. Dasgupta and Y. Delenda, Phys.Lett. B665 (2008) 86, 0804.3786.

[120] P.B. Arnold and R.P. Kauffman, Nucl.Phys. B349 (1991) 381.

[121] J. Kodaira and L. Trentadue, Phys.Lett. B112 (1982) 66.

[122] J. Kodaira and L. Trentadue, Phys.Lett. B123 (1983) 335.

[123] C. Davies and W.J. Stirling, Nucl.Phys. B244 (1984) 337.

[124] C. Davies, B. Webber and W.J. Stirling, Nucl.Phys. B256 (1985) 413.

[125] S. Catani, E. D'Emilio and L. Trentadue, Phys.Lett. B211 (1988) 335.

[126] T. Becher and M. Neubert, Eur.Phys.J. C71 (2011) 1665, 1007.4005.

[127] T. Becher, M. Neubert and B.D. Pecjak, JHEP 0701 (2007) 076, hep-ph/0607228.

[128] T. Becher and M. Neubert, Phys.Rev.Lett. 97 (2006) 082001, hep-ph/0605050.

[129] T. Becher, M. Neubert and G. Xu, JHEP 0807 (2008) 030, 0710.0680.

[130] K. Melnikov and F. Petriello, Phys.Rev. D74 (2006) 114017, hep-ph/0609070.

[131] R. Hamberg, W. van Neerven and T. Matsuura, Nucl.Phys. B359 (1991) 343.

[132] A. Cafarella, C. Coriano and M. Guzzi, JHEP 0708 (2007) 030, hep-ph/0702244.

[133] A. Cafarella, C. Coriano and M. Guzzi, Comput.Phys.Commun. 179 (2008) 665, 0803.0462.

[134] G.P. Korchemsky and G.F. Sterman, Nucl.Phys. B437 (1995) 415, hep-ph/9411211.

[135] A. Guffanti and G. Smye, JHEP 0010 (2000) 025, hep-ph/0007190.

[136] J. Qiu and X. Zhang, Phys.Rev. D63 (2001) 114011, hep-ph/0012348.

[137] S. Tafat, JHEP 0105 (2001) 004, hep-ph/0102237.

[138] A. Kulesza, G.F. Sterman and W. Vogelsang, Phys.Rev. D66 (2002) 014011, hep-ph/0202251.

[139] P. Schweitzer, M. Strikman and C. Weiss, JHEP 1301 (2013) 163, 1210.1267.

[140] D0 Collaboration, V.M. Abazov et al., Phys.Rev.Lett. 108 (2012) 151804, 1203.0293.

[141] CDF Collaboration, T. Aaltonen et al., Phys.Rev.Lett. 108 (2012) 151803, 1203.0275.

[142] G. Bozzi, J. Rojo and A. Vicini, Phys.Rev. D83 (2011) 113008, 1104.2056.

[143] U. Baur et al., Phys.Rev. D65 (2002) 033007, hep-ph/0108274.

[144] V. Zykunov, Phys.Rev. D75 (2007) 073019, hep-ph/0509315.

[145] C. Carloni Calame et al., JHEP 0710 (2007) 109, 0710.1722.

[146] A. Arbuzov et al., Eur.Phys.J. C54 (2008) 451, 0711.0625.

[147] S. Dittmaier and M. Kramer, Phys.Rev. D65 (2002) 073007, hep-ph/0109062.

[148] U. Baur and D. Wackeroth, Phys.Rev. D70 (2004) 073015, hep-ph/0405191.

[149] Q.H. Cao and C.P. Yuan, Phys.Rev.Lett. 93 (2004) 042001, hep-ph/0401026.

[150] V. Zykunov, Phys.Atom.Nucl. 69 (2006) 1522.

[151] A. Arbuzov et al., Eur.Phys.J. C46 (2006) 407, hep-ph/0506110.

[152] C. Carloni Calame et al., JHEP 0612 (2006) 016, hep-ph/0609170.

[153] E. Barberio and Z. Was, Comput.Phys.Commun. 79 (1994) 291.

[154] A. Martin et al., Eur.Phys.J. C63 (2009) 189, 0901.0002.

[155] J. Pumplin et al., Phys.Rev. D65 (2001) 014013, hep-ph/0101032.

[156] J. Pumplin et al., JHEP 07 (2002) 012, hep-ph/0201195.

[157] . http://hep.pa.msu.edu/resum/code/resbos_p/resbos.tar.gz.

[158] . http://hep.pa.msu.edu/resum/grids/resbos_p/w_z/tev2/general_purpose/; http://hep.pa.msu.edu/resum/grids/resbos_p/w_z/lhc/general_purpose/.

[159] J. Collins and T. Rogers, Phys.Rev. D91 (2015) 074020, 1412.3820.

[160] V. Guzey et al., Eur.Phys.J. A49 (2013) 35, 1212.5344.